EFFECT OF PULSED LASER DEPOSITED CERAMIC COATINGS ON MICROHARDNESS AND CORROSION BEHAVIOR OF TITANIUM, Ti6Al4V AND INCONEL

Thesis

Submitted in partial fulfillment of the requirements for the degree

of

DOCTOR OF PHILOSOPHY

by

SUJAYA .C

DEPARTMENT OF PHYSICS

NATIONAL INSTITUTE OF TECHNOLOGY KARNATAKA,

SURATHKAL, MANGALORE -575025

February, 2012

D E C L A R A T I O N

by the Ph.D. Research Scholar

I hereby *declare* that the Research Thesis entitled ***Effect of Pulsed Laser Deposited Ceramic Coatings on Microhardness and Corrosion Behavior of Titanium, Ti6Al4V and Inconel*** which is being submitted to the **National Institute of Technology Karnataka, Surathkal** in partial fulfillment of the requirements for the award of the Degree of **Doctor of Philosophy** in Physics *bonafide report of the research work carried out by me*. The material contained in this Research Thesis has not been submitted to any University or Institution for the award of any degree.

Sujaya C.,
(Reg. No. 050621PH05P01)

Department of physics

Place: NITK-Surathkal
Date: 16-02-2012

C E R T I F I C A T E

This is to *certify* that the Research Thesis entitled ***Effect of Pulsed Laser Deposited Ceramic Coatings on Microhardness and Corrosion Behavior of Titanium, Ti6Al4V and Inconel*** submitted by **Sujaya C,** (Register Number: **050621PH05P01**) as the record of the research work carried out by him/her, is *accepted as the Research Thesis submission* in partial fulfillment of the requirements for the award of degree of **Doctor of Philosophy**.

Research Guide
(Name and Signature with Date and Seal)

Chairman - DRPC
(Signature with Date and Seal)

ACKNOWLEDGEMENT

It gives me immense pleasure to acknowledge the guidance and encouragement throughout my research work that I received from many people.

First and foremost I must be thankful to Dr.H.D.Shashikala for her insight, support and encouragement throughout this process. Without her guidance and expertise, none of this would have been possible. I leave my heartfelt gratitude for her unequivocal support and guidance.

I must thank the members of RPAC; Dr.S.M Kulakarni, Dr.N.K.Udayashankar, for their valuable suggestions and feedbacks. I would also like to thank Prof. G.Umesh, for his kindness, generous help and valuable suggestions.

I also thank Dr. Chitharanjan Hegde, HOD Chemistry, Prof. Narayana Prabhu , HOD, Metallurgical & Materials Engineering, N.N. Sampath Kumar, Former Co-ordinator, R&D centre, NITK Surathkal, Prof, Guru Raw and Prof. Sathish Vasu Kailas from Indian Institute of science, Bangalore, Mr Vyanatheyan from CPRI, Bangalore, Mr Swaminathan, BHEL Bangalore, who have rendered their valuable time and energy in helping me in my research work.

I cannot forget encouragement given by Prof. Jayagopal Uchil , Former Chairman, Department of Materials Science, Mangalore university, who encouraged me to take up research.

The support received from the faculty members, the non-teaching staffs and the research scholars of the department is gratefully acknowledged.

I also remember at this moment, my family members, friends, who have inspired me to achieve this ambitious goal.

I would like to acknowledge the Indian Space Research Organization (ISRO) for financial assistance in carrying out this research work and Vikram Sarabhai Space Centre (VSSC), Thiruvananthapuram for supplying materials for research.

Abstract

Coatings are used to modify and increase the functionality of a bulk surface or substrate without modifying the bulk properties of the material. The present work aims at obtaining uniform adhesive coatings of alumina and silicon carbide on different substrates viz., titanium, Ti6Al4V and inconel by pulsed laser deposition technique using Q-switched Nd: YAG laser at low temperature. Processing parameters such as laser fluence, substrate target distance, substrate temperature and target density during deposition were standardized to get adhesive films. Coated films were characterized using scanning electron microscopy, energy dispersive X-ray spectroscopy, spectrophotometer, optical microscope, nanoindentation, surface roughness measurements using 3D optical profilometer, adhesion test. Microhardness and corrosion studies were carried on substrates and after coating. Composite microhardness of ceramic coated substrates was measured using Knoop indenter and its film hardness was separated from composite hardness using a mathematical model based on modified area-law of mixture. Then by including indentation size effect the film hardness was compared with values obtained using nanoindentation method. Composite hardness as well as film hardness of the ceramic coating was found to be higher compared to the substrates. Corrosion behavior of substrates after ceramic coating was studied using 3.5% NaCl solution by potentiodynamic polarization and electrochemical impedance spectroscopy measurements. The Nyquist and the Bode plots obtained from the electrochemical impedance spectroscopy data are fitted by appropriate equivalent circuits. The pore resistance, the charge transfer resistance, the coating capacitance and the double layer capacitance of the coatings were obtained from the equivalent circuit. Alumina coated substrates showed more corrosion resistance than silicon carbide coated substrates. After the corrosion testing, the surface topography of the uncoated and the coated system were examined under scanning electron microscopy. Experimental results confirmed the possibility of using Nd: YAG laser for ceramic film deposition which improves the microhardness and corrosion resistance of the substrate considerably.

Key words: Ti6Al4V; Inconel; Titanium; Silicon carbide; Alumina; Hardness; Pulsed laser deposition; Corrosion; Ceramic coatings.

Contents

List of figures

List of tables

Nomenclature

Al_2O_3	aluminium oxide
SiC	silicon carbide
Nd:YAG	neodymium-doped yttrium aluminium garnet
SEM	scanning electron microscope
EDAX	energy-dispersive X-ray spectroscopy
3D	3-dimension
NaCl	sodium chloride
EIS	electrochemical impedance spectroscopy
R_{pore}	pore resistance
R_{ct}	charge transfer resistance
Q_{coat}	coating capacitance
Q_{dl}	double layer capacitance
HCP	hexagonal close packing
BCC	body centered cubic
FCC	face centered cubic
Cr	chromium
Fe	iron
Mn	manganese
Mo	molybdenum
V	vanadium
TiC	titanium carbide
TiN	titanium nitride
ZrN	zirconium nitride
PLD	pulsed laser deposition
PVD	physical vapor deposition
CVD	chemical vapor deposition
PECVD	plasma enhanced chemical vapor deposition
MBE	molecular beam epitaxy
RMS	root mean square

FTIR	Fourier transfer infrared Spectroscopy
XPS	X-ray spectroscopy
RT	room temperature
H	hardness
E	elastic modulus
TiAlN/CrN	titanium aluminium nitride/ chromium nitride
UV	ultra violet
XRD	X-ray diffraction
DCP	direct current polarization
ArF	argon fluoride
KrF	krypton fluoride
XeBr	xenon bromide
XeCl	xenon chloride
XeF	xenon fluoride
IR	infra red
R_a	average roughness
AP	apparent porosity
BD	bulk density
TD	true density
BSE	back scattered electrons
CRT	cathode ray tube
SCE	saturated calomel electrode
E_{corr}	corrosion potential
I_{corr}	corrosion current density
R_p	corrosion resistance
CR	corrosion rate
EW	equivalent weight
FRA	frequency response analyzer
Z″	imaginary impedance
Z	real impedance
R_s	electrolyte resistance

EC	equivalent circuit
CDC	circuit description code
CPE	constant phase element
JCPDS	joint committee on powder diffraction standards
CP	commercially pure
E_g	energy gap
E_u	Urbach energy
ISE	indentation size effect
HK	hardness knoop
P	applied load
L	indentation diagonal
l	path length
CRT	cathode ray tube
AFM	atomic force microscopy
WE	working electrode
Q	total capacitance of the CPE
EIS	electrochemical impedance spectroscopy
h_c	contact depth.
h_s	displacement of the surface at the perimeter contact
h_f	final depth
H	hardness
E	elastic modulus

CHAPTER -1

INTRODUCTION

1.1 Need for coating

Coating is a covering that is applied to the surface of an object, usually referred to as the substrate. Coatings are used to modify and increase the functionality of a bulk surface or substrate without modifying the bulk properties of the material. Surface coating is now being used in virtually every area of technology, including automotive, aerospace, missile, power, electronic, biomedical, textile, petroleum, petrochemical, chemical, steel, power, machine tools, and construction industries. They are being used to develop a wide range of advanced functional properties, including physical, chemical, electrical, electronic, magnetic, mechanical properties at the required substrate surfaces. Either thick or thin films can be used as coatings. In many cases thin films do not affect the bulk properties of the material. They can, however, totally change the optical, electrical transport, and thermal properties of a surface or substrate, in addition to providing an enhanced degree of surface protection. Thin film coatings are widely used in a variety of applications either as structural overcoats or as functional coatings. The former case implies thin films on machine tools to decrease wear or protective overcoats to shield surfaces from an adverse environment. The latter case, for example, implies thin films on optical components for reflection modifications or gas proof films as ion conductors in high-temperature fuel cells.

1.2 Importance of substrate materials

1.2.1 Titanium and Ti6Al4V

Titanium and titanium alloys, especially Ti6Al4V, are excellent candidates for aerospace applications such as aircraft turbine engines, chemical apparatus, surgical implants and heat exchangers owing to their high strength to weight ratio and excellent corrosion resistance. After their introduction in the early 1950s, these materials, in a

relatively short time, became backbone materials for many industries. The largest consumer of titanium alloys is aerospace industry.

The major requirements to the materials for the aircraft industry are their characteristics of specific strength and heat resistance, fatigue resistance, crack resistance, and sufficient corrosion resistance. Of great importance is the processibility of titanium alloys in manufacturing aircraft items and components – their plasticity in deformation, weldability, and machinability (Valentin, N. and Moiseyev 2006). Titanium alloys are used for a variety of components including critical structural parts, fire walls, landing gear, exhaust ducts (helicopters), and hydraulic systems. In fact, about two thirds of all titanium metal produced is used in aircraft engines and frames. In engine applications, titanium is used for rotors, compressor blades, hydraulic system components, and nacelles. The use of titanium and its alloys have expanded in recent years to include applications in nuclear power plants, chemical machine building, shipbuilding, the auto industry, in equipment for the oil and gas industry, the food industry, medicine, and civil engineering, food processing plants, marine components and medical prosthesis etc.

Wide range use of titanium and its alloys in aerospace industry is in making various parts which have moving contact. There have been many attempts at increasing the wear resistance of these alloys. High friction coefficient and low wear resistance of titanium and its alloy, seriously limit extensive usage, especially in situations involving rotating mechanical linkage (Zaytouni, M. and Riviere, J.P. 1996). The high corrosion resistance of titanium alloys is also decreased when local mechanical abrasion removes the protective oxide film (Mischler, S. et al. 1998). However, their poor room-temperature wear resistance and high-temperature oxidation resistance require surface treatments. Use of coating would enhance the wear resistance and oxidation resistance of these materials. There are also many other industrial applications where it is necessary to improve the surface mechanical properties of engineering components without modifying its bulk properties. However in all these applications where there are important stresses

imposed on the surface of the moving part, the adhesion performance of the coating is crucial for durable use.

Background of titanium alloys

Titanium is a relatively light, silver-gray metal. Pure titanium has high melting point of 1668°C. Titanium is allotropic, with HCP crystal structure (α) at low temperatures and a BCC structure (β) above 882°C. The existence of the two different crystal structures and the corresponding allotropic transformation temperature is of central importance since they are the basis for the large variety of properties achieved by titanium alloys. The addition of other metals to a titanium base will favor one or other of the two crystallographic forms. Titanium alloys are classified into three groups depending on the phases present, alpha, alpha-beta, and beta alloys. The alpha-phase alloys of titanium, which is categorized as commercially pure titanium, is relatively weak in strength but offers a combination of good corrosion resistance, good weldability, creep resistance, receptive to heat treatment coupled with ease of processing and fabrication (ASM Metals Handbook 1990 and Donachie, M.J.Jr. 2000). The beta-phase alloys are receptive to forging while offering excellent fracture toughness. The dual phase, i.e. alpha + beta alloys offer a combination of excellent ductility and strength when proper heat treatment is given, which makes them stronger than the alpha-phase and beta-phase counterparts (Boyer R.R. 1996 and Askeland,D.R 2007). Atomic weight of titanium is 47·9 (Askeland, D.R 2007). The density of pure titanium metal is 4500Kg/m^3, which is about 60% that of steel (Donachie, M. J. Jr. 2000 and Askeland 2007).

Alloying elements are added to stabilize one or the other of these phases as shown in Figure 1.1, by either raising or lowering the transformation temperatures (Collings, E.W. 1984). Aluminum is the strongest metallic alpha stabilizer, used in commercial alloys, which raises the beta transus and imparts high-temperature strength to the alloy. Certain alloying elements used in commercial alloys (e.g., Cr, Fe, Mn, Mo, V) are beta stabilizers, which lower the beta transus. Addition of these elements strengthens the beta solid solution and increase the amount of beta retained at room temperature. Thus, the beta may be changed from an unstable form to a stable form, even below room

temperature. In alpha-beta alloys, the beta phase is in an unstable condition. These alloys can be heat treated to achieve strengthening by partial transformation of the beta phase to alpha, which is finely dispersed in the beta phase. Among the alpha-beta alloys, Ti6Al4V is by far the most popular titanium alloy. More than 50% of all alloys in use today are of this composition. The alloy was developed in the early 1950s in the United States at the Illinois Institute of Technology and is therefore one of the very first titanium alloys to be made. There are two reasons for the success of Ti6Al4V. First, the good balance of its properties like hardness, yield strength elastic modulus, tensile strength etc. Second, it is by far the most intensively developed and tested titanium alloy, which is a major advantage – especially in the aerospace industry, the largest user of Ti6Al4V. The next largest application of Ti6Al4V is medical prostheses, which accounts for 3% of the market. The automotive, marine, and chemical industries also use small amounts of Ti6Al4V.The typical ultimate tensile strength of Ti6Al4V is around 900-1100 MPa, which is affected by heat treatment (microstructure), composition (oxygen content) and texture (primarily in sheet) (Collings, E.W. 1984 and Donachie M.J.Jr. 2000). The ultimate shear strength of Ti6Al4V is generally 60% of the tensile strength. This applies to all wrought and cast forms and includes both annealed and solution treated and aged conditions. Depending on heat treatment condition, shear strengths range from 480 to 700 MPa. (Donachie M.J.Jr. 2000).

1.2.2 Inconel

Inconel belongs to a family of austenitic nickel-chromium-based superalloys. This family of alloys was developed for high-temperature oxidizing environments. These alloys typically contain 50–80% nickel, which permits the addition of other alloying elements to improve strength and corrosion resistance while maintaining toughness. Inconel alloy is a standard engineering material for use in severely corrosive environments at elevated temperatures. It is resistant to oxidation at temperatures up to 1177^0C. In addition to corrosion and oxidation resistance, inconel has desirable combination of high strength and workability, and is hardened and strengthened by cold-working. This alloy maintains strength, ductility, and toughness at cryogenic as well as

elevated temperatures. Inconel retains strength over a wide temperature range, attractive for high temperature applications where aluminum and steel would succumb to creep as a result of thermally-induced crystal vacancies. It is used in gas turbines, rocket engines, pressure vessels, tooling, and aircraft structures. Because of its resistance to chloride-ion stress-corrosion cracking and corrosion by high-purity water, it is used in nuclear reactors. Other typical applications are furnace muffles, electronic components, heat-exchanger tubing, chemical-and food-processing equipment, carburizing baskets, fixtures and rotors, reactor control rods, nuclear reactor components, primary heat-exchanger tubing, springs, and primary water piping (Myer Kutz, 2002). Density of inconel is 8740Kg/$m^{3.}$ Melting point of the inconel lies in the range of 1355-1413^{0} C.

Inconel alloys which are widely used in high-temperature applications show an undesirable loss of wear resistance under those conditions. So it is necessary to improve the surface mechanical properties of engineering components without modifying their bulk properties. A well established method to overcome this surface loss of the alloy is by coating with high hardness ceramic materials. Thin film coatings of ceramics exhibit enhanced mechanical, tribological, anti-corrosion and anti-oxidation properties in hostile atmosphere. So, it is necessary to have a homogeneous adhesive coating of ceramic material on the surface of inconel.

1.3 Importance of coating materials

Ceramics are defined as solid materials composed of inorganic nonmetallic materials (Kingery, W.D. et al. 1976). Ceramics have unique thermal, mechanical, chemical and electrical properties, but their high fabrication cost, brittleness, size and shape limitations as monolithic components restrict many potential applications. One way to avoid these drawbacks is to use ceramics as coatings on metallic substrates.

Ceramic films and coatings are both active fields of research and widely used areas of technology. The relatively high hardness and inertness of ceramic materials make ceramic coatings of interest for protection of substrate materials against corrosion, oxidation and wear resistance. The electronic and optical properties of ceramics make

ceramic films and coatings important to many electronic and optical devices. (John, B. W. and Richard, A. H. 1993)

The increasing need to extend life and maintenance cycles of components has also been a motivator for the use of these materials as coatings in gas turbines, power plants, cement plants, gas burners, incineration plants. Thus, many researchers have devoted themselves to developing coatings that can be tailored for numerous applications. Although conventional techniques such as electroplating were popular, they often suffered from adhesion, and hence reliability problems. Other techniques, such as sol-gel, were useful in selected applications but do not offer universal capability to create coatings sufficiently thick to withstand the high temperatures of exposure. Thin ceramic coatings deposited by vapour deposition techniques such as physical vapor deposition and chemical vapor deposition are widely used as wear and corrosion resistant coatings. These coatings include diamond, TiC, TiN, ZrN, Al_2O_3, SiC etc. Since the deposition processes operate at atomic or molecular level, the structure of the coatings can also be controlled on that level and well developed, dense structures having properties of dense monolithic materials can be produced. However, the thickness of these coatings is typically less than 10 μm, since thicker coatings suffer from high internal stresses or the same brittleness as dense monolithic ceramics. In our studies the two important ceramic elements used for coating on the substrate materials are silicon carbide (SiC) and aluminuin oxide (Al_2O_3).

1.3.1 Silicon Carbide (SiC)

Recent interest in silicon carbide originates from its excellent mechanical, thermal and electronic properties. Wide band gap (2.0 to 7.0 eV), high breakdown electric field strength , high electron saturation drift velocity, high thermal conductivity, and extreme resistance to chemical and radiation attacks make SiC a very promising material for high power and high frequency electronic devices. (Morkoc, H. et al. 1994 and Zopal, J.C. and Skowronski, M. 2005). SiC is covalently bonded and exhibits high hardness and high melting temperature. Therefore, SiC coatings exhibit many interesting properties as materials for high temperature mechanical and tribological applications in hostile

environments. (Zaytouni, M. and Riviere, J.P. 1996). SiC has the key property like low density, high strength, low thermal expansion, high thermal conductivity, high hardness, high elastic modulus, excellent thermal shock resistance and superior chemical inertness. It has been employed to protect various kinds of tool and machine parts from excessive wear (Mernagh, V.A. et al. 1991) and, in space applications, it has been used to preserve the outer shell of thermionic energy converter against the high heat found in combustion atmosphere (Louis-Claude, D. et al.1989). Because of its chemical stability and resistance to attack in radiation environments, the nuclear industry has investigated the use of SiC coatings to protect steam generator tubes from intergranular stress corrosion cracking and radioactivity build up and as first–wall alloys of fusion reactors for high levels of induced radioactivity and hydrogen uptake (Gruss, K. A. and Davis, R. F. 1999 and Ho, S. K. et al. 1993).

Silicon carbide (SiC) is the most widely used non oxide ceramic. It occurs in two crystalline forms: the cubic β .-phase, which is formed in the range 1400–1800^{0}C, and the hexagonal α – phase formed at 2000^{0}C (Barry, C. and Grant Norton, M. 2007).

1.3.2 Alumina (Al_2O_3)

Alumina is an outstanding ceramic material due to its several excellent physical and chemical properties like high compression strength, high hardness, resistant to abrasion, resistant to chemical attack by a wide range of chemicals even at elevated temperatures, high thermal conductivity, resistant to thermal shock, high degree of refractoriness, high dielectric strength, high electrical resistivity even at elevated temperatures, transparent to microwave radio frequencies (Atul Khanna, et al. 2006). Also availability in abundance has made alumina attractive for engineering applications. According to their excellent mechanical, optical and electrical properties, aluminium oxide thin films are used in a very large range of applications, such as wear-resistant coatings (Wang, J. et al. 2001) corrosion resistant barriers (Haanappel, V. A. C. et al. 1995), optical waveguides (Pillonnet, A. et al. 2000) and passivation barriers in metal oxide semiconductor devices (Yi-Shung, C. and Nripen, R. 1990).

Alumina is a very interesting crystalline material exhibiting many crystalline phases. The alpha (α), kappa (κ), and xeta (χ) phases are called the "alpha series" with hcp stacking of oxygen atoms; whereas, the gamma (γ), theta (θ), eta (η) , and delta (δ) phases form the "gamma series" with fcc stacking of oxygen atoms. The most thermodynamically stable form is α-aluminium oxide and is known as corundum. Various properties of Al_2O_3 and SiC are summarized in Table 1.1

Ceramic coatings can be produced by chemical vapor deposition and various physical vapor deposition processes such as thermal evaporation, arc ion plating, magnetron sputtering, thermal spraying etc. Among these methods, pulsed laser deposition (PLD) is found to be a powerful technique to produce adherent thin films.

1.4 Introduction to surface coating techniques

Coating technologies are commonly classified according to coating thickness. Usually, those up to 10 μm are considered thin-film coatings. The main aspect, however, is that thin films can have completely different properties compared to bulk material and thicker coatings, in part due to their different microstructure. Common processes in recent thin-film technology include chemical vapor deposition (CVD) and physical vapor deposition (PVD) technology. The fact that coating material is applied to the substrate on an atomic scale, in the form of individual atoms, ions, clusters, or molecules, is common to nearly all processes. CVD and PVD techniques deposit coating material via the gas phase

1.4.1 Chemical vapor deposition (CVD)

CVD is a process in which the substrate is exposed to one or more volatile precursors, which react and/or decompose on the substrate surface to produce the desired thin film deposit. The resulting solid material is in the form of a thin film, powder, or single crystal. By varying experimental conditions, including substrate material, substrate temperature, composition of the reaction gas mixture, gas flows pressure, etc., materials with a wide range of physical, tribological, and chemical properties can be grown. A characteristic feature of the CVD technique is its excellent throwing power, enabling the production of coatings of uniform thickness and properties with a low porosity even on

substrates of complicated shape. Another important feature is the capability of localized or selective deposition on patterned substrates. In CVD, the chemical reactions require temperatures of up to 2000^0C to provide the necessary activation energy. CVD and related processes are employed in many thin film applications, including dielectrics, conductors, passivation layers, oxidation barriers, conductive oxides, tribological and corrosion-resistant coatings, heat-resistant coatings, and epitaxial layers for microelectronics. In CVD, the chemical species being deposited is generally reduced or decomposed on the substrate surface, usually at high temperatures. Care must be taken to control the interfacial reactions between coating and substrate and between substrate and gaseous reaction products. In contrast to PVD, the process can operate under low-pressure conditions and atmospheric pressure.

1.4.2 Physical vapor deposition (PVD)

PVD processes encompass a wide range of vapor-phase technologies and a variety of methods to deposit thin solid films by the condensation of a vaporized form of the solid material onto various surfaces. PVD involves physical ejection of material as atoms or molecules and condensation and nucleation of these atoms onto a substrate. The vapor-phase material can consist of ions or plasma and is often chemically reacted with gases introduced into the vapor, called reactive deposition, to form new compounds. PVD processes include thermal evaporation, electron beam (e-beam) evaporation and reactive electron beam evaporation , sputtering (planar magnetron, cylindrical magnetron, dual magnetron, high-power pulsed magnetron, unbalanced magnetron, closed field magnetron, ion beam sputtering, diode, triode) and reactive sputtering , filtered and unfiltered cathodic arc deposition (non-reactive and reactive), ion plating, pulsed laser deposition etc. PVD coatings are used in various applications. Not only applicable for conventional wear-resistance coatings, PVD can produce decorative coatings, thermal-barrier coatings, and optical surfaces, e.g. for microelectronics. Usually, PVD involves high-vacuum technology. PVD allows thin-film deposition of metalloid and ceramic coating materials on virtually any technically relevant substrate. Apart from alloys and metals, ceramic, as well as glass substrates, even plastics can be PVD coated using high

energy pulses (lasers) in order to reduce process temperature. PVD process has the ability to produce unusual microstructures and new crystallographic modifications, e.g. amorphous deposits. In this process the substrate temperature can be varied within very wide limits from low to high temperatures. The deposits having very high purity can be obtained in PVD process. The main disadvantages of PVD processes are the low deposition rates and the difficulty in applying oxide coatings efficiently. Because of the technology used in PVD manufacturing, particles of the source material can only travel in a straight line. Therefore, it's more difficult to make finishes for odd-shaped objects. Additionally, this technology can require very high temperatures as compared to PLD, which need to be monitored closely by workers. Installation and operating costs for PVD can also be quite high.

1.4.3 Pulsed Laser Deposition (PLD)

Soon after the discovery of the laser, researchers began focusing their lasers at materials to observe the interaction. Smith H M and Turner A F (1965) were amongst the very first to irradiate materials for the purpose of thin film growth. In their study they observed some of the qualities that make pulsed laser deposition (PLD) one of the main advances of the last two decades in the field of laser material processing. Due to the inherently short duration of laser pulses, even energies of the order of hundreds of mJ, when focused, correspond to enormous peak power levels from megawatts cm^{-2} for nanosecond lasers to gigawatts cm^{-2} and terrawatts cm^{-2} for picosecond and femtosecond laser pulses, respectively. Any material, even those that absorb poorly at the wavelength of the incoming photons, when irradiated at such high laser intensities will be almost instantaneously heated beyond their boiling temperature and a vaporization process will subsequently be initiated from the surface. The interaction of the laser pulse with the vaporized particles can even create a dense plasma plume containing highly energetic ions, neutral atoms and electrons. Regardless of the incoming direction of the initial laser pulse, the plume expansion will be highly forward-directed with the distribution centered normal to the local target surface. The ejected material contained in the plume (predominantly atoms, ions and small molecules) is then incident on a substrate located

typically between 0.03 to 0.1 m in front of the target. Because of the highly forward-directed nature of the PLD plume, the material incident on the substrate contains nearly the same relative ratio of atoms, or stoichiometry, as the target. If the sticking fraction is close to unity, and if the substrate is heated to approximately half the melting temperature, the material will often self-assemble into complex crystalline structures highly oriented or even epitaxial with the substrate.

The ability to transfer the stoichiometry of a multicomponent target to a growing film is the most important advantage of PLD compared to other conventional physical vapour deposition techniques and it makes PLD the premier technique for ceramic thin film research. Other advantages of PLD include the ability to deposit material in high pressures of reactive gases (because there are no filaments or discharges) and the simplicity of the PLD set-up. For ceramic thin films, the ability to easily control multicomponent stoichiometry, especially the oxygen content, in a simple set-up makes PLD a highly reproducible technique (Colin, E. W. and Julian, D. C. J. 2004).

1.4.3.1 Advantages and disadvantages of PLD

PLD is the technique using the energy of a laser to vaporize a target material. This laser ablation is based on the interaction between matter and very short laser pulses. The duration of a laser pulse is short such that extremely high power can be delivered by each pulse. Further, these energetic pulses are focused to very small areas yielding high energy densities. When the energy densities are high enough to melt the target and break the bonds of the material, ionized components are ejected and form a plasma plume which is subsequently transported to the heated substrate and react on the surface to form a thin film. PLD can produce films whose stoichiometries are nearly the same as that of the targets because of the extremely high temperatures generated at the lasers focus point, which can evaporate all elements without preference. This is of great benefit when films of relatively complex composition are grown. By easily adjusting the ratio of different elements when targets are made, films with identical ratios of different elements can be achieved. PLD requires lower deposition temperatures than most other deposition techniques because of the high kinetic energies (up to about 100 eV) (Kuzma, M. et al.

2000) of the ablated ionized components from the targets. So the substrate temperature can be relatively low compared with other film growth techniques, which is important for the growth of materials whose growth temperature is high (Chrisey, D. B. and Hubler, G. K. 1994 and Miller, J.C. and Haglund, R. F. 1998). This technique can be used to produce quality films of various kinds such as semiconductors, high T_c superconductors, ceramics, ferroelectrics, multilayer polymers, etc. (Otsubo, S. et al. 1990, Kidoh, H. et al. 1991, Tsuboi, Y. et al. 1999 and Tsuboi, Y. et al. 1998). In particular, PLD is useful for ablating materials in the combinational forms that cannot be easily produced by other methods (Lowndes, D. H. et al. 1998 and Agostinelli, E. et al. 2000). Recently, PLD has also been used to synthesize nanotubes (Zhang, Y. et al. 1998), nanopowders (Geohegan, D.B. 1995), quantum dots (Goodwin, T. et al 1997), and some organic thin films that have applications in optoelectronics (Wang, L. D. and Kwok, H. S. 2000).

There are a number of advantages of PLD over other film deposition methods. Some of them are listed below:

(i) The biggest advantage is that it is versatile. A very wide range of materials, including oxides, metals, semiconductors and even polymers, can be grown by PLD. All that required is a target of the desired composition. Whereas in Molecular Beam Epitaxy (MBE) and Chemical Vapor Deposition (CVD), different source of precursors are required for each element of the desired compound.

(ii) It has the ability to maintain target composition in the deposited thin films. Because of the very short duration and high energy of the laser pulse, target material plumes instantly move toward the substrate and also every component of the phase has a similar deposition rate. This makes optimization of the deposition process much easier.

(iii) The energy associated with the high ionic content in laser ablation plumes (typically of the order of 10% and rising with increasing incident laser power density) and high particle velocities (of the order of 10^4 $m.s^{-1}$) appear to aid crystal growth and lower the substrate temperature required for epitaxy.

(iv)Other advantages are that PLD is clean, low cost, and capable of producing multilayered films simply by switching between several different targets.

There are certain disadvantages to PLD. These include:

(i) The ablation plume cross section is generally small (of the order of cm^2) due to a limited laser spot size. This, in turn, limits the sample size that can be prepared by PLD. In addition, this also brings difficulty in controlling thickness uniformity across the sample. This problem can be overcome, to some extent, by scanning the laser beam on a larger size target.

(ii) The plume of ablated material is highly forward directed, which causes poor conformal step coverage. It also makes thickness monitoring difficult.

(iii) Finally, there is an intrinsic "splashing" associated with laser ablation itself, which produces droplets or big particles of the target material on the substrate surface. From an industrial perspective, this is particularly serious as it will result in device failure.

By standardizing the processing parameters these disadvantages can be overcome and uniform adhesive films can be obtained on the substrate using PLD.

1.5 Summary of literature review

Titanium and its alloys are well known for their high specific strength and outstanding corrosion resistance, but the friction and wear properties of these materials can cause problems in various industrial sectors. There are great interests to overcome the poor corrosive-wear resistance of titanium alloys through appropriate surface techniques. A series of surface modification processes, including thermo chemical diffusion treatment (Muraleedharan, T. M. and Meletis, E. I. 1992 and Galliano, F. et al. 2001), laser surface melting (Tian, Y. S. 2005), ion implantation (Qiu, X. et al. 1990 and Lidong, Z. and Erich, L. 2002) chemical and physical vapor deposition (Met, C. 2003) and Kessler, O. et al 2002) and spraying (Lidong, Z. and Erich, L. 2002), successfully improved their wear resistance through surface hardening. In most processes, however, the request in industrial applications for titanium and its alloys is not completely satisfied because the modified surfaces with improved wear resistance show deteriorated corrosion resistance, and/or the modified surfaces and deposited films no longer have the improved properties due to the insufficient thickness or peeling off. Therefore, developing new surface engineering techniques is necessary for the improvement in wear and corrosion

resistance of titanium and its alloys.

High temperature materials such as nickel-base superalloys are currently used in numerous high temperature applications which require both mechanical strength and oxidation resistance (Pieraggi, B. 1987). In these conditions an undesirable loss of wear resistance of inconel has been observed. So it is necessary to improve the surface mechanical properties of engineering components without modifying their bulk properties. Garbacz, H. et al. (2006) reported on Al_2O_3+Ni–Al multilayer coatings, which have been produced on inconel 600 by glow discharge, assisted oxidizing of substrates pre-coated with aluminum by magnetron sputtering. These layers have a diffusive structure and can be produced on parts of complicated shapes. The presence of the Al_2O_3 layer on intermetallic Al–Ni imparts high hardness (7.2 GPa) and good wear resistance. In this paper, the influence of the multilayered coatings on the mechanical properties of inconel 600 was investigated. The structure of layers was examined on a scanning electron microscope with energy dispersive spectrometer and the surface topography using a profilometer.

Coated materials have many applications in industry. Coatings permit one to obtain wear-resistant metal-tools, thermal barriers in the aircraft and automobile industry, insulating layers in microelectronics, etc. The reliability of coated materials has become a growing field of interest in the recent past. Audoly, B. (2000) reported about particular mode of failure of these materials, the buckle-driven delamination.

PLD is well known as a reliable, economical technique for the growth of thin films. There are number of interesting characteristics, however, that distinguish this method from other thin film techniques. In particular, the vapor species are typically characterized by average energies far above those encountered in thermal evaporation and chemical vapor based approaches. As a result, PLD may have the potential to realize films with a smoother morphology at low substrate temperatures if the surface species can retain some portion of the initial kinetic energy after adsorption.

Gottmann, J. et al. (1998) and Hirschauer B.et al.(1996) reported that alumina deposits can be produced by evaporating metallic aluminium target in the presence of

oxygen gas, or alternatively, by straight evaporation of alumina target. In the latter case, the application of background oxygen is also possible, to ensure the desired stoichiometry of the deposit.

Hirschauer, B. et al. (1996) & (1997) showed that alumina films grown near room temperature show an amorphous microstructure. Increasing the substrate temperature increases the crystallinity and orientation of the deposit. Highly crystalline and oriented structures require as high substrate temperatures as 850 °C. Similar effect can be obtained by annealing the specimens after the deposition. Substrate heating and / or post-annealing also induce the growth of grain size, as well as phase transformations, since PLD alumina has several possible crystalline forms, e.g. α, γ, δ and θ. Cibert, C.et al. (2008) studied and compared the properties of alumina thin films deposited by PLD and plasma enhanced chemical vapor deposition (PECVD) at room temperature and at 800^0C. At room temperature films are found amorphous while at 800 ^{0}C the γ-type structures are found. Analysis indicates that films deposited by PLD are of high purity, density and stoichiometric compared to PECVD. Alumina films deposited by PLD showed interesting chemical, structural mechanical, optical properties compared to PECVD.

Conventionally silicon carbide thin films have been grown by chemical vapor deposition. This technique has, however, few major drawbacks, namely, substrate suffering from high temperatures (typically 1300-1600 °C) and relatively high hydrogen content of the film. Jipo, H. et al. (1999) and Tang, Y.H. et al. (2006) reported that SiC films can be grown at lower temperature without deviating the stoichiometry. Silicon carbide films grown in lower temperatures (250^0C or lower) usually show amorphous microstructure. In these cases, Si and C atoms are not always covalently bonded (as is the case of SiC polytypes); also systems, where undefined Si- and C-rich phases coexist or Si- and C-atoms form a solid solution, are possible. However, the formation of stoichiometric SiC is usually necessary, to obtain the desired properties of the film. Generally, good thermal, mechanical and chemical stability are characteristic of pulsed laser deposited SiC. Thus, it can be used as a coating material under extreme environments and the application field is wide. Most of the applications are in high-

power and high-frequency electronic devices or optoelectronic components. In addition, SiC thin films are used as protective and tribological coatings.

Jamey, S.P. et al. (2000) examined the PLD growth of SiC thin films on (100) silicon and (0001) sapphire substrates over a substrate temperature range of 250- 900^0C. In-situ characterization using reflection high-energy electron diffraction indicates that films deposited on sapphire above 700^0C, using low laser fluence, initially grow as single crystal material. X-ray diffraction shows either 3C-SiC features or no features at all, independent of the type of substrate. Atomic force microscopy shows very smooth films, with an average surface roughness of 3 Å at a substrate temperature of 250^0C and 0.7 Å at 900^0C.SiC films deposited using PLD technique at room temperature, 370^0C and 480^0C are carried out by Katharria,Y.S. et al. (2008). XPS and FTIR analysis showed the formation of Si - C bonds in the films. TEM and electron diffraction were used to study the structural properties of nanocrystallites formed in the films. Nearly stoichiometric thin films containing nanocrystals of α-SiC were prepared by PLD at RT as a result of high supplied energy to evaporate particles by the laser. This makes surface diffusion easier, the grown films were found to be very smooth having root mean square (RMS) roughness of about 2nm or less.

Direct measurement of film hardness by conventional microhardness testing is not possible for a large range of indentation loads because the substrate also participates in the plastic deformation occurring during the indentation process. It is often assumed that this phenomenon, which involves the two materials, begins to be noticeable for loads such that the depth of the indent exceeds one tenth of the film thickness (Cai, X. and Bangert, H. 1995). In this situation the hardness number H_c is thus the result of combined substrate and film contribution. In order to determine the true hardness of the film, it is necessary to separate these combinations using numerous mathematical models. These models were proposed for that purpose on the basis of different assumptions. G. Guillemot et al.(2010) compared Jönsson and Hogmark model (Jönsson, B. and Hogmark, S. 1984), Burnett and Rickerby model (Burnett, P.J. and Rickerby, D.S. 1987), Chicot and Lesage model (Chicot, D. and Lesage, J. 1995), Korsunsky, A.M. et al.

(1998) and Puchi-Cabrera model (Puchi-Cabrera, E.S. 2002). Models with the objective to fit the entire range of the experimental data were proposed. The authors concluded that both Korsunsky and Puchi-Cabrera models allow well predicted hardness of the film since they give an adequate fitting of the observed composite hardness data. On the other hand, the Jönsson–Hogmark and Chicot–Lesage models are both obviously not able to fit the composite hardness data and consequently are not usable to predict the film hardness. However they showed that that both the Jönsson and Hogmark and Chicot and Lesage models can be made suitable to find the film hardness by incorporating the indentation size effect (ISE) by taking into account a linear relation between hardness and the reciprocal indentation depth.

Nanoindentation technique is now widely used in evaluating the mechanical properties of small volumes such as thin-film. Jeong-Hoon, A. (2000) reported the hardness (H) and elastic modulus (E) of Al_2O_3 film, glass, and stainless steel. These were evaluated by analyzing the load–depth curve measured by nanoindentation technique.

William, G.V.K. et al. (2006) studied the corrosion properties of TiAlN/CrN multilayer coatings. Potentiodynamic polarization and electrochemical impedance spectroscopy (EIS) were used to study the corrosion behavior of the coatings. Scanning electron microscopy and energy dispersive X-ray analysis were used to characterize the corroded samples. The potentiodynamic polarization tests showed lower corrosion current density and higher polarization for the coatings compared to substrate. The porosity values were calculated from the potentiodynamic polarization data. The Nyquist and the Bode plots obtained from the EIS data were fitted by appropriate equivalent circuits. The pore resistance, the charge transfer resistance, the coating capacitance and the double layer capacitance of the coatings were obtained from the equivalent circuit. Corrosion pits were observed after corrosion testing while examining the corroded samples under scanning electron microscopy. Liu, C.et al. (2003) reported on corrosion behavior of PVD coated steels in 0.5 N NaCl aqueous solutions by EIS and established equivalent circuits for EIS model and also reported on EIS interpretation of corrosion behavior.

1.6 Scope and objective of the present work

Thin film coatings on the surface of a material will modify the surface related properties of the material without modifying its bulk properties. As the literature survey indicates, there had been some work done by earlier investigators on pulsed laser deposition of Al_2O_3 and SiC on different substrates like silicon, sapphire, glass etc. These films were deposited at room temperature and slightly above that show amorphous nature and have poor adhesion to the substrate. In the present work, films were deposited from room temperature to 450^0C, so that the minimum temperature needed to get adhesive coatings could be determined. Further, improvement in microhardness and corrosion resistance of the substrates after coating was studied. Titanium and its alloy Ti6Al4V and inconel were chosen as substrate materials to improve the hardness and corrosion resistance by the application of thin ceramic film coating on their surface. Al_2O_3 and SiC coating were applied separately on surface of substrate material. Coating was carried out using PLD technique. After deposition effect of processing parameters like target-substrate distance, temperature of substrate, target density, laser energy on the coated ceramic films were studied. Coated substrates were characterized using XRD, SEM, UV-Visible spectroscopy and optical microscope. Hardness, adhesion, surface roughness, corrosion resistance of the ceramic film coated titanium and its alloy Ti6Al4V and inconel were studied in detail.

Objective of the present investigation is

- To obtain adhesive coatings of Al_2O_3 and SiC on different substrates viz., titanium, Ti6Al4V and inconel by pulsed laser deposition technique at low temperature.
- To obtain adhesive coatings of Al_2O_3 and SiC, the laser processing parameters like temperature, target substrate distance, laser energy, and target density are standardized.
- Characterization of substrate, target materials using XRD, SEM, chemical analysis.
- Characterization of coated films using XRD, SEM and optical studies.
- To carryout microhardness and nanoindentation studies of the substrates and after coating. Separation of film hardness from the composite hardness using a model

based on area-law of mixtures and compared with the film hardness measured using nanoindentation technique.

- Conducting corrosion studies of substrates before and after coating.

1.7 Overview of the thesis

The thesis work present here is divided into six chapters. Chapter 1 describes the need for taking up the present work by supporting it with literature survey. This chapter also presents the objective of the work that has been carried out.

Chapter 2 gives the detailed experimental description of the PLD technique used to develop SiC and Al_2O_3 thin film coatings on substrates. It also concludes description of different characterization techniques like XRD, SEM and absorption spectroscopy. Hardness measurements using microhardness tester and nanoindentation technique and corrosion studies by Direct Current Polarization (DCP) and Electrochemical Impedance Spectroscopy (EIS) is described.

Chapter 3 begins with a characterization of substrate and coating materials using XRD, EDAX, and chemical analysis. It is followed by standardization of PLD processing parameters like target-substrate distance, substrate temperature, target density, laser energy to obtain uniform adhesive ceramic coatings. Characterization of the PLD coated substrates are also explained using XRD, EDAX and by optical method using uv –visible spectrometer.

Chapter 4 starts with a microhardness studies on coated substrates using Knoop indenter. Separation of film hardness from composite hardness by using a mathematical model is discussed. Film hardness obtained using this model is compared using nanoindentation method.

Chapter 5 includes corrosion studies on substrates before and after ceramic coating using direct current polarization and electrochemical impedance spectroscopy.

Chapter 6 summarizes the results obtained and conclusions drawn from the present investigations.

Figures of different chapters are collected and shown in appendix I. Tables are given in appendix II. The references for the research work carried out are followed by appendix

II. Brief bio-data containing contact address, qualification and list of publications are enclosed at the end of the thesis.

CHAPTER -2

EXPERIMENTAL DETAILS

2.1 Pulsed laser deposition of thin films

2.1.1 Lasers

Conventionally two basic types of lasers are used in PLD, excimer and Nd: YAG. An excimer laser typically uses a combination of an inert gas (argon, krypton, or xenon) and a reactive gas (fluorine or chlorine). An excimer gain medium is pumped with short (nanosecond) current pulses in a high-voltage electric discharge (or sometimes with an electron beam), which create so-called *excimers* (excited dimers) – molecules which represent a bound state of their constituents only in the excited electronic state, but not in the electronic ground state. After stimulated or spontaneous emission, the excimer rapidly dissociates, so that reabsorption of the generated radiation is avoided. This makes it possible to achieve a fairly high gain even for a moderate concentration of excimers. Different types of excimer lasers typically emit wavelengths between 157 and 351nm, which includes ArF (argon fluoride), KrF (krypton fluoride), XeBr (xenon bromide), XeCl (xenon chloride), XeF (xenon fluoride).

The Nd: YAG laser is the most commonly used type of commercial solid state laser. Neodymium-doped yttrium aluminum garnet $Y_{3-x}Nd_xAl_5O_{12}$ (Nd: YAG) possesses a combination of properties uniquely favorable for laser operation. The cubic structure of YAG favors a narrow fluorescence line width, which results in a high gain and a low threshold for laser operation. The YAG host is hard, of good optical quality and has a high thermal conductivity. Pulsed Nd: YAG lasers are typically operated in the so called Q-switching mode: An optical switch is inserted in the laser cavity waiting for a maximum population inversion in the neodymium ions before it opens. Then the light wave can run through the cavity, depopulating the excited laser medium at maximum population inversion. In this Q-switched mode output powers of 20 megawatts and pulse

durations of less than 10 nanoseconds are achieved. Nd: YAG lasers typically emit light with a wavelength of 1064 nm, in the infrared. The high-intensity pulses may be efficiently frequency doubled to generate laser light at 532 nm, or higher harmonics at 355 and 266 nm.

2.1.2 Laser ablation – principle & origin

The PLD can be typically divided into four stages: 1) Laser radiation interaction with the target, 2) The formation of plasma plume and transportation towards the substrate, 3) Interaction of the ablated species with the substrate, 4) Nucleation and growth of thin film on the substrate (Bauerle, D. 2000 and Metevand, S. and Meteva, K.1989).

Laser radiation interaction with the target

The first process step of the PLD technique is the interaction of the high-intensity laser pulse with the target. This mechanism depends strongly on the properties of the laser, like fluence, frequency, pulse duration and wavelength. Laser radiation from IR to UV interacts primarily with the outer electrons of atoms and sometimes, though less commonly, with a particular set of atomic or molecular vibrations or phonons. These wavelengths do not induce nuclear disturbances nor do they affect the energy levels of the inner core electrons of atoms. The optical properties of any material will therefore be mainly affected by the nature of its outermost electrons and thus can be predicted by knowing their electronic configurations. In the case of PLD, electronic sputtering is the main mechanism of laser-target-interaction.

Electronic sputtering consists of various processes, all of which involve some kind of excitation or ionization. As the photons hit the target, they produce electron-hole-pairs and electronic excitations. As a consequence of the electron-lattice interactions, the temperature of the lattice increases strongly. This is followed by desorption of particles. Lattice defects and loose interatomic bonding facilitate the desorption.

Formation of plasma plume and its transportation

The ejection of particles from a surface induced by irradiation with a high intensity laser beam leads to the formation of a cloud of ablated material called plume,

which moves rapidly away from the surface. Usually, such a laser ablation cloud (plume), consists of excited or ground-state electrons, and ions. An example of a plume is a strongly light-emitting cloud growing in all directions, but preferentially along the target normal. The physical parameters in the plume, e.g. the mass distribution, ion and atom velocity, and the angular distribution of the plume species, play an important role for applications of laser ablation in mass analysis of laser induced plasma and in the production of thin films by PLD (Chrisey, D.B and Hubler, G.H, 1994).

Interaction of plume with the substrate

The thickness distribution in film deposition on a substrate is determined by the plume shape that has evolved during the expansion from the target surface to the substrate. The behavior of the plasma depends on whether the process is carried out in vacuum or presence of background gas. The profile of the plume is described by $\cos^n\varphi$ curve, where $4 < n < 15$, and n depends particularly on gas pressure. The presence of the background gas has an influence on scattering and kinetic energy of the particles in the plasma, as well as on the rate of deposition (Boyd, W. 1996). As a result of fluorescence and recombination processes occurring in the plasma, the plume emits visible light. This phenomenon offers a mean to monitor the deposition process. Laser ion mass spectroscopy and optical emission spectroscopy are examples for techniques used for plume monitoring. The ablated species have high kinetic energy of typically greater than 30eV and high initial velocities of greater than 10^4 m/s (Chrisey, D. B. and Hubler, G. K. 1994). They may impinge onto the surface of the substrate and may induce various types of damage to the substrate. However, the reduced kinetic and internal excitation energies of the ablated species can also be used to assist film formation and to promote chemical reactions.

Nucleation and growth of thin films

Nucleation and growth of thin films depend on many factors such as density of the target of laser, energy of laser, degree of ionization, types of condensed particles on the substrate. In general, when considering the theoretical models of film nucleation and growth in PLD, there are three conventional modes: three-dimensional growth of islands,

two-dimensional growth of monolayers and the formation of full monolayers followed by the growth of separate three-dimensional islands. The thermodynamics related to the surface energies of the film and the substrate determines which mode dominates the growth of the film. The three-dimensional growth of islands (also called Volmer-Weber nucleation and growth) involves a number of atomic scale processes taking place after the particles arrive on the substrate. The total free energy of each atomic cluster determines the balance between the growth and dissolution processes. By decreasing the temperature or increasing the deposition rate the free energy of the cluster nucleation and growth can be made more negative, i.e. the nucleation rate of the clusters can be increased. The lowering of the temperature may, however, decelerate the formation of the equilibrium structure of the deposit, which increases the possibility of metastable or amorphous phases (Chrisey, D.B. and Hubler, G.K. 1994). Depending on the size and shape of the nuclei and the interface energies of the cluster, substrate and vapor, it can be energetically made favorable for the film to grow as complete monolayers instead of three-dimensional islands. This growth mode (also called Frank-van der Merwe nucleation and growth) is more possible in the conditions, where the film surface energy is low and the substrate surface energy is high. However, the atomic processes during the Frank-van der Merwe nucleation and growth are essentially the same as in Volmer-Weber-mode, but the thickness of the islands corresponds only one monolayer. Similarly, the nucleation rate can be controlled by changing the temperature or the deposition rate, as described earlier.

The third possible mode is called Stranski-Krastinov nucleation and growth. The film formation begins with complete monolayers, but after 1-5 monolayers the growth continues by island formation. The reason for this kind of behavior is probably the lattice stress, which is higher on the surface of the deposited monolayers than on the bare substrate. In the nucleation and growth modes, it is assumed that the nucleation occurs on random sites, homogeneously on the whole substrate surface. In practice, the surface of the substrate is not uniform enough to ensure the homogeneous nucleation: there may be defects and dislocation intersections providing more favorable nucleation sites. Thus, for

example, the preparation of the substrate can have a remarkable effect on the nuclei density and nucleation rate.

2.1.3 Effect of processing parameters

The parameters that are important for the growth of the film, which have to be optimized, are the laser wavelength, pulse duration and fluence, target-substrate distance, the ambient gas and its pressure, the substrate temperature and target density.

For a choosen material and a fixed laser wavelength, the laser fluence on the target has the most significant effect on the particulate size and density. The laser fluence can be varied by varying the laser power or the laser spot size. At constant laser power, the particulate number density is higher with tighter focus. In general, there exists threshold laser fluence, below which the particulates are barely observable. Above the threshold laser fluence, the particulate number density increases rapidly with increasing fluence. However, the rate of increase reduces at a higher fluence, indicating saturation. The saturation of the particulate deposition and film deposition is largely due to the saturation in the ablation process.

The laser wavelength (λ) comes into play mainly in effectiveness of the absorption of the laser power by the target. For most metals, the absorption coefficient (α) decreases with decreasing λ. Hence the laser penetration depth in metals is larger in the UV range than in the infrared range. For other materials, the variation of absorption coefficient with wavelength is more complex since various absorption mechanisms, such as lattice vibration, free carrier absorption, impurity centers or band gap transition, can take place. The absorbance decreases with increasing wavelength, green light at 533 nm is almost 10 times less absorbed than at its 266nm counterpart. A deeper penetration depth (that is larger α^{-1}) achieved by Nd: YAG laser in IR 1064 nm wavelength than the excimer laser in UV is perhaps the most significant factor that determines the particulate size density. (Colin, E. W. and Julian, D. C. J. 2004).

During the film deposition in vacuum, the effect of target-to-substrate distance is mainly reflected in the angular spread of the ejected flux. Increasing the target-substrate-distance is useful in coating large area substrates, since the plasma plume becomes wider

as it gets further away from the target. The films grown at the longest possible ablation distance results in very uniform films with the drawback of low growth rate and low yield (Hirschauer, B et al. 1996)

The substrate temperature should be at least higher than 0.3 T_m, where T_m is the melting temperature in K, to obtain good crystallinity, although epitaxial films have been grown at lower temperatures than those used by other techniques. However, a lower deposition temperature will prevent or at least limit harmful film and/or ambient gas-substrate interaction, (Park, J. et al 1998 and McKee, R.A. et al. 1991), unwanted substrate interdiffusion process, and re-evaporation of volatile component. (Prusseit, W. 1992).

The incoming laser will dig a deep hole if it falls on a stationary target. When the target is rotated, the laser beam will dig a much shallower trench. There are several scanning techniques to ensure uniform erosion of the target, which are economically justified. Moreover, changing randomly the direction of the incoming laser beam avoids the formation and development of micro-relief that will unpredictably change the removal rate. The denser the target, the better the crystallinity and morphology of the grown film.

2.2 Deposition of film on the substrate

2.2.1 Substrate preparation

Substrate materials Titanium, Ti6Al4V and Inconel of size 0.22x0.22 m^2 were used for ceramic coating. The surface of the substrate was sequentially polished using polishing grinder (Chennai Metco) at a rotation speed of 500rpm with SiC waterproof abrasive paper from 320 grit to 2000 grit size and smooth polishing was done on velvet cloth using Al_2O_3 suspension of 1, 0.5, 0.3-micron size, to an average roughness (R_a) of 30-50 nm. After polishing, the substrate surfaces were cleaned in acetone in ultrasonic bath for 20 minutes.

2.2.2 Target density measurement

Al_2O_3 and SiC pellets of purity 99%, having different densities were used as targets for ablation. Its density was measured by water absorption test method (Singer, F.

and Singer, S.S. 1963). Initially dry weight of the pellet was determined (D). Then the pellets were immersed in water and boiled for one hour and then cooled, retained at room temperature for 24 hours. The surface of the cooled pellet was slightly wiped off using wet cloth and its saturated weight is determined(S). The cooled pellet was suspended in water and its immersed weight was determined (I). Using the following formulae true density and porosity of the pellets were determined.

$$\text{Apparent Porosity} = (AP) = \frac{S-D}{S-I} \tag{2.1}$$

$$\text{Bulk density} = (BD) = \frac{D}{S-I} \tag{2.2}$$

$$\text{True or Apparent density} = (TD) = \frac{BD}{1-AP} \tag{2.3}$$

2.2.3 Pulsed Laser Deposition System

The essential parts of a pulsed laser deposition (PLD) system are the vacuum chamber, vacuum pumps, laser, laser optics, target holder and substrate heater.

In the present study, the depositions were carried out in a laser ablation vacuum coating unit (HIND HIVAC) consisting of a vacuum chamber and a diffusion pump backed by an oil sealed rotary pump. The schematic diagram and photograph of the PLD unit are given in figure 2.1 and figure 2.2 respectively. The pressure of the chamber was monitored by Pennig and Pirani vacuum gauges. The laser used for the deposition process is a Q-switched Nd: YAG laser (Laser spectra) which can produce a laser beam of 1064, 532, 355 nm wavelengths and up to 800 mJ pulse energies. For the present work wavelength of 1064nm was used. This laser has pulse duration of 10 ns and is capable of a maximum repetition rate of 10 Hz and laser beam has a diameter of 0.01 m.

The laser beam was focused using a convex lens of focal length 0.5 m to a point size with diameter of approximately 0.001 m on the target. So the fluence is approximately 170 KJ/m^2, when laser energy of 135 mJ pulse was made to fall on the

target. The target substrate distance was varied to obtain the uniform film thickness. The rotation speed of the target was maintained at 40 rpm. The laser beam was directed on to the target at an incidence angle of 45^{o}. The pressure in the chamber was maintained at 10^{-5} mbar. Silver paint was used to bond the target to the target holder. Since the evaporants are ejected as a highly forward – directed plume of material along the target normal, the substrate must be held directly opposite to the target. The substrate was kept on the substrate holder with heating arrangement using simple clamping mechanism. The temperature was recorded using a thermocouple. Nicrome wires were used to heat the substrate. Figure 2.3 shows the photograph of plume formed due to laser interaction getting deposited on substrate inside the laser ablation chamber. The following parameters were varied during deposition.

1) Target–to-substrate distance (0.03, 0.05, 0.08, 0.1 m)

2) Substrate temperature (Room temperature, 100, 200, 300 & 450^{0}C)

3) Laser energy (85, 135 mJ)

4) Apparent target density (Al_2O_3: 3690 Kg/m^3, 3490 Kg/m^3, 315O Kg/m^3.)

(SiC: 2840 Kg/m^3, 2430 Kg/m^3)

2.2.4 Heat treatment

Heat treatment is used under two different conditions to improve film adhesion to the substrate.

Substrate heating: During deposition of the coating material on the substrate, it is maintained at certain temperature in the ablation chamber. Temperature effect on adhesion is studied by maintaining the substrate at different temperatures namely RT, 100, 200, 300, 450^{0}C

Heat treatment after deposition: Al_2O_3 coated substrates were heat treated in air at 450^{0}C after deposition. SiC coated substrates were heat treated at 850^{0}C in vacuum. These heat treated coatings were used for XRD studies.

2.3 Roughness measurement

Profilometer is a measuring instrument used to measure a surface's profile, in order to quantify its roughness. A diamond stylus is moved vertically in contact with a

sample and then moved laterally across the sample for a specified distance and specified contact force. A profilometer can measure small surface variations in vertical stylus displacement as a function of position. A typical profilometer can measure small vertical features ranging in height from 10 nanometres to 1 millimetre. The height and position of the diamond stylus generates an analog signal which is converted into a digital signal stored, analyzed and displayed. The radius of diamond stylus ranges from 20 nanometres to 25 μm, and the horizontal resolution is controlled by the scan speed and data signal sampling rate. The stylus tracking force can range from less than 1 to 50 milligrams.

Surface roughness can affect a component's chemical and physical stability. Surfaces that have to stand up to hostile environments (temperature, humidity, or hostile chemicals) must be as smooth as possible in order to present the minimum surface area for attack, and to have as few defects or weak spots as possible. Mechanical malfunction can be found in high performance engine machine parts which are required to move or rotate at high speed without wear. Excess surface roughness can lead to unacceptably high levels of frictional heating, causing damage and even failure (http://www.schmitt-ind.com/support-technical-papers-scatter.shtml/ 10/12/2010).

When stylus of the profilometer moved across coated–uncoated junction region, it will indicate surface variation across this region. Coating thickness can be measured by surface variation at coated–uncoated junction region. Taylor Hubson stylus profilometer is used to measure the thickness of the coated film.

Average surface roughness of substrates and films coated under different conditions were measured using 3-D optical surface profilometer. Vecco 3D optical surface profilometer was used to measure the surface roughness based on the principle of interference of light between the ray reflected from the surface of interest and the ray from an optically flat reference surface. Deviation in the fringe pattern and dark and bright lines produced by the interference are related to differences in the surface height. 3D image is obtained by using an imaging array.

2.4 Hardness measurement

2.4.1 Microhardness test

Indentation microhardness is a reliable test method for the evaluation of mechanical characterization of the coatings. In microhardness testing a diamond indenter with specific geometry is indented onto the surface of test specimen using a known applied load from 10^{-3} to 1 Kg. Usually to measure microhardness of hard thin films, standard indenters like Knoop, Vicker, Berkovich etc., are used. The Knoop indenter is a better choice for hard brittle material where the indentation cracking would be relatively minimized when compared to Vicker's indenter at the same load. It is reported that by Ferro, D. et al. (2006), that measurement error of Knoop indenter diagonal is less compared to Vickers diagonal. The Knoop indentation is shallower (depth approximately 1/30 the long diagonal) than the Vickers indentation (depth is approximately 1/7 the average diagonal) when the same load is applied on the material. Hence, the Knoop test is better suited for testing thin coatings. Hardness of thin films has combined effect due to the influence of the substrate and the film that leads to the so-called "composite hardness". The composite hardness includes the component of the substrate hardness depending on the relative depth of penetration and mechanical properties of the both film and the substrate. Film hardness is separated from the composite hardness based on a mathematical model.

Microhardness is determined by using CLEMEX Microhardness tester. Knoop and Vickers indenters were used for the test. Loads of 0.025, 0.050, 0.1, 0.2, 0.3 and 0.5 Kg were applied and were maintained for 10 sec on each coating surface. Averages of 10-15 indentations at each load were used to measure hardness.

2.4.2 Nanoindentation

Intrinsic hardness of coated material is found using Hysitron Tribo indenter. This instrument can measure the hardness and elastic constants of thin films and coatings. Berkovitch type diamond indenter is used to measure the nanoindentation. A load of 1000-1500μN was applied to the surface and the penetration depth of the tip was

continuously recorded. From the loading and unloading curves nano mechanical properties were evaluated.

2.5 Scratch test

It is qualitatively performed using TQCCC2000 Adhesion test kit, in which two cuts/scratches were made perpendicular to each other (lattice type pattern) on the coated substrate. Then pattern was brushed several times back and forth along each of the diagonal lines of the lattice pattern. An adhesive tape was applied parallel to scratched lattice pattern and pulled off steadily at 60^0 angle. Careful examination of the magnified scratch areas using optical microscope (400x) reveals the adhesion of the film to the substrate.

2.6 Spectrophotometer

Ultraviolet-visible (UV-vis) spectroscopy is used to obtain the absorbance spectra of a compound in solution or as a solid. UV-vis spectroscopic data can give qualitative and quantitative information of a given compound or molecule**.** Spectroscopically we observe the absorbance of light energy or electromagnetic radiation, which excites electrons from the ground state to the first singlet excited state of the compound or material. The UV-vis region of energy for the electromagnetic spectrum covers 1.5 - 6.2 eV which relates to a wavelength range of 800 - 200 nm. The Beer-Lambert Law,

$$A=\varepsilon cl \qquad (2.4)$$

where A is absorbance (unitless, usually seen as arb. units or arbitrary units), ε is the molar absorptivity of the compound or molecule in solution ($M^{-1}cm^{-1}$), l is the path length of the cuvette or sample holder (usually 1 cm), and c is the concentration of the solution (M).

UV –Visible Fiber Optic spectrophotometer (SD-200, Ocean optics Inc) is used to record the optical spectrum of coated films on optically flat glass substrates.

2.7. Scanning Electron Microscopy (SEM)

Scanning electron microscopy (SEM) is a method for high-resolution imaging of surfaces. The advantages of SEM over light microscopy include much higher magnification (>100,000X) and greater depth of field up to 100 times that of light microscopy. The electrons interact with the atoms that make up the sample producing signals that contain information about the sample's surface topography, composition, and other properties such as electrical conductivity. The types of signals produced by an SEM include secondary electrons, back-scattered electrons (BSE), characteristic X-rays, light (cathodoluminescence), specimen current and transmitted electron

The SEM generates a beam of incident electrons in an electron column above the sample chamber. The electrons are produced by a thermal emission source, such as a heated tungsten filament, or by a field emission cathode. The energy of the incident electrons can be as low as 100 eV or as high as 30 KeV depending on the evaluation objectives. The electrons are focused into a small beam by a series of electromagnetic lenses in the SEM column. Scanning coils near the end of the column direct and position the focused beam onto the sample surface. The electron beam is scanned in a raster pattern over the surface for imaging. The beam can also be focused at a single point or scanned along a line for X-ray analysis. The beam can be focused to a final probe diameter as small as about 10 Å.

The incident electrons cause electrons to be emitted from the sample due to elastic and inelastic scattering events within the sample’s surface and near-surface material. High-energy electrons that are ejected by an elastic collision of an incident electron, typically with a sample atoms nucleus, are referred to as backscattered electrons. The energy of backscattered electrons will be comparable to that of the incident electrons. Emitted lower-energy electrons resulting from inelastic scattering are called secondary electrons. Secondary electrons can be formed by collisions with the nucleus where substantial energy loss occurs or by the ejection of loosely bound electrons from the sample atoms. The energy of secondary electrons is typically 50 eV or less. To create an SEM image, the incident electron beam is scanned in a raster pattern across the sample's

surface. The emitted electrons are detected for each position in the scanned area by an electron detector. The intensity of the emitted electron signal is displayed as brightness on a cathode ray tube (CRT). By synchronizing the CRT scan to that of the scan of the incident electron beam, the CRT display represents the morphology of the sample surface area scanned by the beam.

In our studies surface topography of the coated ceramic films were studied using a scanning electron microscope (JEOL JSM 5800) and energy- dispersive X-ray spectroscopy (EDAX) was carried out for the compositional analysis.

2.8 X- ray diffraction (XRD)

X-ray scattering techniques are a family of non-destructive analytical techniques, which reveal information about the crystallographic structure, chemical composition, and physical properties of materials and thin films. X-rays are electromagnetic radiation with a wavelength of approximately 1 Å, which is about the same size as an atom. XRD uses X-rays diffracted by a sample to get the crystalline information. When the incident X-ray beam is diffracted by a sample, enhanced diffraction occurs only when the following Bragg's condition is achieved:

$$2d \sin\theta = n\lambda \qquad (2.5)$$

where d is the spacing between two crystal lattice planes of the sample, λ is the X-ray wavelength, θ is the angle between the incident/diffracted beam and the sample crystalline planes, and n is a natural number, as shown in Figure 2.4. Therefore, by scanning the specimen over a range of angle θ, the count of the diffracted X-ray is related with crystalline information such as the d space between the crystal planes. The detecting area of XRD is normally in the range of square millimeters.

Characterization of the substrate and coating material was done using X-ray diffractometry (JEOL) using CuK_{α} radiation (1.54 Å) with nickel filter.

2.9 Corrosion studies

The general techniques used for corrosion performance evaluation of the coatings are DC Polarization (DCP) and Electrochemical Impedance Spectroscopy (EIS). The corrosion behavior of the coated and uncoated substrates in the present work was studied using DCP and EIS. All studies were carried out by immersing samples in 3.5% NaCl solution in open air and at room temperature, using potentiostat/Galvanostat Gamry Instruments (PCI 4G750-47065) system.

2.9.1 Direct Current Polarization (DCP)

DC polarization test is a potential dynamic corrosion testing technique. When an electrode is polarized, it can cause current to flow via electrochemical reactions that occur at the electrode surface. The amount of current generated is controlled by the kinetics of the reactions and the diffusion of reactants both towards and away from the electrode. In a cell where an electrode undergoes uniform corrosion at open circuit, the open circuit potential is controlled by the equilibrium between two different electrochemical reactions. One of the reactions generates cathodic current and the other anodic current. The open circuit potential is also the potential at which the cathodic and anodic currents are equal (Figure 2.5). It is referred to as a mixed potential. The value of the current for either of the reactions is known as the corrosion current. Mixed potential control also occurs in cells where the electrode is not corroding.

All electrochemical measurements are performed using conventional three electrode cell, using a platinum plate as an auxiliary electrode, saturated calomel electrode (SCE) as a reference electrode. The exposed area to the corrosive medium is 1 cm^2. The sample is cleaned in distilled water before loading to the sample holder. The sample is placed in such a way that Luggin capillary of the reference electrode is close to the working electrode and this arrangement is used for all tests. The current density is measured and usually plotted on a logarithmic scale. The corrosion potential (E_{corr}) and the corrosion current (I_{corr}) are obtained from the Tafel plots. The corrosion potential (E_{corr}) or the open-circuit potential is the potential a metal will assume when placed in

contact with a conductive medium. The value of the corrosion potential is determined by half-reactions of the corrosion process. E_{corr} is characteristic of the corroding system and is unrelated with the electrochemical instrumentation. The Tafel plot provides a direct measure of corrosion current, which can be used to calculate the corrosion rate. **(**Nestor, P. 2004). The corrosion resistance R_p is given by

$$R_p = \frac{B}{I_{corr}} = \left[\frac{\Delta E}{\Delta I}\right]_{\Delta E \to 0} \tag{2.6}$$

Where, I is the total current at a potential E, E_{corr} is the open circuit potential.

$$B = \beta_a \beta_c / 2.303(\beta_a + \beta_c) \tag{2.7}$$

β_a & β_c are the Tafel proportionality constants for the anodic and the cathodic reactions respectively. The corrosion rate (*CR*) is calculated from the Faraday's law (Dean, S.W. 1977) using the following equation

$$CR(\mu m/y) = (3.27 * I_{corr} * EW)/d \tag{2.8}$$

where *EW* is the equivalent weight of the testing material and *d* is the density of testing sample in Kg/m^3. By substituting the value of I_{corr}, *CR* is calculated. Variations of the Tafel plot may occur depending on the nature of the protection mechanism of the coating.

2.9.2 Electrochemical Impedance Spectroscopy (EIS)

EIS is considered as one of the most important technique for investigation of the electrochemical behavior of passive films. Impedance measurements were conducted using a frequency response analyzer (FRA). The spectrum was recorded in the frequency range 10mHz – 300KHz. The applied alternating potential had root-mean-square amplitude of 10mV. After each experiment the impedance data was displayed as Nyquist and Bode plots. The Nyquist plot is a plot of imaginary impedance (Z″) versus real (Z).

From the Nyquist diagram it is possible to obtain the value of the both resistance i.e., the electrolyte resistance (R_s), at high frequencies and charge transfer resistance (R_{ct}), at low frequencies. The Bode plot is a plot of log Z versus log f (magnitude plot), and phase angle (θ) versus log f (phase plot), where log Z is the absolute impedance and f is the frequency. The advantage of the Bode plot is that the data for all the measured frequencies are displayed along with the impedance values. Furthermore, the frequency dependence of the phase angle indicates whether one or more time constants occur, which could be used to determine equivalent circuit (EC) parameters. A circuit description code (CDC) is assigned for the acquired data and the acquired data are curve fitted and analyzed using ZSimpWin software.

CHAPTER -3

CHARACTERIZATION OF SUBSTRATE, TARGET AND COATED FILMS

3.1 Characterization of substrate and target materials

Three different materials namely CP titanium, Ti6Al4V and inconel were choosen as substrate materials and SiC and Al_2O_3 as target materials. Characterization of substrate and target materials has been done using XRD, EDAX and by chemical analysis. X-ray diffraction data of target, substrate and coated films was collected and compared with the standard data (JCPDS data) to determine the phases present in it. Compositions of the materials were determined using EDAX and chemical analysis.

3.1.1 Substrate materials

Basic characterization of substrate material is done by X-ray diffraction, optical microscopy, EDAX and chemical analysis.

3.1.1.1 Titanium (commercial purity 99.2%)

Commercially pure titanium sheets of 0.10 m x 0.1 m x 0.002 m were procured from Alfa Aesar.

i) X-ray Diffraction

In X-ray pattern no extra peaks were found other than Titanium. All the peaks correspond to α-Ti phase. Figure 3.1 shows the XRD pattern of Titanium.

ii) Microstructure

The microstructure of the commercial purity titanium after etching with Kroll's reagent at 400x magnification is shown in figure 3.2. It shows bright and dark regions.

The dark regions in the above micrograph are due to twinned alpha grains of cp titanium. (http://www.feppd.org/ICB-Dent/campus/materials for prosthetic dentistry/ Alloying effect.htm, June 2, 2011).

iii) Chemical composition

Chemical composition of the titanium as determined by chemical analysis and EDAX is listed in table 3.1. Figure 3.3 shows the EDAX of titanium substrate.

3.1.1.2 Ti6Al4V

Ti6Al4V substrates used for coating were cut from slabs of dimensions 0.05m x 0.05m x 0.0025m. These substrates were provided by Vikram Sarabhai Space Centre, Trivandrum. The results of characterization of Ti6Al4V substrates are given below.

i) X-ray diffraction

Figure 3.4 shows the X-ray diffraction pattern of Ti6Al4V. XRD pattern shows the existence of α & β -Ti phases, which is the characteristic of two phase (α + β) Ti6Al4V alloy.

ii) Microstructure

Optical microscopy also confirms the existence of α & β phases. Fine polished surface of the Ti6Al4V is etched with Kroll etchant (10% HF, 5% HNO_3, and 85% H_2O) and optical micrographs were taken at 400X magnification as shown in figure 3.5. α and β phases were clearly observed**.**

iii) Chemical composition

Chemical composition of the Ti6Al4V is listed in table 3.2. Figure 3.6 shows the EDAX of Ti6Al4V substrate. The discrepancy in composition among the two methods can be due to the two phase structure of the titanium alloy.

3.1.1.3 Inconel

Inconel 601 substrates used for coating were cut from slabs of dimensions 0.05m x 0.05m x 0.0010m. These substrates provided by Vikram Sarabhai Space Centre, Trivandrum, were characterized using the following method.

i) X-ray Diffraction

By comparing the obtained XRD data with JCPDS files (33-0945) it has been found that diffraction angles were matching with inconel 601. Figure 3.7 shows the X-ray diffraction pattern of Inconel.

ii) Microstructure

Fine polished inconel was etched with etchant (97 ml HCl, 2 ml H_2SO_4, and 1 ml HNO_3). Microstructure observed at 400x magnification was shown in figure 3.8. Different microstructures were observed at different regions on the surface.

iii) Chemical composition

Chemical composition of the inconel as obtained by two different methods is listed in table 3.3. Figure 3.9 shows the EDAX of inconel substrate. The discrepancy in composition between chemical analysis and EDAX could due to different microstructures in different regions on the surface which is characteristic of inconel 601.

3.1.2 Target materials

3.1.2.1 SiC

i) X-ray Diffraction

SiC in the form of pellet of diameter 0.04m was supplied by BHEL, Bangalore. The pellet was powdered to collect the XRD data using X-ray diffractometer. Figure 3.10 shows the XRD pattern of SiC. All peaks correspond to α-SiC.

ii) Density measurement

SiC pellets of two different densities were used as target to study the effect of density on ablation rate. The density of these pellets was measured using water absorption test method (Singer, F. and Singer, S.S. 1963). The apparent densities of these pellets were found to be 2840 Kg/m^3 and 2430 Kg/m^3.

3.1.2.2 Alumina

i) X-ray Diffraction

XRD pattern of Alumina is given in Figure 3.11. All the peaks correspond to α - Al_2O_3.

ii) Density measurement

The apparent densities of Al_2O_3 pellets using water absorption test method were found to be 3690 Kg/m^3, 3490 Kg/m^3 and 3150 Kg/m^3.

3.2 Standardization of processing parameters of PLD

Generally in PLD, laser beam interaction with target results in plume, which contains a mixture of atoms molecules electrons ions clusters and micron, sized solid particles. The plume rapidly expands in the vacuum with narrow forward angular distribution towards the substrate to form the deposit. Material deposition on the substrate depends on the laser processing parameters like laser fluence, frequency & spot size, ambient gas pressure in the vacuum chamber, target–substrate distance, target density and surface topography of the target material, substrate temperature during deposition, etc. The above mentioned predominant factors influence film uniformity which in turn affects surface topography, structure, orientation and properties of the deposited thin films. In our studies the following parameters were varied and standardized to obtain uniform adhesive ceramic coatings. The processing parameters were target-substrate distance, substrate temperature, target density and laser energy.

3.2.1 Target -substrate distance

The effect of variation of target-substrate distance on the deposited ceramic film was studied. Alumina was coated at different target substrate distances (d), viz., 0.03, 0.05, 0.08 and 0.10m using Al_2O_3 target of density 3150 Kg/m^3 while maintaining all other deposition parameters constant. The top view photograph of the coated sample at different target substrate distance is shown in figure 3.12. It was observed that the angular spread of the plume resulting from the interaction of the laser beam with target broadens with increasing distance as shown schematically in the figure 3.13**.** Non-uniform films with different thickness deposited at 0.03 and 0.05 m target substrate distance show larger thickness at the central region. Three distinct regions were observed at 0.03 m distance (sample A) and it merged into two at 0.05 m distance (sample B). Films deposited at 0.08, 0.10 m distances (sample C) were showing single uniform region. The resulting coatings were of different thickness and microstructures as shown in the

figure 3.14. Uniformity in the film can be improved by increasing the target substrate distance d, but the rate of deposition will decrease with increasing distance. Different surface morphology, non-uniform thickness, different average surface roughness, microhardness variation were found in the different regions of films deposited at 0.03 and 0.05 m.

The optical microstructure of particle distribution of the sample A in 3 distinct regions (I, II, III) of figure 3.13 are shown in figure 3.15. In the region I, distribution density of the particle is more and also bigger sized particles can be seen. The heavier particle having slow velocity tends to concentrate in the central region of the plume. Since the substrate is kept normal to the plume, region I receives the heavier and more number of particles in addition to lighter particles..

Particle distribution continues with this sequence in the region II & III. Table.3.4 shows the variation of hardness and average roughness with distance, which correlates the properties of the film with the characteristics of the plume interaction with substrate. The density and size of the deposited particle on the substrate reduces as the target-substrate distance increases. Uniform films were also obtained at 0.8 m target substrate distance. The coated films were observed to be uniform even at the target substrate distance of 0.10m. But the thickness of the film obtained at 0.10 m was less. So, the minimum target substrate distance to grow uniform film was optimized as 0.8 m.

Figure 3.16 a), b), c) shows the 3-D surface profilometer photographs of the Al_2O_3 coated on Ti6Al4V at d =0.03 m. It shows three different regions with 3 different average roughness R_a values. Similarly Figure 3.16 d), e) is at taken at d=0.05 shows two distinct regions with two different R_a values and Figure 3. 16 f) is the photograph of d=0.10m showing single uniform region.

3.2.2 Target density

Target density is another parameter that alters the rate of ablation and the film thickness. Sintered pellets were used as target materials. Targets of different density were chosen for our studies. It is well known that high density and highly homogeneous targets yield the best films. Al_2O_3 was deposited using three targets of different apparent density

3690, 3490, & 3150 Kg/m^3 and SiC targets of apparent density 2840 and 2430Kg/m^3 under identical conditions. Rate of ablation varies with density of the target as follows:

Al_2O_3

Density (Kg/m^3)	Ablation rate (nKg/sec)
3690	0.833
3490	1.190
3150	2.944
SiC	
2840	2.500
2430	4.416

It was observed that the rate of ablation is less for more dense targets and more for less dense targets. Deposition period should be increased to obtain the required film thickness using high-density targets. The optical microstructures of the alumina coated samples are shown in figure 3.17 a), b), c) and silicon carbide coated samples in figure 3.17. d), e). The particle size in the deposited material is almost same for different density targets. But the density of particles is less with increase in density of the target. The ablation of the high-density targets reduces the deposition rate to a large extent. Uniform films were found to be obtained at low density targets (alumina target of apparent density 3150 Kg/m^3 and silicon carbide 2430 Kg/m^3). In addition to that required film thickness will be obtained at shorter period. Still lower density targets could not be ablated by laser, since the laser beam penetrates deeper into the target by crater formation in a short period without much ablation of the material.

Density of the target should have certain optimum value to ablate it to form deposit on the substrate surface below which ablation is not possible due to the crater formation into the depth of the ablating pellet and above which the ablation rate is very small.

3.2.3 Temperature of the substrate

Good adhesion of the film to the substrate is an important factor that protects the substrate surface from the damage. Film adhesion to the substrate was studied for silicon carbide and alumina at room temperature and by varying temperature up to 450^0C. Optical micrograph of Al_2O_3 and SiC deposited on Ti6Al4V substrate at different temperatures is shown in figure 3.18 a), b), c), d), e), and f). Delamination of the film was observed in both SiC and Al_2O_3 films deposited at room temperature and at 100^0C as shown in figure 3.18 a), b), c) and d). The ripples formed as observed were caused by the large compressive stresses in the film (Chopra, K.L. 1969). Substrate heating during deposition reduces the stress produced during the deposition of the film and results in good adhesion with the substrate due to the enhanced diffusion of the particle on to the substrate surface. The substrate temperature effect during deposition on the adhesion was studied for Al_2O_3 and SiC film at 100^0C, 200^0C, 300^0C and 450^0C. Films grown at 100^0C also show film delamination in certain regions of the coating. Delamination was not observed in films grown above 200^0C. So to obtain adhesive films substrate temperature should be greater than 200^0C.

Generally films grown near room temperature were amorphous. Increasing the substrate temperature increases the crystallinity and orientation of the deposit. Similar effects can be obtained by annealing the specimens after the deposition. Substrate heating and /or annealing also induce growth of grain size, as well as phase transformation.

Alumina coated at room temperature on Ti6Al4V substrates was annealed in air after the deposition at 600^0C for one hour. It was observed that annealing after the deposition would make the films more brittle resulting in cracking of the films during indentation. But when the films grown at 450^0C on the substrate were again annealed in air, they were not brittle. This may be due to the formation of TiO_2 during heat treatment on the surface in the former case since the adhesion of the film was poor and absence of formation in the second case. To overcome delamination of film, substrate temperature was maintained at 450^0C during deposition.

3.2.4 Laser energy

Alumina target of apparent density 315 Kg/m^3 was ablated for 30 minutes using two different laser energies namely 85 mJ and 135 mJ. Figure 3.19 shows the particle distribution of the deposited alumina film using different laser energies. Particle size of the deposited film remains same in both the films deposited using different laser energies. Only the deposition rate is reduced with decrease in laser energy. So, for ablation, we have chosen 135 mJ laser energy.

After repeated trails and checking the reproducibility of the results, the following processing parameters were standardized.

1. Target substrate distance – 0.08m
2. Density of the target

   Al_2O_3 - 3150 Kg/m^3

   SiC - 2430 Kg/m^3
3. Temperature of the substrate – 450^0 C
4. Laser energy -135 mJ

These processing parameters were kept same for Al_2O_3 and SiC coatings on three substrates viz., titanium, Ti6Al4V, inconel. After coating these substrates were characterized and used for microhardness and corrosion studies.

3.3 Characterization and properties of the PLD coated substrates

3.3.1 XRD

Deposition of ablated alumina on the substrate was confirmed by XRD. XRD pattern was collected on alumina coated inconel after heat treatment. Figure 3.20 shows the XRD pattern of Al_2O_3 coated at 450^0C on inconel and heat treated at 450^0C for 4 hours. Al_2O_3 peak in the pattern confirms its existence in the coating. Since the thickness of the film is very less, intensity of the alumina X-ray peak is very less. Slow scanning between the 30 and 40 ^{0} confirmed the existence of alumina peak. It is clearly shown in the figure 3.21**.** It's found to be α-alumina phase.

Amorphous SiC films were obtained while depositing at 450^0 C. No XRD peaks were found indicating the amorphous nature of as coated film. To convert it into

crystalline film SiC substrate is annealed in vacuum at 850^0C for 1 hour. XRD peak corresponding to α-SiC was found after annealing (figure 3.22). These XRD patterns confirm the presence of target material in the coating.

The presence of coated materials was further confirmed by optical absorption studies.

3.3.2 Scanning electron microscopy (SEM) studies

Surface morphology of the SiC and Al_2O_3 thin film coatings on Ti6Al4V substrate was studied using SEM as shown in figures 3.23 and 3.24. In SiC film, as shown in figure 3.23 we see the existence of spherical particles (micro droplets) of submicron size which ranges from 838 nm to 62 nm. Microstructure of the coated film is found to be uniform throughout the surface. Existence of particles of different size is quite common in PLD films. Particle size does not depend much on the energy of the incident laser beam. Same sized particles were also observed when films were deposited using laser beam of lower energy (85mJ). But decrease in laser energy reduces the ablation rate.

Surface morphology of the Al_2O_3 deposited on the surface of the Ti6Al4V using alumina target of apparent density 3150 Kg/m^3 is shown in figure 3.24. The particle size of the deposited particle varies from 1000 nm to 39 nm. As reported in literature, similar results were obtained for coatings on other substrates also.

3.3.3 Energy-dispersive X-ray spectroscopy (EDAX) analysis

EDAX of SiC on Ti6Al4V and Alumina on Ti6Al4V was collected. This analysis confirmed the presence of relevant element in the deposited coatings. At two different energies EDAX was collected. At low energy Coating element peak was prominent. Due to the very low thickness of the coating, when intensity of the incident beam was increased substrate peak becomes prominent. 3.25 a) and b) was collected at 5 KV and 15 KV incident energy on SiC on Ti6Al4V and figure 3.25 c) and d) show EDAX of Al_2O_3 on Ti6Al4V substrates at low and high KeV incident energy.

3.3.4 Optical characterization of coatings

Optical characterization is another method used to confirm the presence of the target material in the coatings. The optical band gap energy and Urbach energy calculations for SiC and Al_2O_3 coated on glass substrates were carried out using optical absorption data. The Tauc's power law is used to obtain the optical band gap energy E_g. (Tauc, J. 1972)

$$\alpha h\nu = const(h\nu - E_g)^p \tag{3.1}$$

where E_g is the optical band gap energy and $h\nu$ is the photon energy of the incident radiation, the exponent p in the equation is 2 for indirect optical transition and p=1/2 for direct optical transition. The energy band gap E_g of SiC and Al_2O_3 films are calculated by extrapolating linear region of the curve obtained by plotting $(\alpha h\nu)^{1/2}$ as a function of $h\nu$ in the case of SiC (indirect band gap) and $(\alpha h\nu)^2$ versus $h\nu$ in the case of Al_2O_3 (direct band gap) as shown in figures 3.26 & 3.27. The E_g values are found to be 3.32 eV for Al_2O_3 and 2.07 eV for SiC film. These values are comparable with the reported values of 3.2 eV for Al_2O_3 (Rose, V. et al. 2003) and 2 - 2.9eV for SiC (Park, J. 1998). Generally amorphous films have low band gap energy compare to crystalline films. This is observed to be true in case of SiC films coated in the present work.

The coated films in the present work are amorphous in nature. This is confirmed by optical absorption data. At longer wavelength in the spectrum, there is an absorption tail described by Urbach exponential law (Urbach, F. 1953), which describes the amorphous nature of the film. The Urbach energy is related to the absorption coefficient as

$$\alpha(h\nu) = \alpha_o \exp\left(h\nu / E_u\right) \tag{3.2}$$

where α_o is constant. The Urbach energy E_u is the measure of disorder in the system. Figure 3.28 and 3.29 correspond to the plot of $ln\alpha$ as a function of $h\nu$. The value of Urbach energy is calculated by fitting the linear region of figure 3.28 and 3.29 by the

method of least squares to the straight line equation $(ln\alpha = h\nu / E_u + constant)$ and is found to be 1.49eV for Al_2O_3 and 1.39eV for SiC film. The Urbach energy E_u is the measure of structural disorder in the system. The value of Urbach energy obtained for SiC and Al_2O_3 confirms that the obtained films to be amorphous in nature. Absence of sharp XRD peaks also confirms that coated films are amorphous in nature.

3.3.5 Adhesion test

Scratch tests were carried out on SiC coatings deposited on Ti6Al4V at 100^0C, 200^0C, 300^0C and 450^0C. The scratch tracks were produced by applying the same force of 50N on the samples of coating thickness 0.5µm. Figure 3.30 a) shows SEM micrograph of scratch tested SiC coated Ti6Al4V deposited 200^0C and figure 3.30 b) is that of the film deposited at 450^0C. In figure 3.30a), deep cracks were observed compared to SEM image of SiC coated on Ti6Al4V substrate**,** due to the less adherence of film to the substrate surface. Figure 3.31 shows the optical micrograph of the scratch tested Alumina coated Ti6Al4V substrate at 300^0C and 450^0C. Coating thickness and forces applied to produce scratches on SiC coating were same.

In both the cases films deposited at 450^oC show better adhesion with the substrate in comparison with the lower temperature deposited film. Also no cracking of film is observed at the edges of the scratch tracks.

CHAPTER- 4

HARDNESS STUDIES

4.1 Separation of film hardness from composite hardness using microhardness data

Hardness of thin films has combined effect due to the influence of the substrate that leads to the so-called “composite hardness”. The composite hardness includes the component of the substrate hardness depending on the relative depth and mechanical properties of both film and the substrate. At lower loads, coating dominates more on the composite hardness but at higher loads substrate dominates more than the coating on the composite hardness. Relative contributions of the film and the substrate to the hardness have to be separated. In order to determine the true hardness of the film, it is necessary to separate these contributions. A model based on area law of mixtures can be used to find the true hardness of the film. These studies will give information about the selection of appropriate coating thickness and substrate hardness to give a required composite hardness. Numerous mathematical models were proposed on the basis of different assumptions. Most common model is based on the “area law of mixtures” approach. It was originally proposed by Jonsson and Hogmark (1984) for Vickers indentation and it was adapted to the geometrical configuration of the Knoop indenter (Iost, A. 1998 and Ferro, D. et al. 2006). Drawbacks of Jonsson and Hogmarkmodel can be overcome by incorporating the indentation size effect (ISE) in the analysis (Iost, A. 1996).

In the Knoop hardness measurement, the Knoop hardness is obtained from the following relation

$$HK = 14229 P / L^2 \qquad (4.1)$$

where *HK* is the Knoop hardness in GPa, 14229 is a constant dependent on the indenter geometry. *P* is the applied load in N, *L* is the length of long diagonal of the resultant rhombic impression in μm.

The composite hardness H_c of the film-substrate system is expressed as

$$H_c = (A_f / A)H_f + (A_s/A)H_s$$

$$H_f = (A /A_f) (H_c - (A_s/A) H_s) \quad (4.2)$$

where *A* is the contact area; *H* is the hardness; the subscripts *c*, *f* and *s* are related to the composite, film and the substrate, respectively and $A = A_f + A_s$. By means of simple geometrical relations depending on the Knoop indentation, equation for A_f / A can be written as

$$A_f/A = 2ct/L - c^2t^2/L^2 \quad (4.3)$$

where *L* is the length of the large diagonal, t is the thickness of the film, c = 2.908 for brittle film on the soft surface or c = 5.538 for soft film on the soft surface (Torregrosa, F. et al. 1995). Usually, measured hardness varies with load due to ISE which was not been taken into account in Jonsson and Hogmark model. Jonsson and Hogmark model is improved by incorporating the ISE taking into account a linear relation between hardness and the reciprocal indentation depth (Iost, A. 1996 and Guillemot, G. 2010). To obtain the true hardness of the film, the hardness variation with applied load is written as

$$H_f = H_{fo} + B_f/L \quad (4.4)$$

$$H_s = H_{so} + \frac{B_s}{L} \quad (4.5)$$

where H_{fo} and H_{so} are the absolute hardness of the film and the substrate respectively, B_f and B_s are constants and *L* is the indentation diagonal length. Substituting equation (4.3), (4.4) and (4.5) in (4.2) and neglecting second order 1/L terms, the composite hardness becomes

$$H_c = H_{so} + B_c/L \quad (4.6)$$

where $B_c = \left(B_s + 2ct(H_{fo} - H_{so})\right)$. To evaluate H_{so} and B_s values, hardness measurements on substrate were performed. The experimental plot H_s versus $1/L$ is approximated well by a linear regression. The experimental data on the hardness of the film-substrate H_c was plotted against 1/L and the intrinsic hardness of the film (H_{fo}) was calculated from the slope of the regression line (B_s + 2ct (H_{fo} -H_{so})). The intrinsic hardness of the substrate was evaluated from the microhardness data on the substrate.

To verify whether the film is brittle or soft we observed the nature of indentation on the surface of the coating. If the film is brittle it accommodates the indenter by crack formation. If it is a soft film it plastically deforms to match the shape of the indenter. When the film is soft for Vickers indenter c = 1 and for Knoop indenter c = 5.538 where the film is plastically strained to match the shape of diamond indenter. c = 0.5 for Vickers indenter and c = 2.908 for Knoop indenter when the film is brittle and accommodates the indenter by crack formation.

During the indentation, impression was observed after the indentation using diamond indenter. If the film is brittle, it accommodates the indenter by crack formation. If it is a soft film it plastically deforms to match the shape of the indenting indenter. Figure 4.1 shows the difference in brittle and soft film after indentation. The indentation shown in figure 4.1 a) and b) are made with load of 10N on the SiC film coated on the Ti6Al4V substrate. It can be observed that film shows soft nature by plastically straining to match the shape of the indenting Vickers and Knoop diamond tip. Brittle film accommodates the indenter, during indentation by crack formation in the interior of the impression as shown in figure 4.1 c), d). In this case indentation was made on the heat treated Al_2O_3 films deposited on the Ti6Al4V substrate at the load of 500gf.

So crack formed film after indentation is considered as brittle film and plastically strained film as soft film to choose the value of constant c. From optical micrographs of indentation, we can conclude that heat treated Al_2O_3 films are brittle and SiC films are soft in nature in the present work. But as deposited alumina and SiC films are showing soft nature.

4.2 Hardness measurement of Al_2O_3 and SiC coatings

4.2.1 Inconel

Figure 4.2 a and b shows the dependence of measured composite film-substrate hardness on the inverse of indentation diagonal for Al_2O_3 and SiC coatings on inconel. A least-square fit to the plots of the equation (4.6) results in the slope $B_c = (B_s + 2ct\,(H_{fo} - H_{so}))$. The value of c is chosen depending on whether the film is brittle or soft since the nature of the films will be different from their bulk material. For Knoop indentation its value is 2.908 for brittle film and 5.538 for soft film (Torregrosa, F.et al. 1995 and Ferro, D. et al. 2006).

In the present study, there is no cracking of film as observed in Al_2O_3 and SiC deposited substrates even at high load (10 N) and is shown in figure 4.2. Soft nature of the film is due to the amorphous structure of the coated film (Esteve, J. et al. 2001 and Sridharan, M. et al. 2007). Since the deposition is carried out at low temperature (450^0 C), deposited ceramic films are not transformed into crystalline form as confirmed by optical absorption and XRD data.

From the above reasoning, assuming the film to be soft, the c value is selected as c = 5.538. Using the value of B_s and H_{so} of substrate, the intrinsic hardness of the films is calculated using the equation (4.6). The slope of the straight line obtained by plotting H_c versus $1/L$ (figure 4.3) is used to calculate the intrinsic film hardness H_{fo}. The intrinsic hardness of the coated films is listed in table 4.1. The film hardness is increased 2.4 times (138%) with SiC coating 1.9 times (94%) by Al_2O_3 coating.

Ti6Al4V and Titanium

Hardness measurement of Al_2O_3 and SiC coatings on Ti6Al4V and titanium substrates are tabulated in table 4.2 .The slope of the straight line obtained by plotting H_c versus $1/L$ for Al_2O_3 and SiC coatings on Ti6Al4V and Al_2O_3 and SiC coatings on titanium are respectively represented in figure 4.4 a) and b) and 4.5 a) and b). It was found that film hardness is greater than substrate hardness in both cases. The film hardness is increased in Ti6Al4V substrate 3.1 times (211%) with SiC coating and 3.3 times (229%) with Al_2O_3 coating. In case of titanium substrate the increase in

microhardness is 3.1 times (209%) with SiC coating and by 2.4 times (137%) with Al_2O_3 coating.

4.3 Nanoindentation

Generally it is not possible to measure the properties of a thin film independent of the substrate, unless coating is very thick, using conventional testing equipment. To determine the film hardness indentation depth should be 10% of the film thickness. In such cases nanoindenter is used. The elastic modulus of the film can also be determined using this method. Common feature of this method is that it continuously monitors load and displacement as the indentation is produced. The feature of continuous depth and load recording allows thin film properties to be obtained directly from the data without need to measure indentation diagonals.

A schematic representation of a section through an indentation showing various quantities used in analysis is shown in the figure 4.6. Figure 4.7 shows the schematic representation of indentation load (P) versus displacement (h) data obtained during one full cycle of loading and unloading. As the indenter is driven into the material, both elastic and plastic deformation processes occur, producing a hardness impression that confirms to the shape of the indenter to some contact depth, h_c. As the indenter is withdrawn, only the elastic portion of the displacement is recovered, which effectively allows one to separate the elastic properties of the material from the plastic.

The fundamental relations from which H and E can be determined are

$$H = P/A \tag{4.7}$$

$$E_r = (\Pi/A)^{1/2} * S/(2\beta) \tag{4.8}$$

Where E_r is the reduced elastic modulus and β is a constant that depends on the geometry of the indenter. A is the projected contact area of the indenter, S = dP/dh. A reduced modulus, $E_{r,}$ is used in equation (4.8)

To account for the fact that elastic displacements occur in both the indenter and the sample, the elastic modulus of the test material, E is calculated from E_r using:

$$1/E_r = (1-\nu^2 / E) + (1-\nu_i^2 / E_i) \quad (4.9)$$

where ν is the Poisson's ratio for the test material, and E_i and ν_i are the elastic modulus and Poisson's ratio, respectively, of the indenter. (For diamond E_i =1141 GPa and ν_i=0.07) h_c is the contact depth, h_f is final depth when the indentation if fully drawn, h_s is the displacement of the surface at the perimeter contact where as h is the total displacement.

Table 4.3 and 4.4 lists the hardness and Young's modulus value obtained by nanoindentation on SiC and alumina coated on Ti6Al4V, inconel, and titanium substrate. Atomic force microscopy (AFM) images of the nanoindentation are shown in figure 4.8. The film hardness obtained by nano indentation technique is compared with the value obtained from a model which separates the film hardness from the composite hardness.

4.4 Comparison of film hardness obtained from the model and nanoindentation

During nanoindentation, indentation depth is 10 times less than that of film thickness. The absence of kickbacks and elbows in the unloading curve of Al2O3 or SiC coated different substrates (Figure 4.9 (1), (2), (3)) indicates the absence of substrate effect in the nanoindentation data. So, it can be concluded that the hardness obtained from nanoindentation is solely due to surface film. Similar observations were made in (Beegan D. et al 2008) while studying the effect of the substrate on Cu films. So it is assumed that hardness value obtained using nanoindentation method gives the film hardness. The comparison of film hardness obtained from the model, applied on the composite hardness of the film coated substrate found to agree with the data obtained using nanoindentation technique (table 4.5). In the case of Ti6Al4V substrate we found a little difference in hardness values obtained using model and nanoindentation technique. This could be due to the two phase structure of the Ti6Al4V alloys. Since it is a two phase (α and β) alloy, there is a difference in hardness value of α and β phases of the

Ti6Al4V alloy. So in general, the hardness model is found to be valid for the measurement of film hardness from the composite hardness.

CHAPTER -5

CORROSION STUDIES

5.1 Potentiodynamic polarization measurements

The Tafel plots obtained for Ti6Al4V, titanium, inconel, with Al_2O_3 and SiC coatings of thickness (t) 0.5μm in 3.5% NaCl solution at room temperature are shown in figure 5.1, 5.2 & 5.3 respectively. The corrosion potential (E_{corr}), the corrosion current density (I_{corr}) and the corrosion rate are deduced from the Tafel (log i vs. E) plots. Its values are listed in table 5.1, 5.2 & 5.3. For the Ti6Al4V substrate the I_{corr} is about 0.54 $\mu A/m^2$ which decreases to 0.0457 $\mu A/m^2$ for alumina coatings and 0.085 $\mu A/m^2$ for SiC coatings. Similarly for inconel substrate the I_{corr} is about 0.369 $\mu A/m^2$ decreases to 0.0235 $\mu A/m^2$ for alumina coatings and 0.1007 $\mu A/m^2$ for SiC coatings and titanium substrate the I_{corr} is about 0.506$\mu A/m^2$ decreases to 0.0255 $\mu A/m^2$ for alumina coatings and 0.286 $\mu A/m^2$ for SiC coatings. Corrosion rate is directly proportional to $I_{corr..}$ It is found that CR reduced drastically after ceramic coating. The decrease in corrosion rate of Ti6Al4V substrate is 2 times with SiC coating, 3.7 times with Al_2O_3 coating. On inconel substrate it is reduced to 1.5 times with SiC coating, 3.4 times with Al_2O_3 coating. In case of titanium substrate, corrosion rate reduced to 1.2 times with SiC coating, 6.1 times with Al_2O_3 coating.

Alumina coated substrates exhibit excellent corrosion resistance. Improvement in the corrosion resistance of the substrate after ceramic coating is due to the fact that ceramic coating passivates the surface of the substrate and prevents the corrosion attack by the electrolyte. Generally, in physical vapor deposited coatings, electrolytes enter into the substrate through the defects like pores and micro cracks and cause the corrosion of the substrate (Harish, C. B. 2009). The protective coatings must fulfill the two main requirements to achieve the remarkable effect on corrosion resistance. They are strong adhesion to the substrate and low density of pores and cracks. Absence of pores and

micro cracks, complete surface coverage and good adhesion of the ceramic film coating to the substrate obtained by PLD technique which enhances the corrosion resistance of the substrate. Enhanced corrosion rate of coatings on substrate indicates that the coated films are having negligible concentration of pores and cracks.

5.2 Electrochemical impedance spectroscopy studies

Electrochemical impedance spectroscopy is useful in the study of localized corrosion of coatings/substrate systems, and offers advantages over conventional electrochemical polarization techniques. Modeling and interpretation of EIS spectra becomes the key to extracting useful information with regard to the details of the electrochemical corrosion characteristics. EIS modeling is carried out through an equivalent circuit (EC), which is an assembly of circuit elements, representing the physical and electrical characteristics of the electrochemical interface. The relevant equivalent circuits are developed by non-linear least square curve fitting to the exponential data to build up a description of the influence of different coatings deposited on the substrate.

Figures 5.4 – 5.9 shows the impedance response of Ti6Al4V, inconel and titanium with Al_2O_3 and SiC coatings as Nyquist and Bode plots. The Nyquist plot shows an unfinished semicircle, which is attributed to the charge transfer controlled reaction. Bode plot phase angle versus log f showed that the phase angle approaches 90^o and remains constant between the higher and lower frequency (mHz - KHz) suggesting that a highly stable film is formed on the surface. The simplified equivalent circuits are shown in figure 5.10. The values of solution resistance (R_s), charge-transfer resistance (R_{ct}), Pore resistance (R_p), total capacitance (Q) of the constant phase element (CPE) are listed in Table 5.4. The R_{ct} increases in the following order: substrate (Ti6Al4V, inconel and titanium) < SiC coated substrate < Al_2O_3 coated substrate, which shows that Al_2O_3 coated substrate has higher corrosion resistance. The values of R_{ct} are strongly dependent on the passive film characteristics and are an indication of the corrosion of the materials.

The R_p values obtained from the polarization study also vary in the same order. Figure 5.7, 5.8 and 5.9 (log *Z* versus log *f*) plot show that the absolute impedance

increases in the same order as R_{ct}. The equivalent circuit for the substrate is shown in Figure 5.10 a). It consists of a double layer capacitance, which is parallel to the charge transfer resistance, both of which are in series with the solution resistance between the working electrode (WE) and the tip of the Luggin capillary. The double layer capacitance provides information about the polarity and the amount of charge at the substrate/electrolyte interface. Constant phase element (CPE) describing the non-ideal (eg capacitive) characteristics of the electrochemical interface, designated as Q, is introduced to achieve a more accurate simulation of electrochemical corrosion The capacitance is replaced with CPE for a better quality fit. CPE accounts for the deviation from ideal dielectric behavior and is related to the surface in homogeneities. This element is written in admittance form as

$$Y(\omega) = Y_0(j\omega)^n, \qquad (5.1)$$

where Y_0 is an adjustable parameter used in the non-linear least squares fitting and n is also an adjustable parameter that always lies in between 0.5 and 1. The value of n is obtained from the slope of log Z versus log f plot (Fig. 5.7. 1), 5.8. 1), 5.9. 1)). The phase angle (θ) can vary between 90^0 (for a perfect capacitor (n = 1)) and 0^0 (for a perfect resistor (n = 0)). The CDC for the equivalent circuit proposed for substrate is R(Q)R (figure 5.10 a). When the sample is immersed in the electrolyte the defects in the coating provide the direct diffusion path for the corrosive media. In this process the galvanic corrosion cells are formed and the localized corrosion dominates the corrosion process. In such cases, electrochemical interface can be divided into two sub-interfaces: electrolyte/coating and electrolyte/substrate. The proposed equivalent circuit for such a system is shown in Figure 5.10 b). The parameters in the equivalent circuit R_{pore} and Q_c are related to the properties of the coating and the electrolyte/coating interface reactions. R_{ct} and Q_{dl} are related to the charge-transfer reaction at the electrolyte/substrate interface. The CDC of the proposed equivalent circuit for the coated sample is R (Q[R(QR)]). From

the EIS data given in Table 5.4 it is seen that Q_c decreased from SiC coating to alumina coating indicating that SiC coatings had more pores and less dense microstructure as compared to alumina coatings.

5.3 SEM Studies after corrosion

After the corrosion testing, the surface topography and the corrosion characteristics of the uncoated and the coated systems were studied by scanning electron microscopy and EDAX, respectively. Pits were formed as a result of corrosion attack which appears as a small dark spots. These pits were observed on the uncoated substrate as shown in the figure 5.11 but were absent in SiC or Al_2O_3 coated substrates. EDAX analysis indicates the presence of sodium (Na) and Chlorine (Cl) in the dark regions.

CHAPTER -6

SUMMARY AND CONCLUSIONS

The major requirements to the materials for the aircraft industry are their characteristics of specific strength and heat resistance, fatigue resistance, crack resistance, and sufficient corrosion resistance. Aerospace materials like titanium, its alloy Ti6Al4V and inconel have attractive properties such as specific strength, low density, relatively high melting point, good oxidation and corrosion resistance. But they have poor tribological property, which limits their use in severe wear conditions. The high corrosion resistance of these materials is also decreased when local mechanical abrasion removes the protective oxide film. Coatings are used to modify and increase the functionality of a bulk surface or substrate without modifying the bulk properties of the material. In many cases thin films do not affect the bulk properties of the material. Degradation of surface properties of these materials can be overcome by coating ceramic materials like Al_2O_3 and SiC on their surface using film deposition techniques.

As part of this thesis work the Al_2O_3 and SiC coatings using PLD on three substrates viz., titanium, Ti6Al4V and inconel were deposited and characterized. Characterization of target, substrate materials and coatings were carried out. Effect on microhardness and corrosion resistance due to presence of ceramic coatings was studied. The substrate material surfaces were sequentially polished with silicon carbide papers from 320 to 1500 grit size before the deposition. The samples were polished to a mirror finish of average roughness (R_a) of 20 nm using alumina suspension of 1, 0.5, 0.3 micron size. Fine polished surfaces were cleaned in acetone using ultrasonic bath before deposition. Target and substrate materials were characterized using XRD. The XRD peaks correspond to α phase of titanium, α +β phase of Ti6Al4V, α phase of Al_2O_3 and α- SiC. Densities of the targets were determined by water absorption method. Thin films

of Al_2O_3 and SiC can be deposited on the substrates by pulsed laser ablation using Q-switched Nd: YAG laser of wavelength 1064 nm, of frequency 10Hz, of beam diameter 0.01m was focused by a spherical lens of focal length 0.5m to spot size of 1mm diameter and made to fall on to a flat target surface. Laser beam was directed at an angle of 45^0 on to the rotating target. Target is rotated continuously at the rate of 40 rpm, in order to avoid crater formation. Deposition was done in vacuum level of 10^{-5} mbar. Laser processing parameters play an important role in changing the film properties. The coatings of different microstructure and thickness are obtained by varying the target – substrate distance. Uniform films are obtained at large target substrate distance which greater than 0.08m due to the broadening of angular spread of the plume resulting from the interaction of the laser beam with target. Density of the target material changes the rate of ablation of the depositing particle which results in changes in the film thickness. Longer time duration is required to obtain appropriate film thickness using high density targets. Ablation is not possible in very low density targets due to the crater formation. Density of the target should be certain minimum density to ablate it to form deposit on the substrate surface. Substrate heating during deposition of the coating determines the adhesion of the film to the substrate. Adhesive coating can be obtained by maintaining the substrate temperature at 450^0C. Room temperature deposited films show buckling delamination. Rate of deposition of the target material also depends on laser energy. Deposition rate was less at low energy.

Coated films were characterized using SEM, EDAX, spectrophotometer, optical microscope, nanoindentation, surface roughness measurements using 3D optical profilometer, adhesion test, and corrosion studies. XRD, EDAX and optical absorption studies confirms the existence of deposited coating material. Hardness measurement on the coated substrate gives the composite hardness value due to the influence of substrate and the coating. Film hardness was separated from the composite hardness using a model based on the area law of mixture and by considering the hardness variation with load due to the indentation size effect. Film hardness can be directly measured using nanoindentation technique by continuously monitoring the load and displacement of the

indenter. Young's modulus of the film can also be determined from this technique. Film hardness of the SiC and alumina coating obtained from the model is compared with the nanoindentation technique, it was found to be nearly equal. Corrosion behavior of substrates after ceramic coating is studied using 3.5% NaCl solution by potentiodynamic polarization and electrochemical impedance spectroscopy (EIS) measurements. The Nyquist and the Bode plots obtained from the EIS data are fitted by appropriate equivalent circuits. The pore resistance (R_{pore}), the charge transfer resistance (R_{ct}), the coating capacitance (Q_{coat}) and the double layer capacitance (Q_{dl}) of the coatings are obtained from the equivalent circuit. Experimental results show increase in corrosion resistance of substrate after ceramic coating. Al_2O_3 coated substrates showed more corrosion resistance than SiC coated substrates.

Conclusions

The following conclusions can be drawn from the present thesis work.

- Adhesive uniform Al_2O_3 and SiC coatings can be deposited using PLD technique on titanium, Ti6Al4V, inconel substrates by PLD technique using Nd: YAG laser, of wavelength 1064 nm at a temperature of 450^0C. The minimum temperature needed for adhesion of these films is 200^0C.
- XRD and UV-visible absorption spectrum of Al_2O_3 and SiC coatings using spectrophotometer data of films prove the existence of coating material on the substrate.
- Laser processing parameters like target substrate distance, substrate temperature, target density, laser energy play an important role in changing the film properties
- A thin coating of 0.5µm of Al_2O_3 or SiC on substrates shows considerable improvement in microhardness and corrosion resistance of the substrates.
- The microhardness of inconel substrate has increased by 2.4 times (138%) with SiC coating 1.9 times (94%) by Al_2O_3 coating. Similarly in the case of Ti6Al4V substrate the increase is 3.1 times (211%) with SiC coating and 3.3 times (229%) with Al_2O_3 coating. In case of titanium substrate the increase in microhardness is 3.1 times (209%) with SiC coating and by2.4 times (137%) with Al_2O_3 coating.

- Film hardness is separated from the composite hardness using a model based on the area law of mixture and by considering the hardness variation with load due to the indentation size effect and it is compared with the nanoindentation technique.
- The potentiodynamic polarization and the EIS measurements showed that Al_2O_3 and SiC coatings exhibit better corrosion resistance as compared to that of substrate. The decrease in corrosion rate of Ti6Al4V substrate is 2 times with SiC coating, 3.7 times with Al_2O_3 coating. On inconel substrate it is reduced to 1.5 times with SiC coating, 3.4 times with Al_2O_3 coating. In case of titanium substrate, corrosion rate reduced to 1.2 times with SiC coating, 6.1 times with Al_2O_3 coating.

APPENDIX I

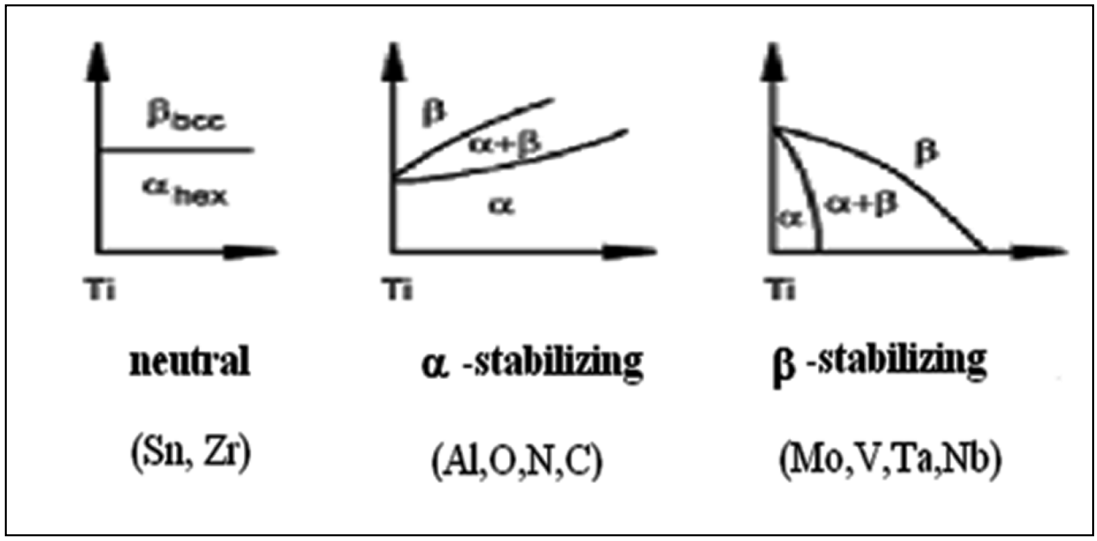

Figure1.1. Influence of alloying element on phase diagram of Ti alloys (schematically) (Christoph, L.and Manfred, P. 2003)

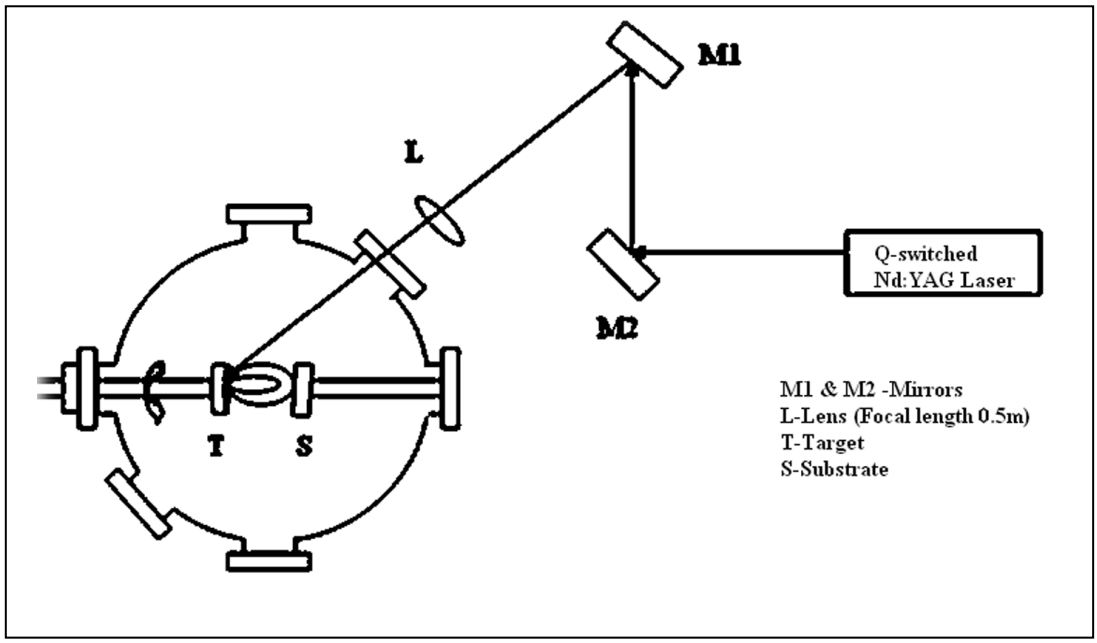

Figure 2.1 Schematic representation of the PLD system.

Figure 2.2 Photograph of the ablation chamber

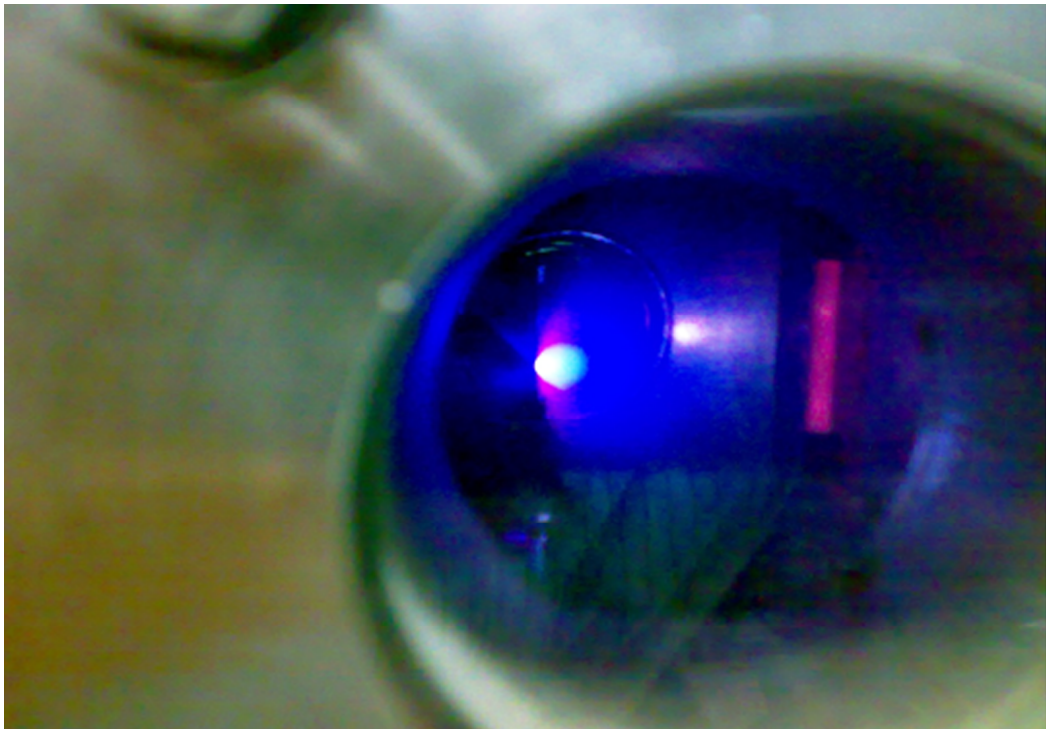

Figure 2.3 Photograph of plume formation due to laser interaction with target

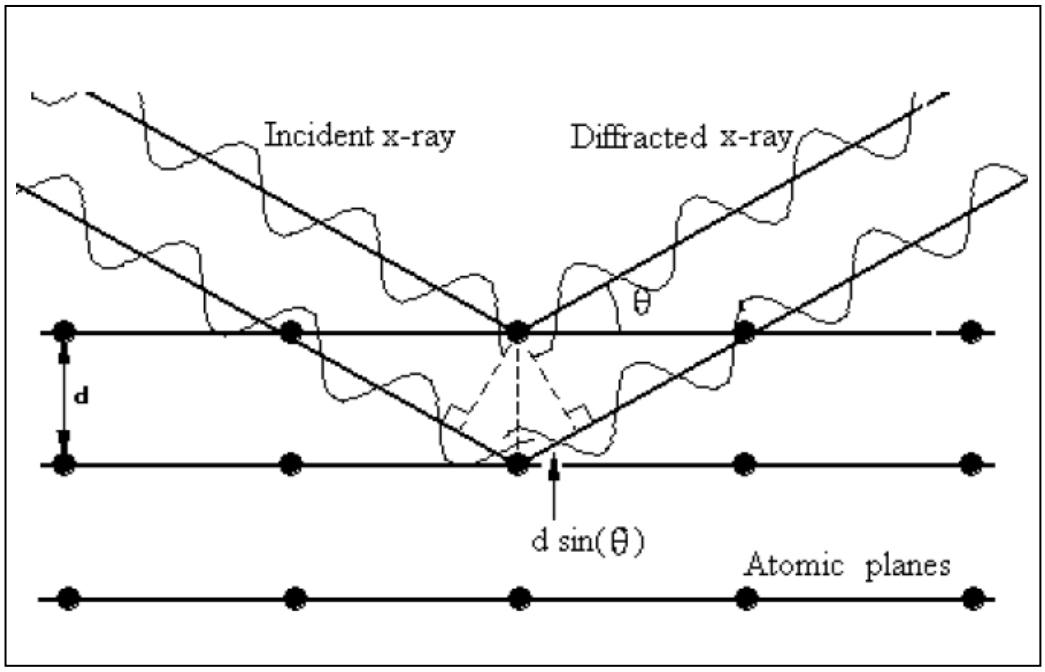

Figure 2.4 Sketch of X-ray diffracted by atomic planes showing the mechanism of Bragg's law.

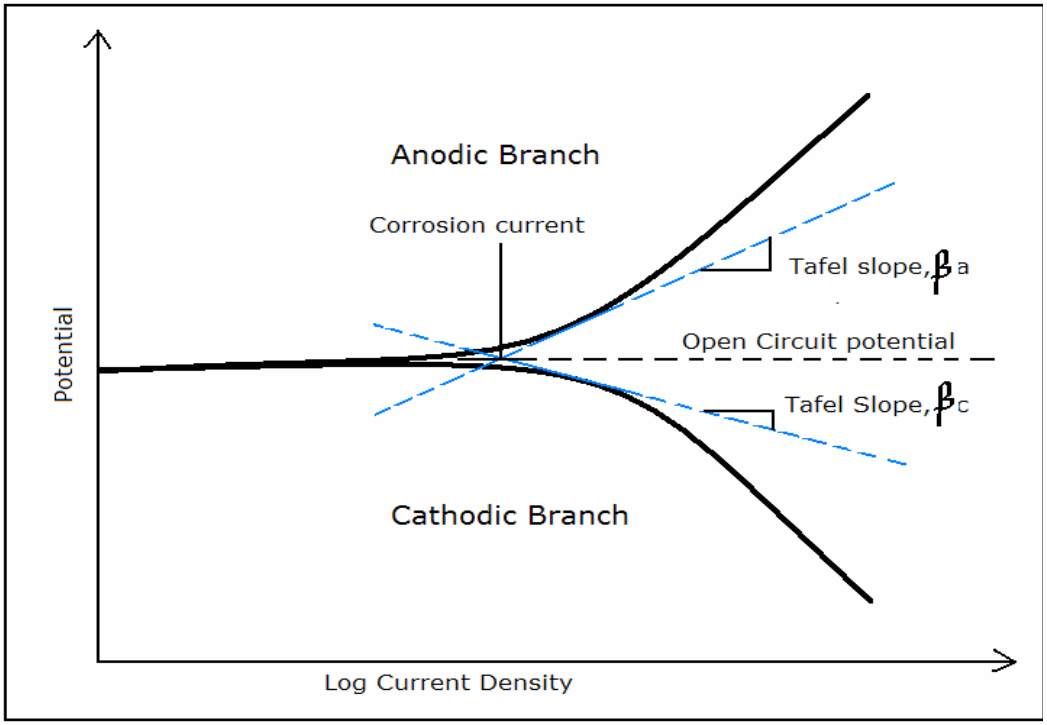

Figure 2.5 Diagram showing DC Polarization Tafel plot

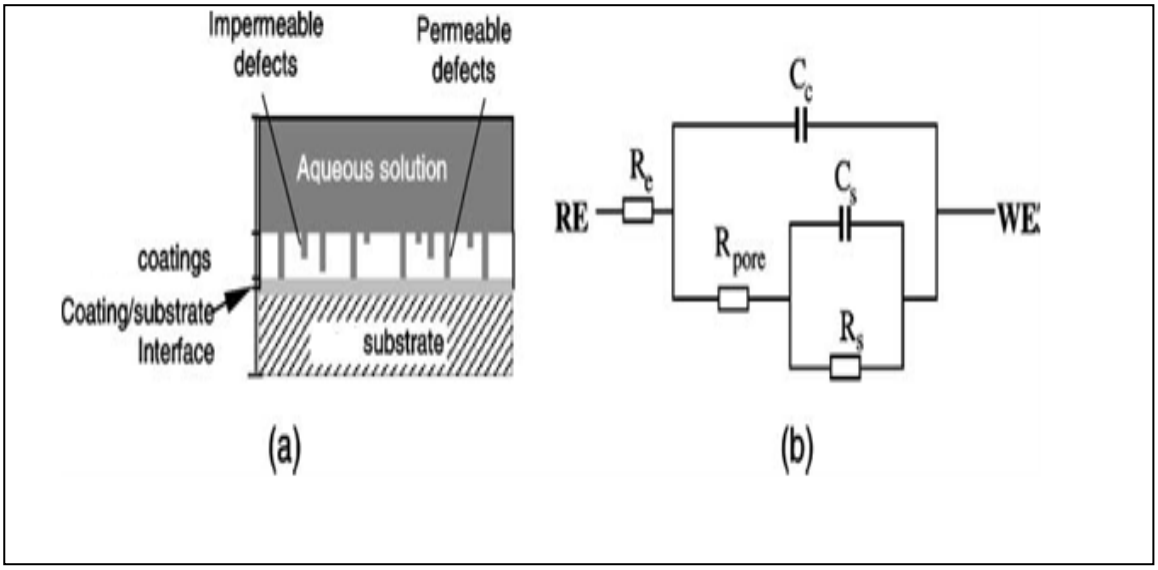

Figure 2.6 a) Schematic description of surface coated substrate immersed in an aqueous solution b) General EC proposed to describe localized corrosion at pores shown in (a).

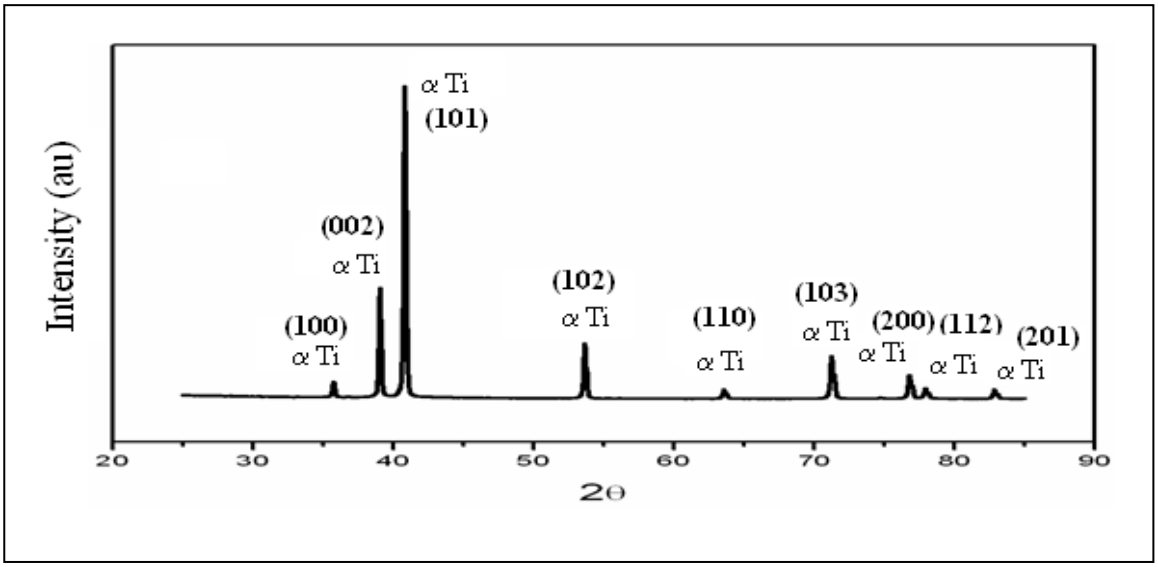

Figure 3.1 XRD pattern of titanium

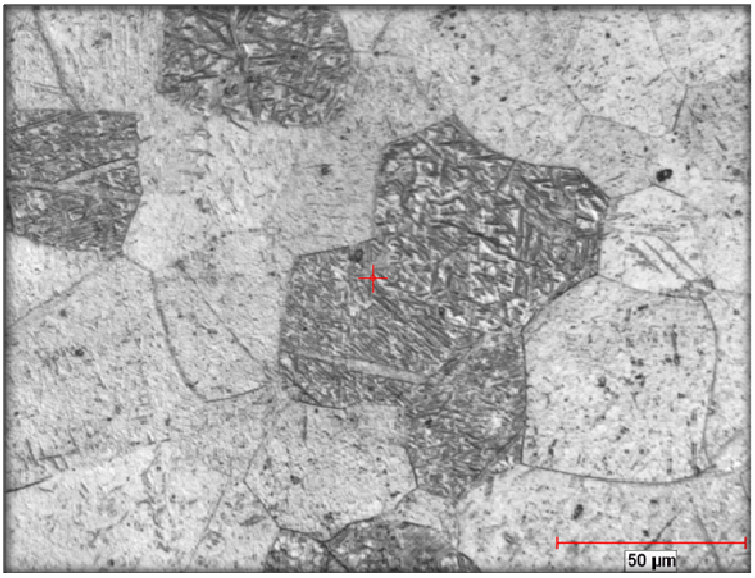

Figure 3.2 Optical micrograph of titanium at 400x magnification

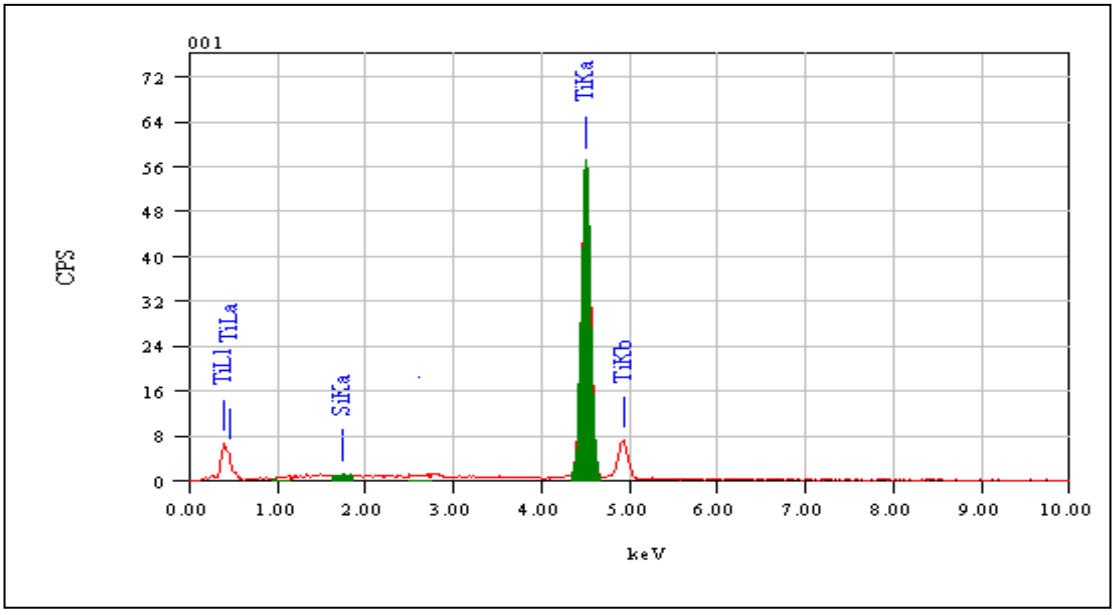

Figure 3.3 EDAX of titanium substrate

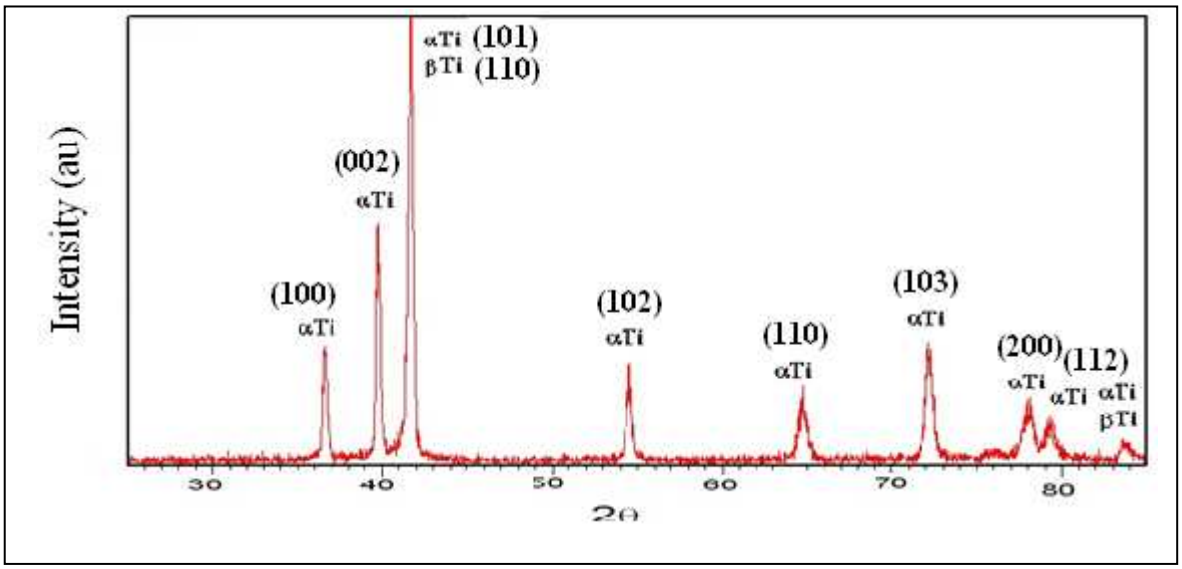

Figure 3.4 XRD pattern of Ti6Al4V.

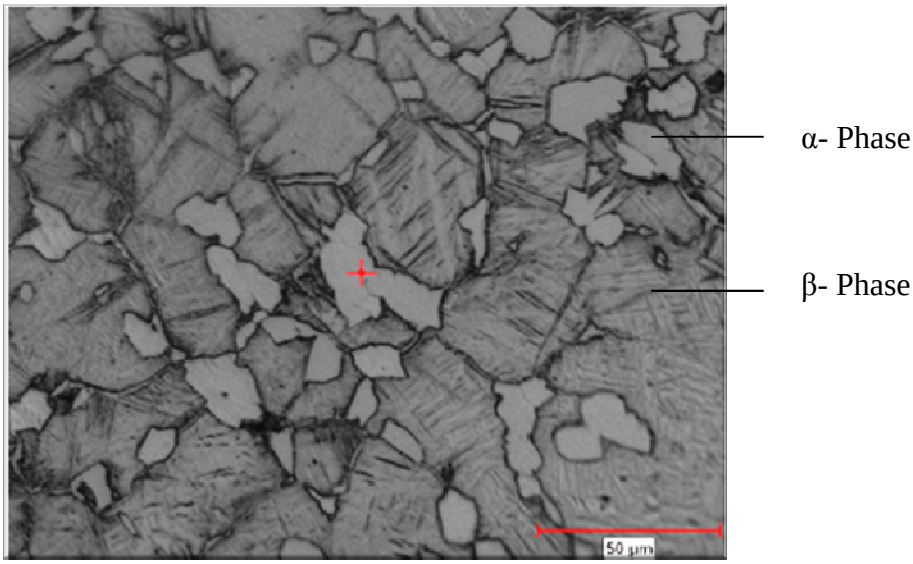

Figure 3.5 Optical micrograph of Ti6Al4V at 400x magnification

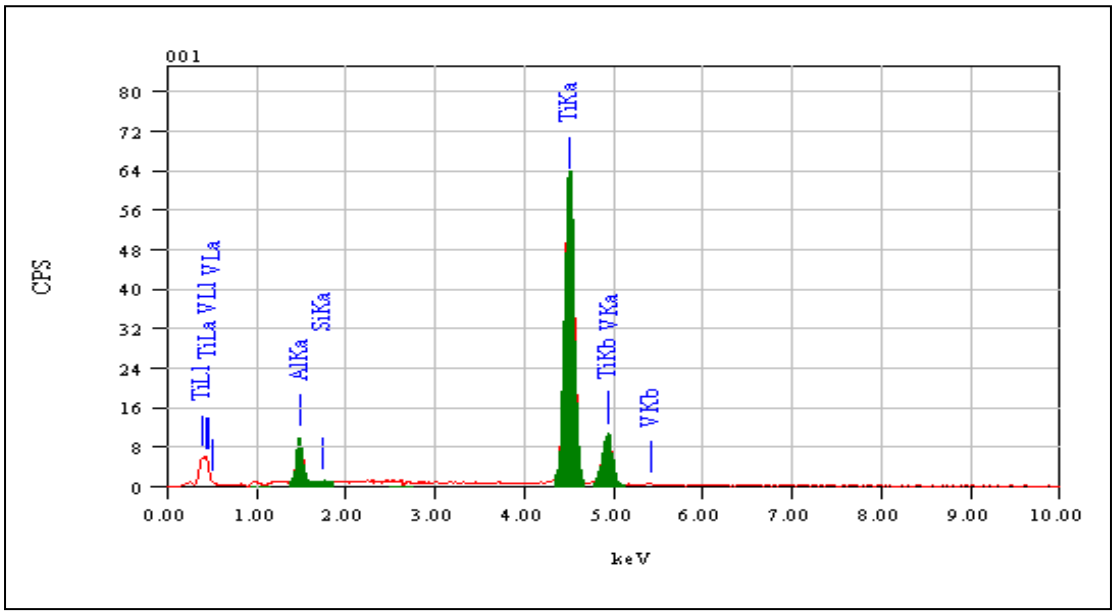

Figure 3.6 EDAX of Ti6Al4V substrate.

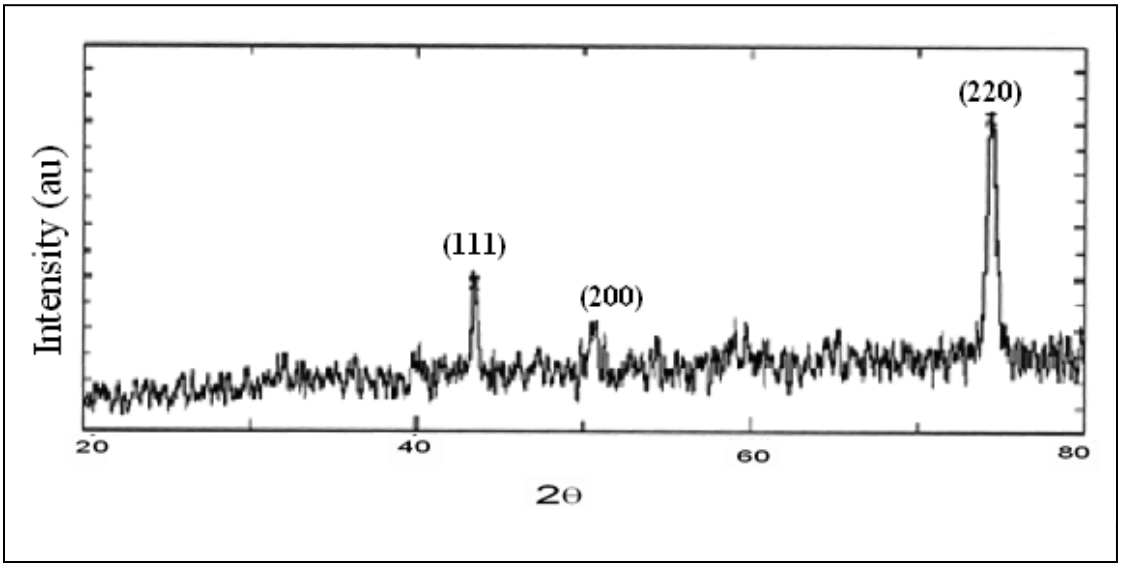

Figure 3.7 XRD pattern of inconel

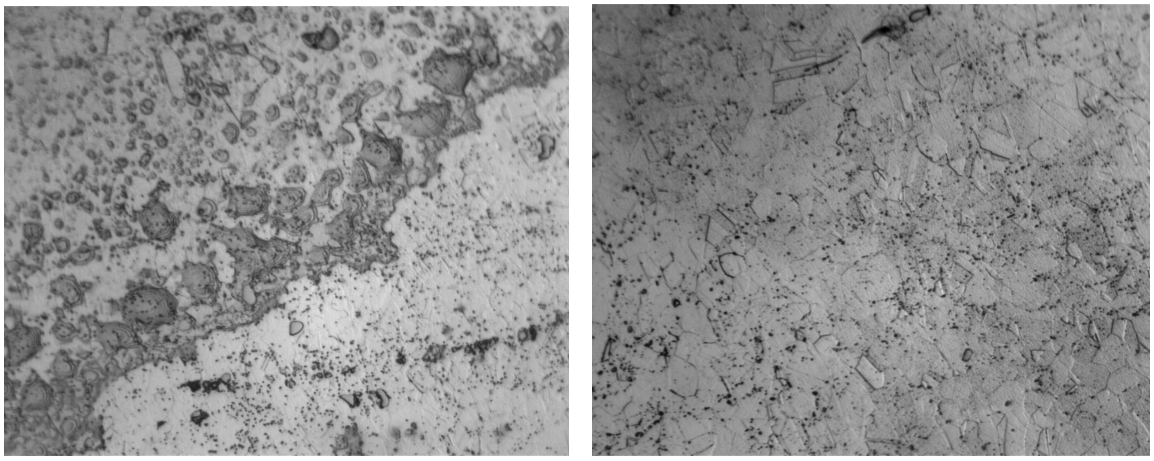

Figure 3.8 Optical microstructure of inconel at 400 x, at different regions on the surface.

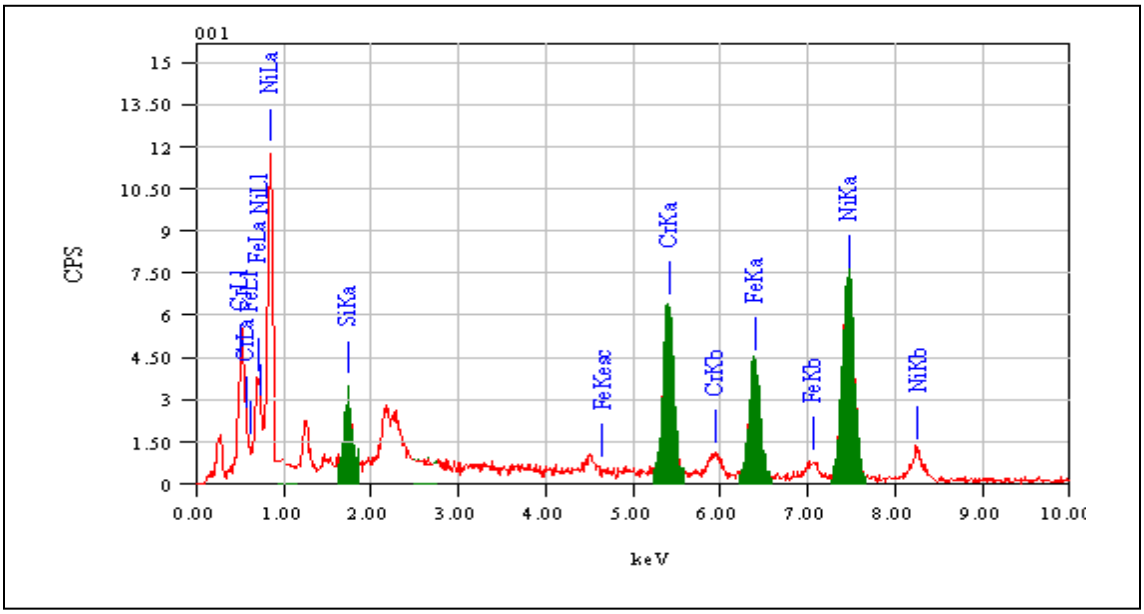

Figure 3.9 EDAX of inconel substrate.

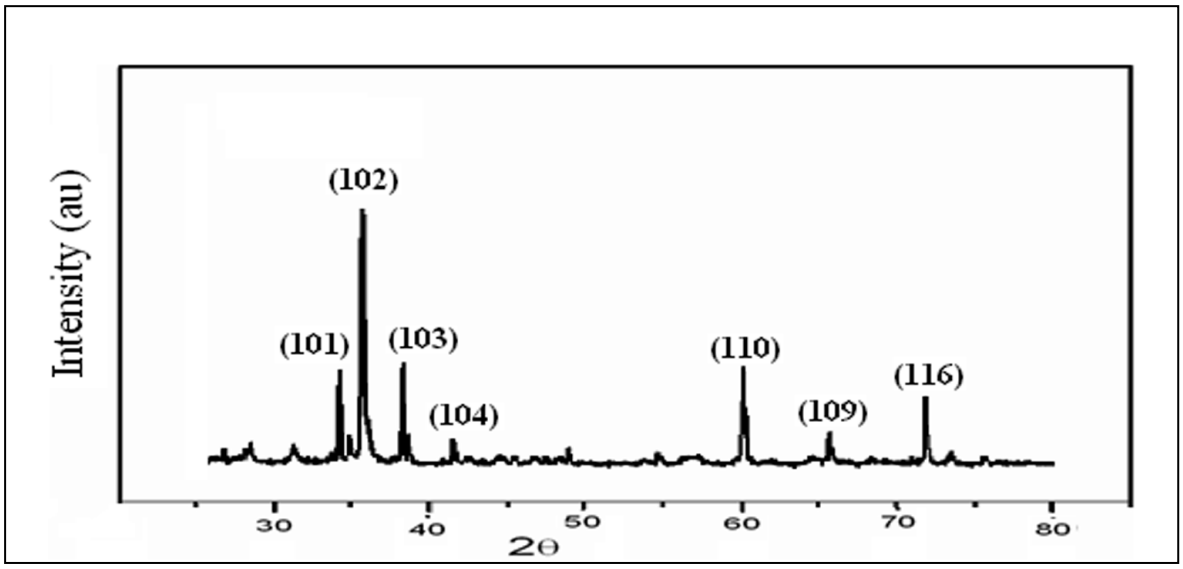

Figure 3.10 XRD pattern of SiC.

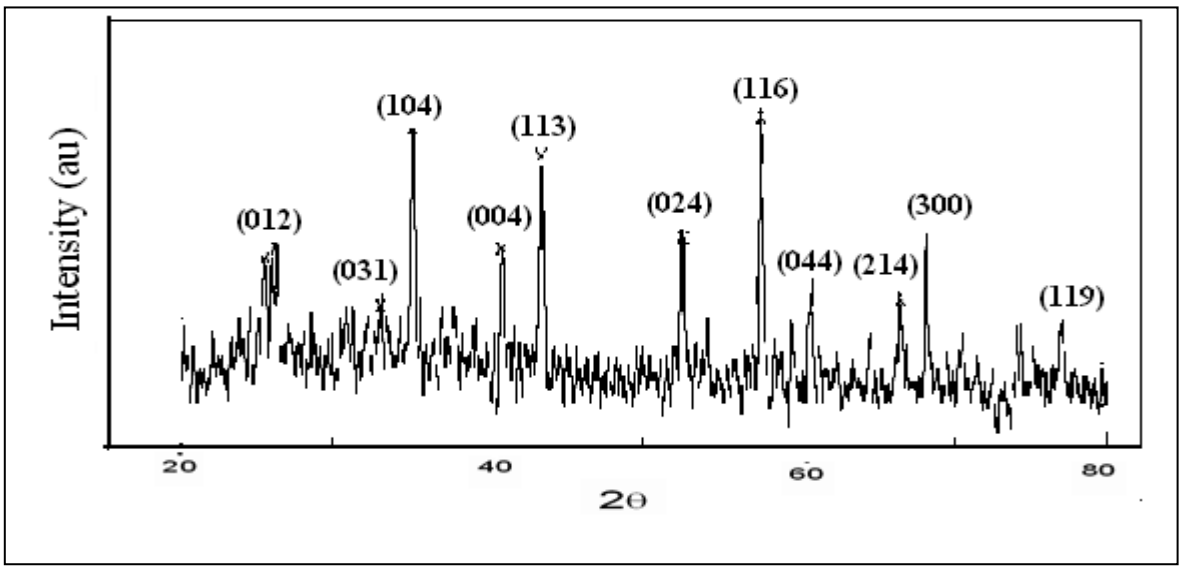

Figure 3.11 XRD pattern Al_2O_3.

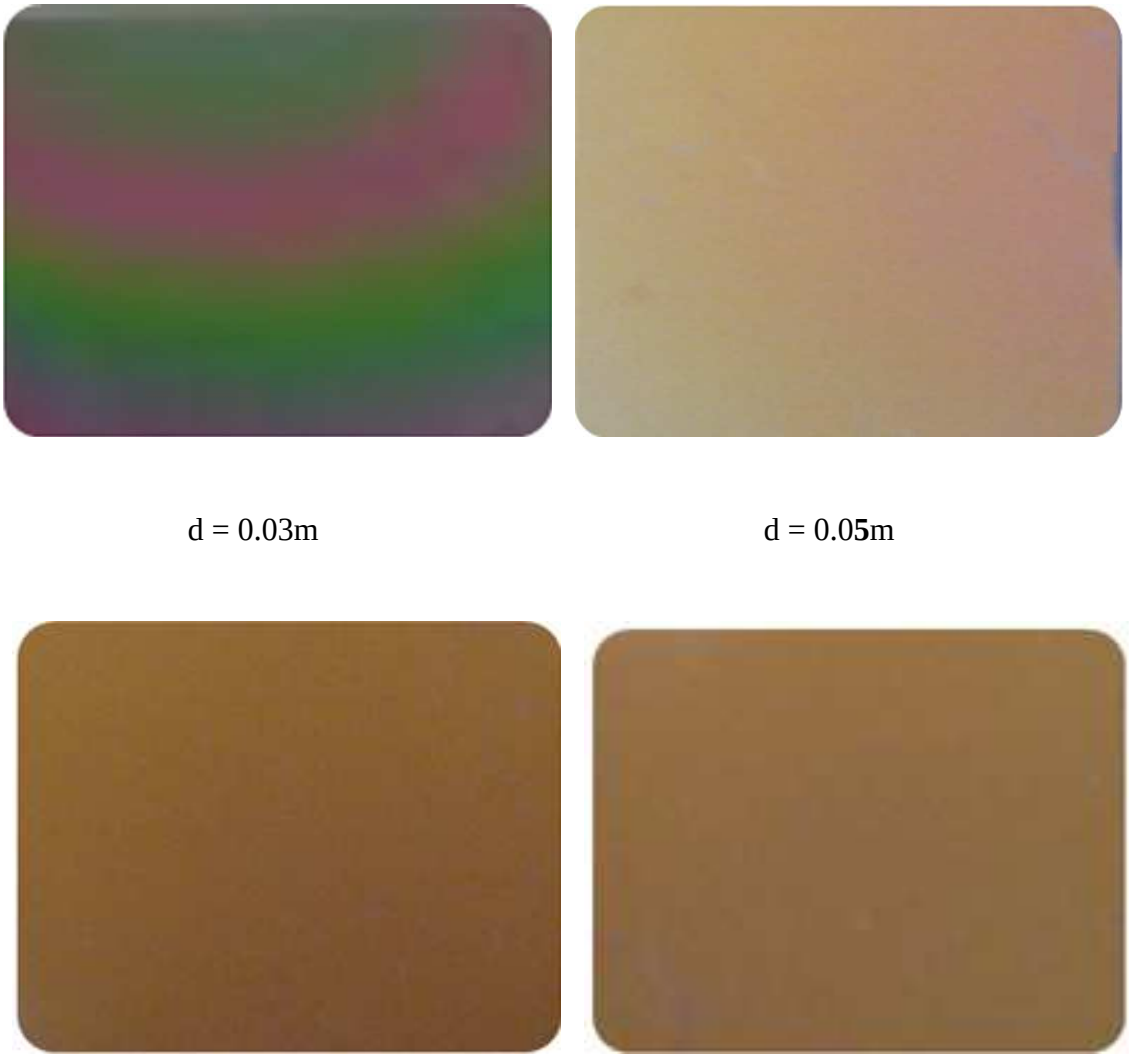

d = 0.03m d = 0.05m

d = 0.08m d = 0.10m

Figure3.12 Photograph of the substrates coated at different distance (d) from the substrate .

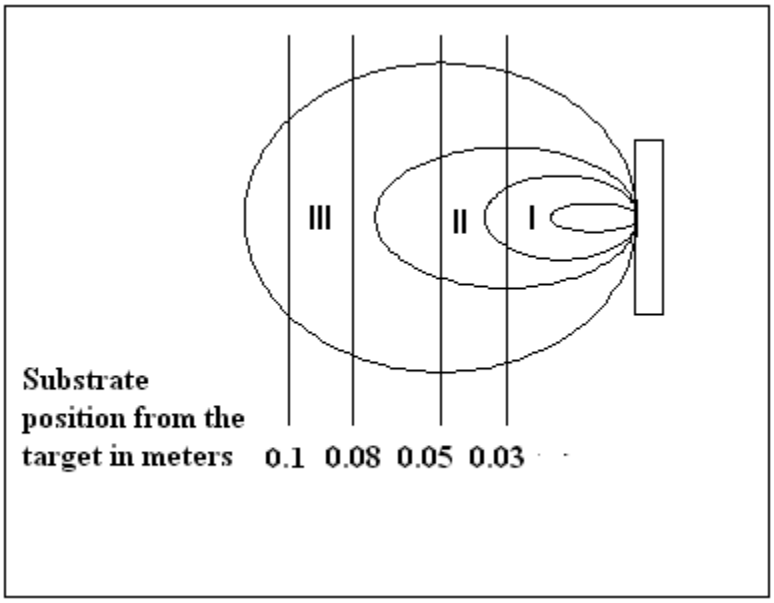

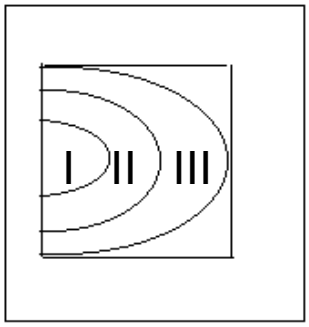

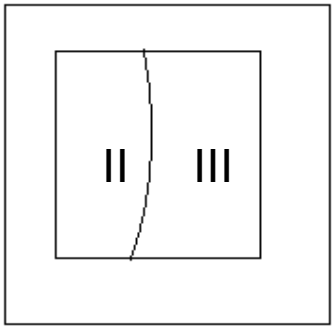

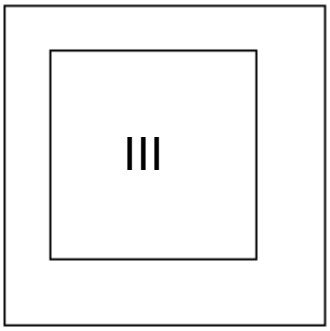

Sample A (d = 0.03m) Sample B (d = 0.05 m) Sample C (d = 0.08, 0.10m)

Figure 3.13 Schematic representation of the angular distribution of the plume at different target – substrate distances.

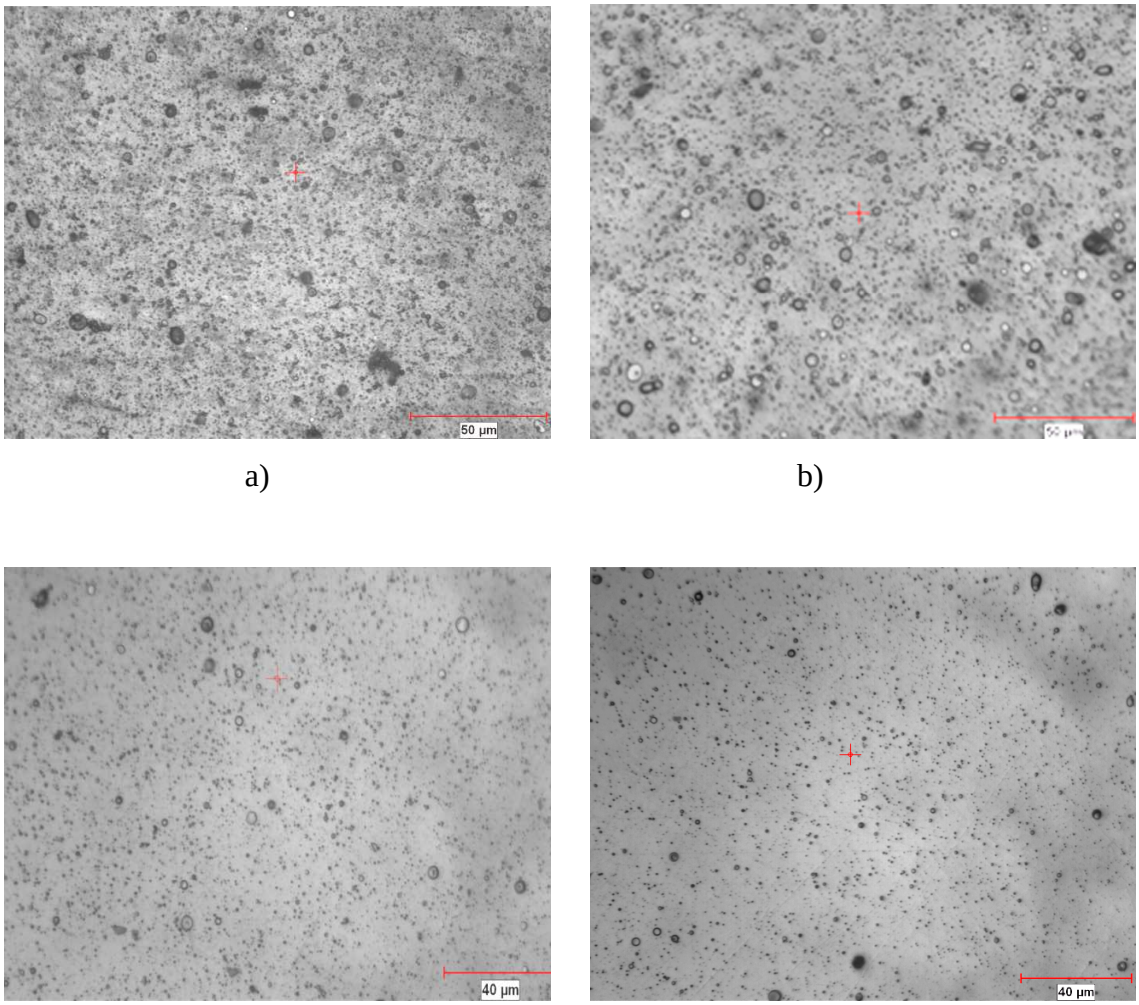

a) b)

c) d)

Figure3.14. Surface morphology at 400x, of the alumina coated on Ti-6Al-4V substrate at a target–substrate distance of a) 0.03m b) 0.05m c) 0.08m d) 0.10m.

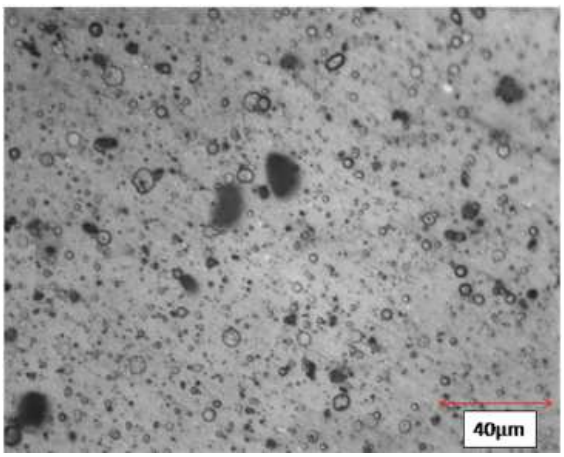

a)

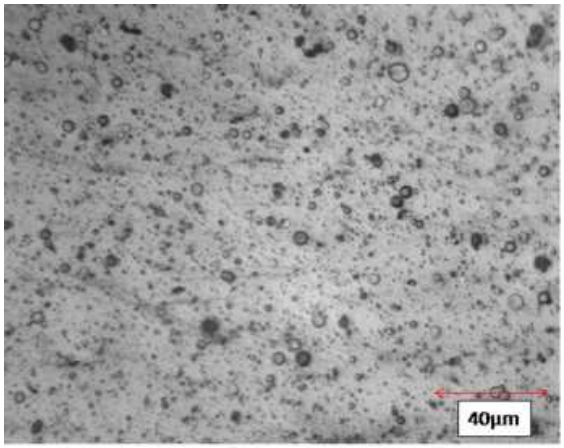

b)

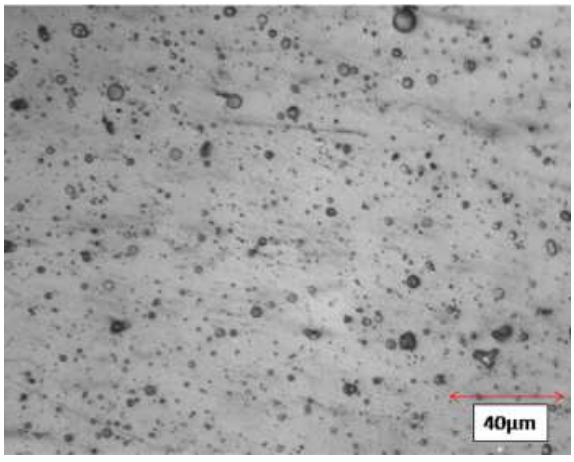

c)

Figure 3.15. The optical microstructure of particle distribution of the sample A (d=0.03 m) in 3 distinct regions a) I, b) II, c) III) on the surface.

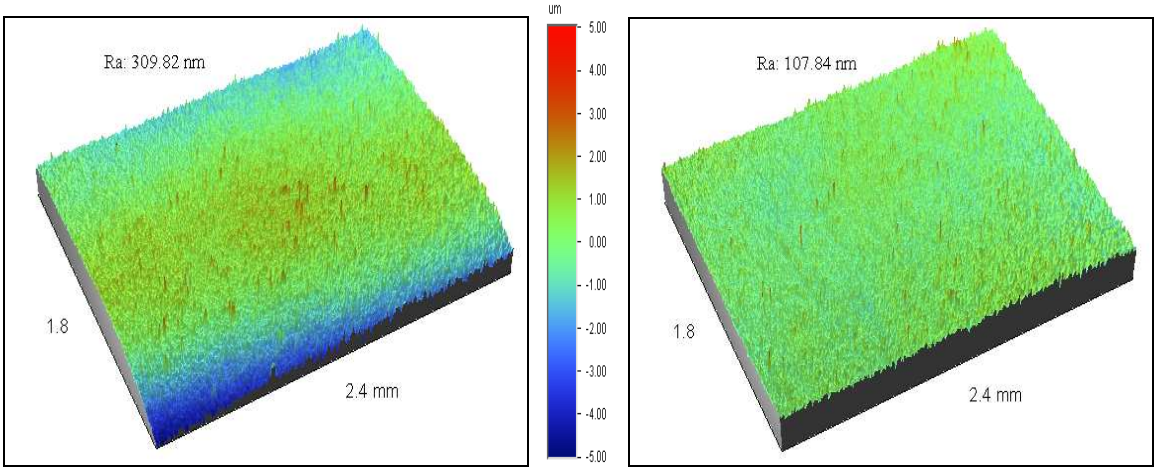

a) Al_2O_3 coating at d= 0.03 m (Region I) b) Al_2O_3 coating at d= 0.03 m(Region II)

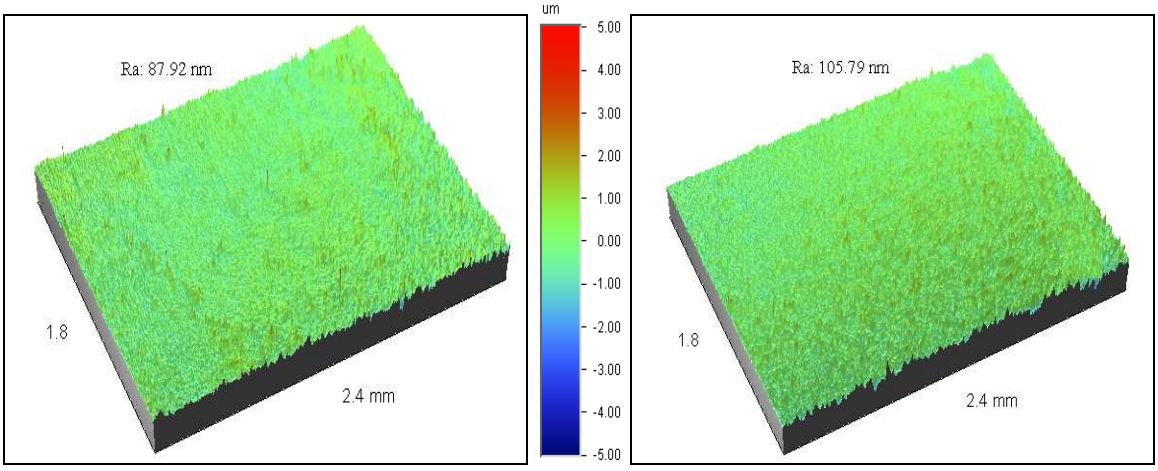

c) Al_2O_3 coating at d= 0.03 m (Region III) d) Al_2O_3 coating at d= 0.05 m (Region II)

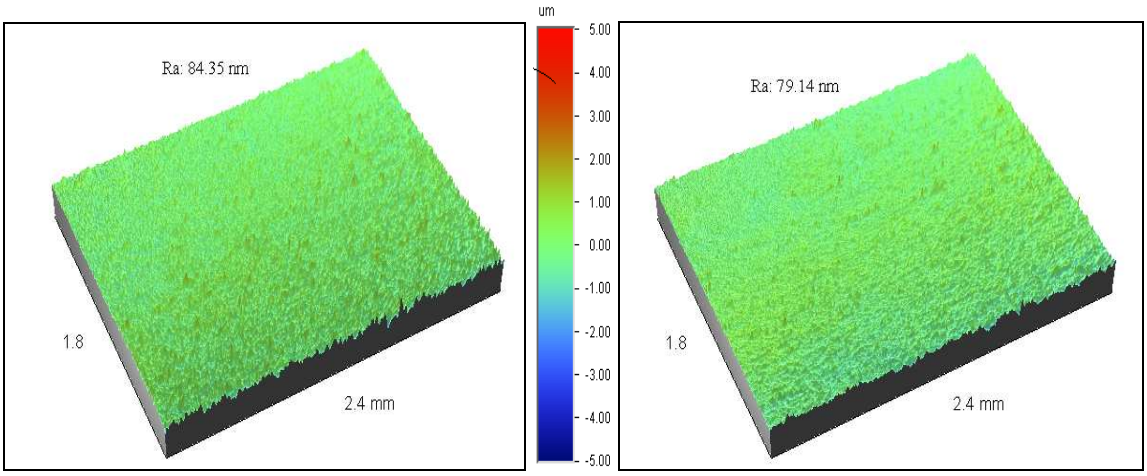

e) Al_2O_3 coating at d= 0.05 m (Region III) f) Al_2O_3 coating at d= 0.10 m (Region III)

Figure 3.16 3-D Surface profilometer photograph of the Al_2O_3 coated on Ti6Al4V substrate at different d values.

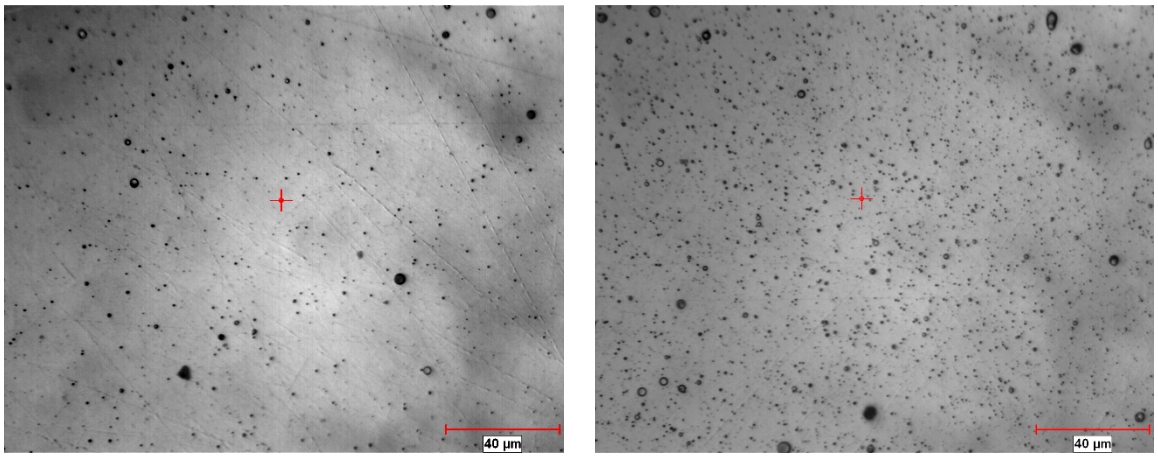

a) b)

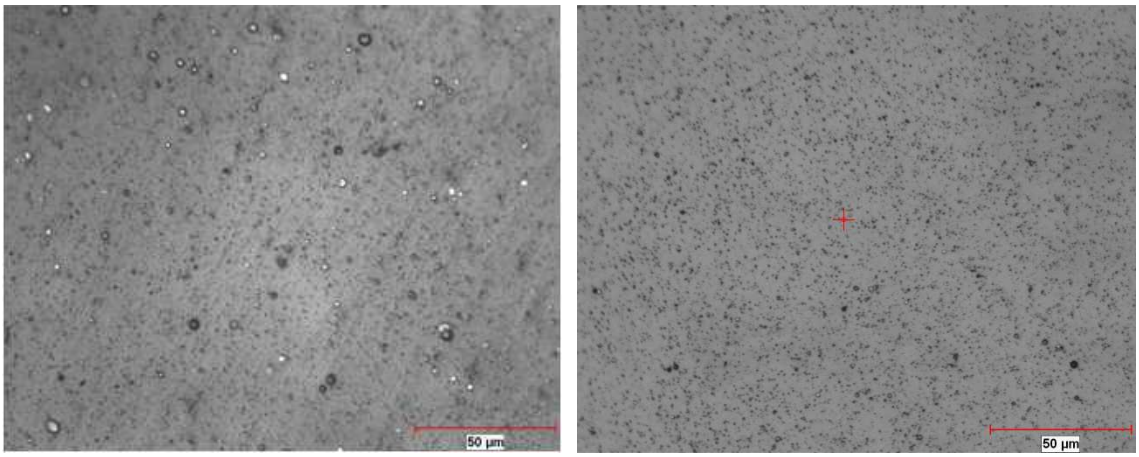

c) d)

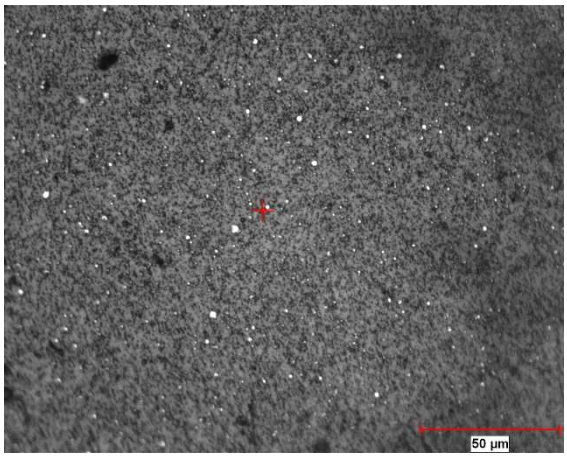

e)

Figure 3.17 Surface morphology of coated Ti6Al4Vsubstrate at a target–substrate distance of 0.08 m using Al_2O_3 target of density a) 3690 Kg/m^3, b) 3490 Kg/m^3,c) 3150 Kg/m^3 and SiC target of density d) 2840 Kg/m^3, e) 2430 Kg/m^3 during 60min deposition.

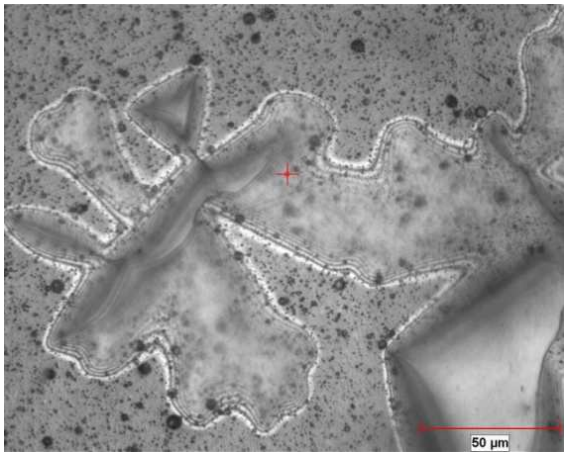

a)

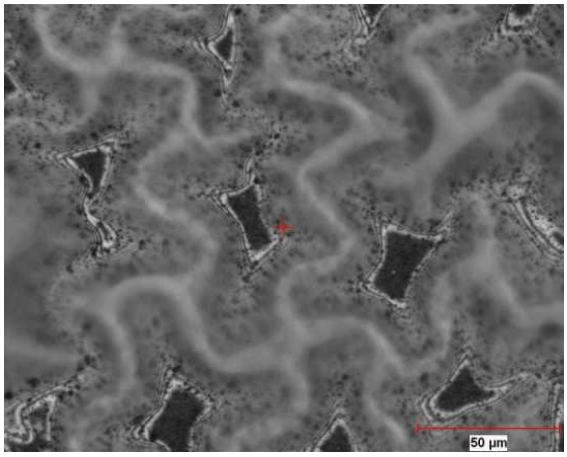

b)

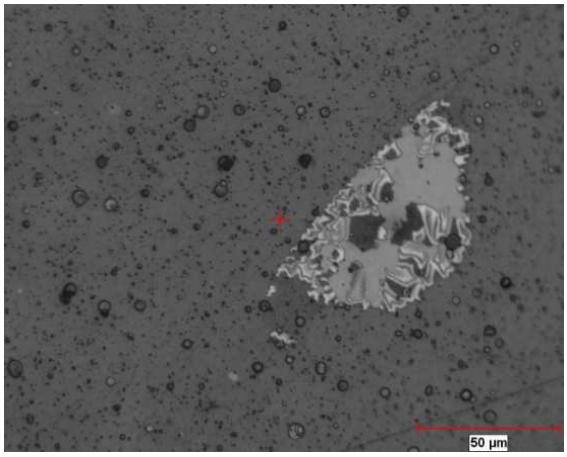

c)

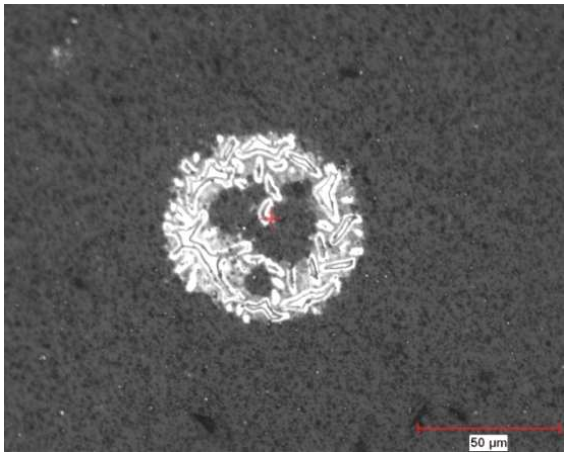

d)

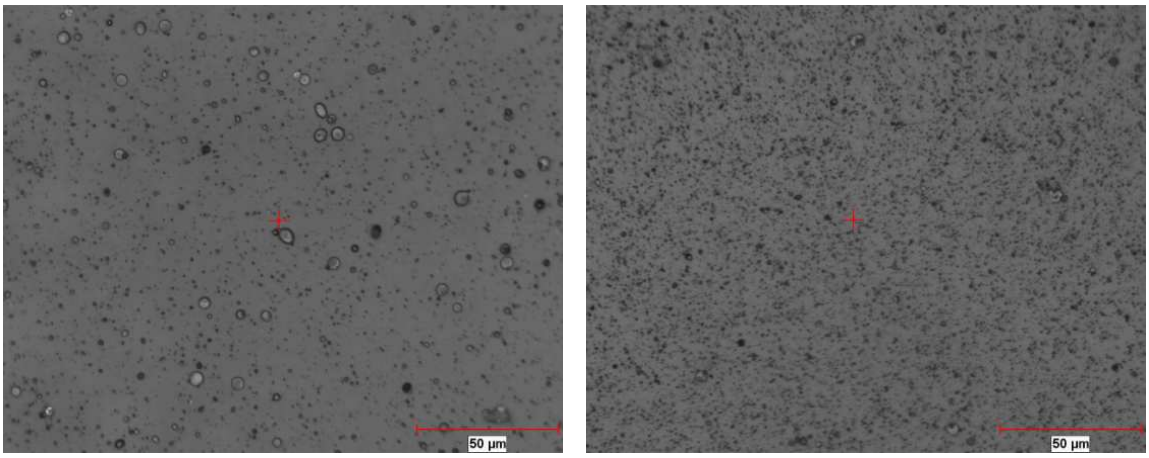

e) f)

Figure 3.18. Optical microstructure of Al_2O_3 and SiC films deposited at different temperatures on Ti6Al4V, a) Al_2O_3 and b) SiC deposition at RT, c) Al_2O_3 and d) SiC deposition at 100^0C , e) Al_2O_3 and f) SiC deposition at 200^0C.

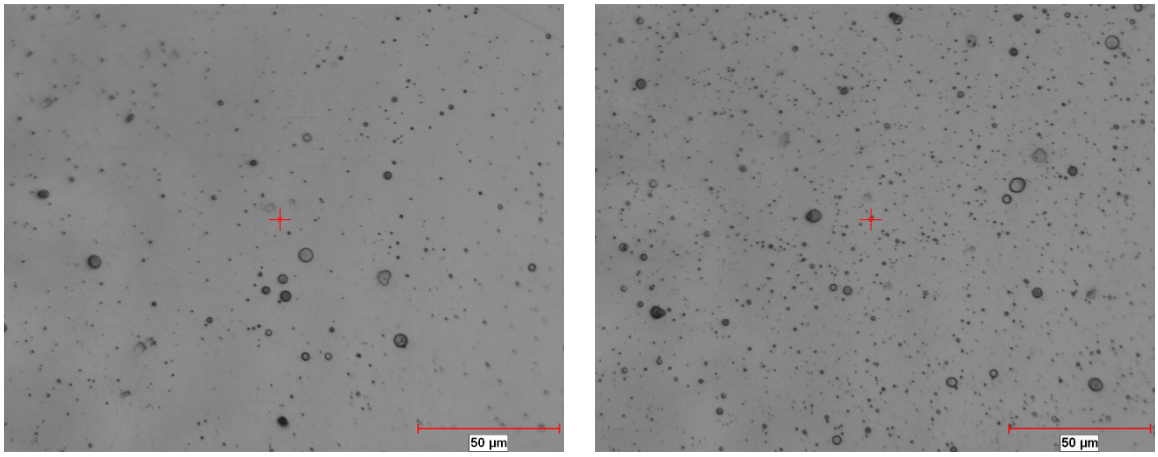

a) b)

Figure 3.19. Surface morphology of the alumina deposit using laser energy a) 85 mJ b) 135mJ.

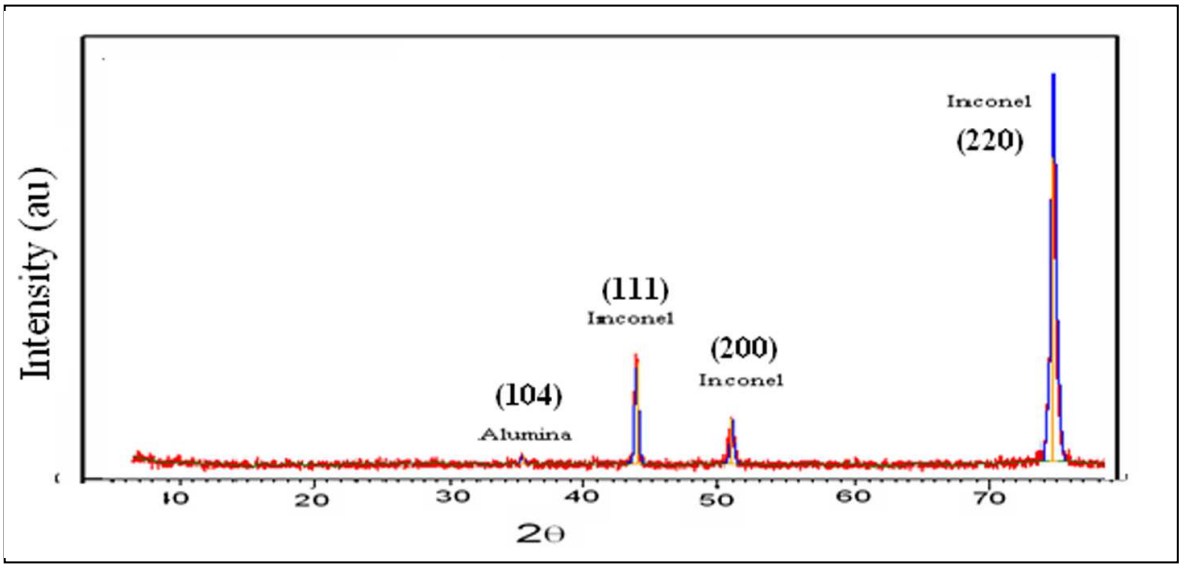

Figure 3.20 XRD of Al_2O_3 coated inconel substrate.

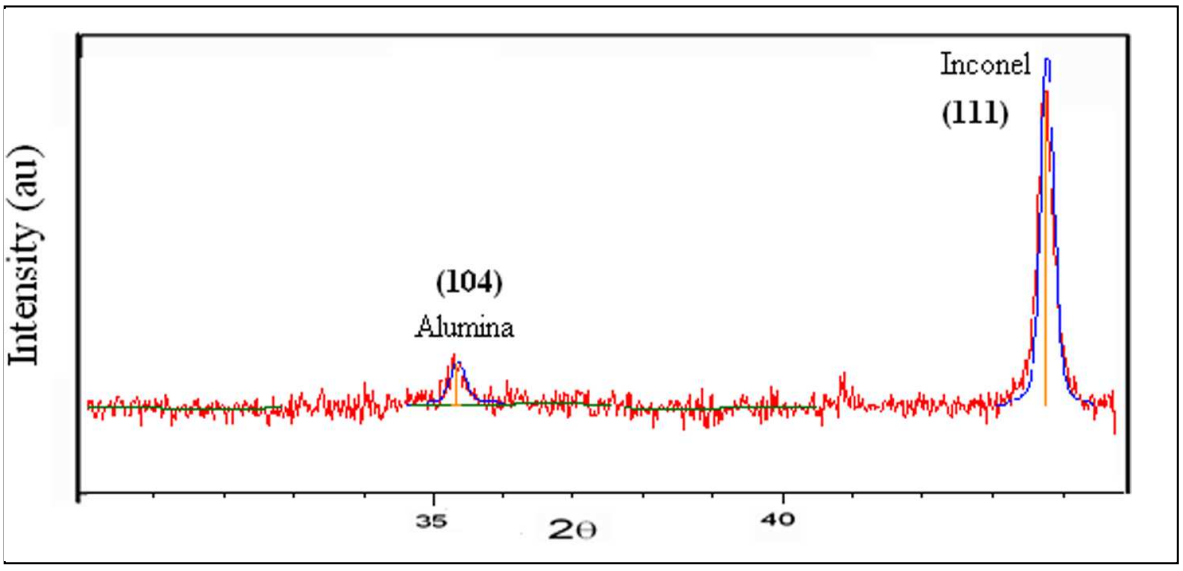

Figure 3.21 XRD of Al_2O_3 coated inconel substrate (slow scan).

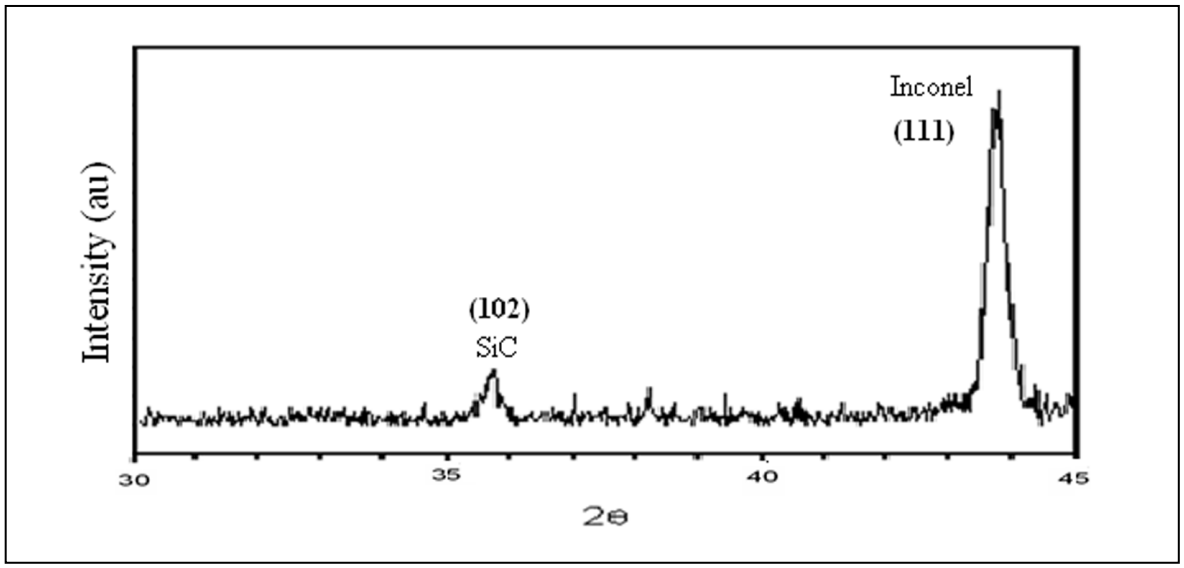

Figure 3.22 XRD of SiC coating on the inconel substrate (slow scan).

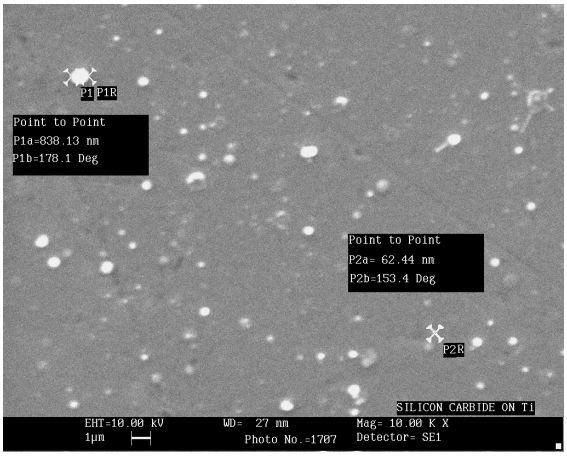

Figure 3.23 SEM image of SiC coated on Ti6Al4V substrate

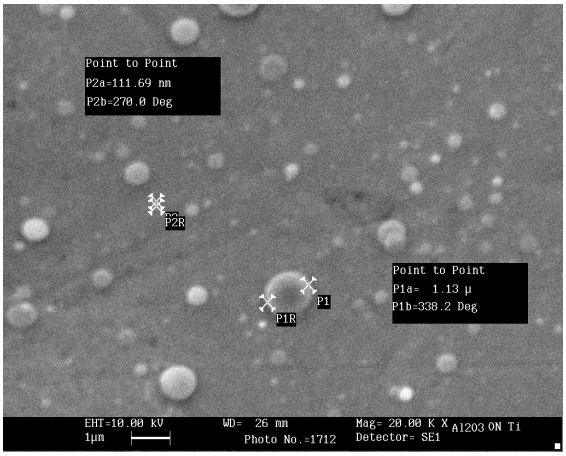

Figure 3.24 SEM image of Al_2O_3 coated on Ti6Al4V substrate

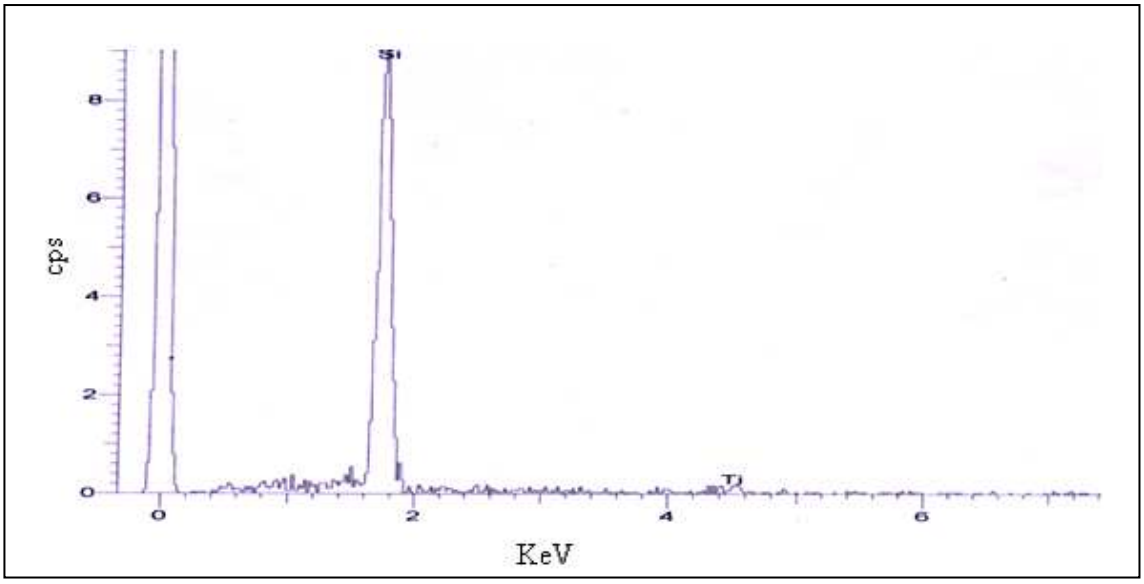

a) EDAX of SiC on Ti6Al4V at 5 KV

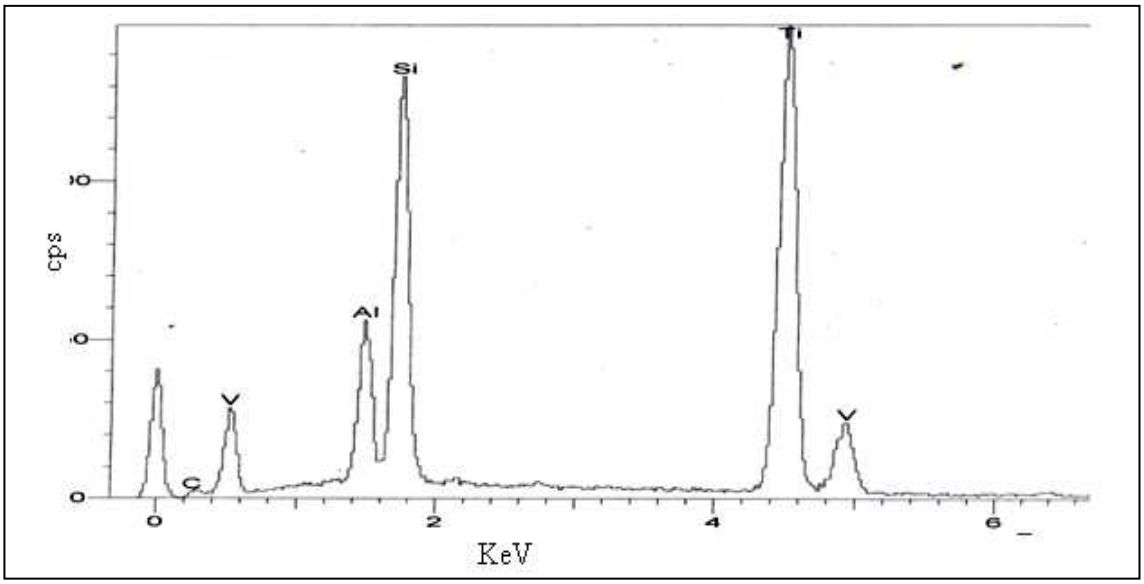

b) EDAX of SiC on Ti6Al4V at 15 KV

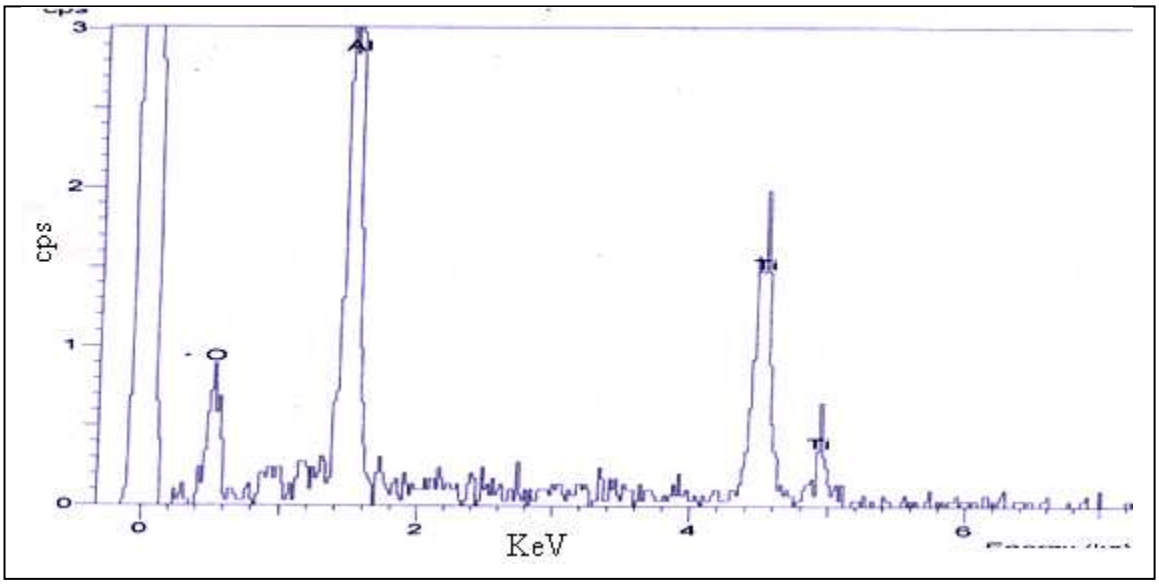

c) EDAX of Alumina on Ti6Al4V at 5 KV

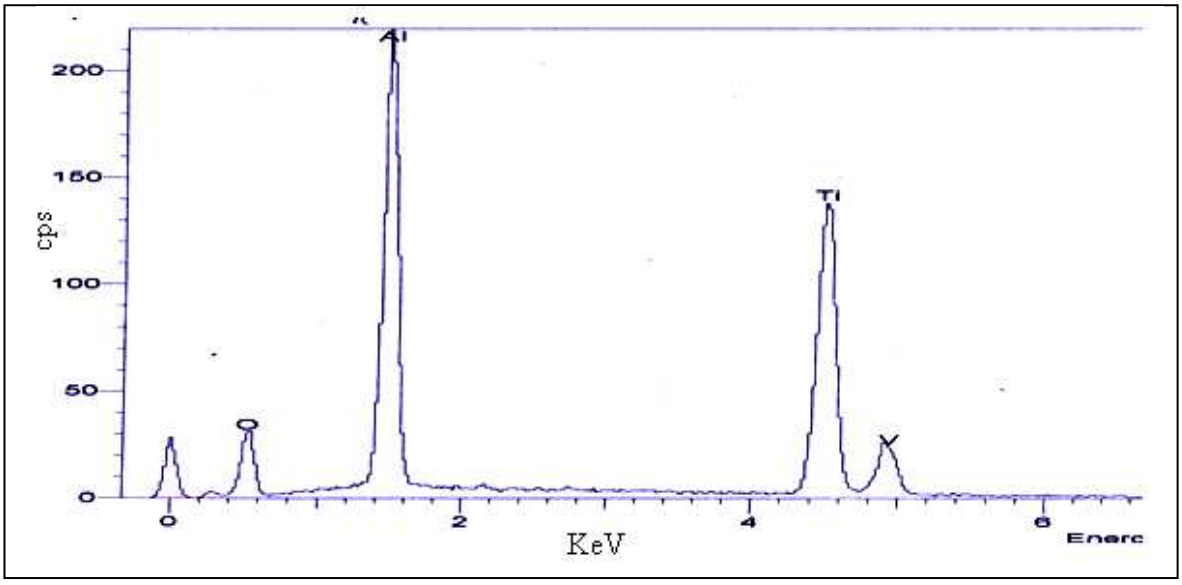

d) EDAX of Alumina on Ti6Al4V at 15 KV

Figure 3.25 a) b) c) and d) EDX of SiC and Al_2O_3 on Ti6Al4V at 5 and 15 KV

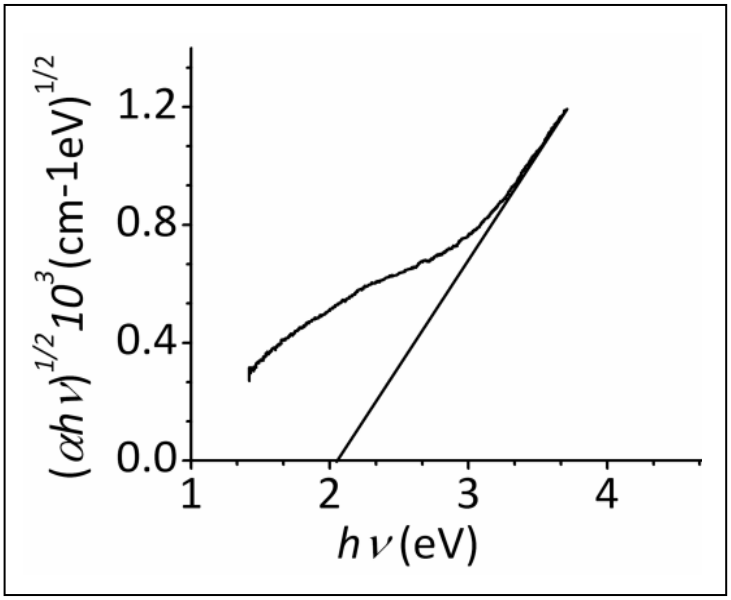

Figure 3.26. Absorption coefficient versus energy of an Al_2O_3 film.

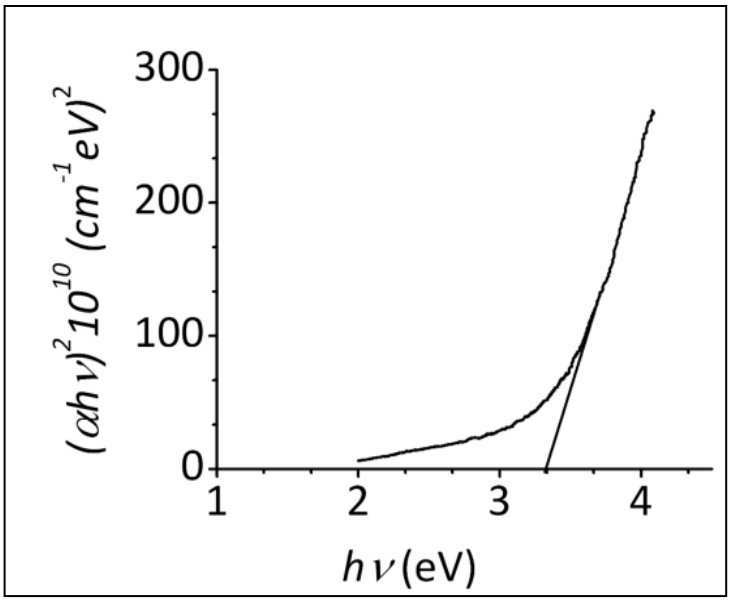

Figure 3.27 Absorption coefficient versus energy of a SiC film.

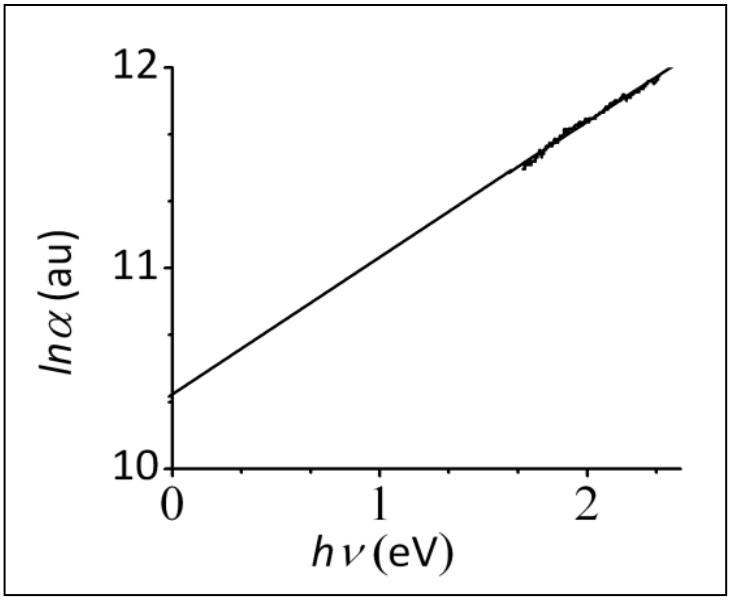

Figure 3.28. lnα as a function of energy (hυ) Al_2O_3 film

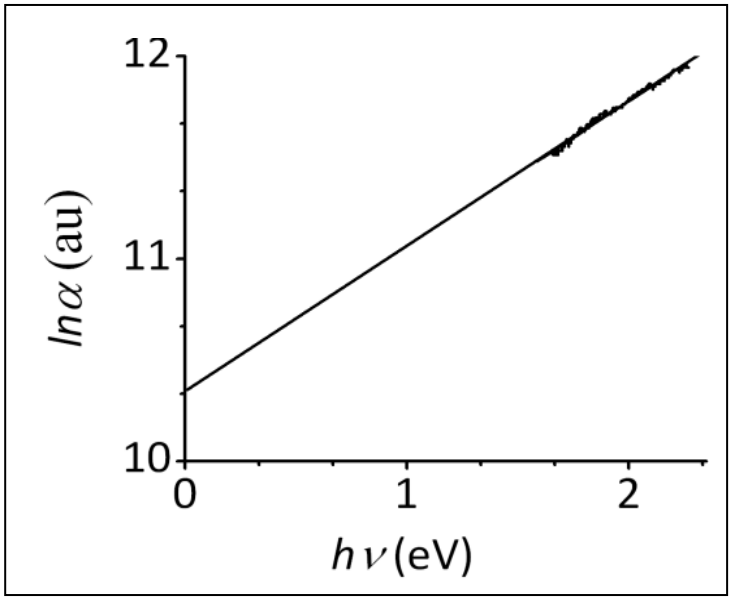

Figure 3.29. lnα as a function of energy (hυ) SiC film .

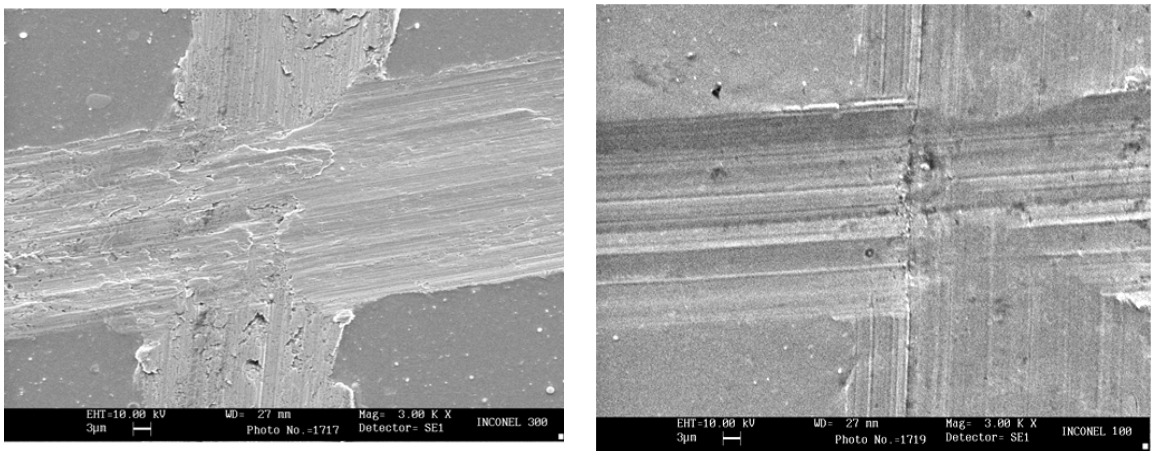

a) b)

Figure 3.30 SEM photograph after adhesion test on SiC film deposited at (a) 200^0C, (b) 450^0C on Ti6Al4V substrate.

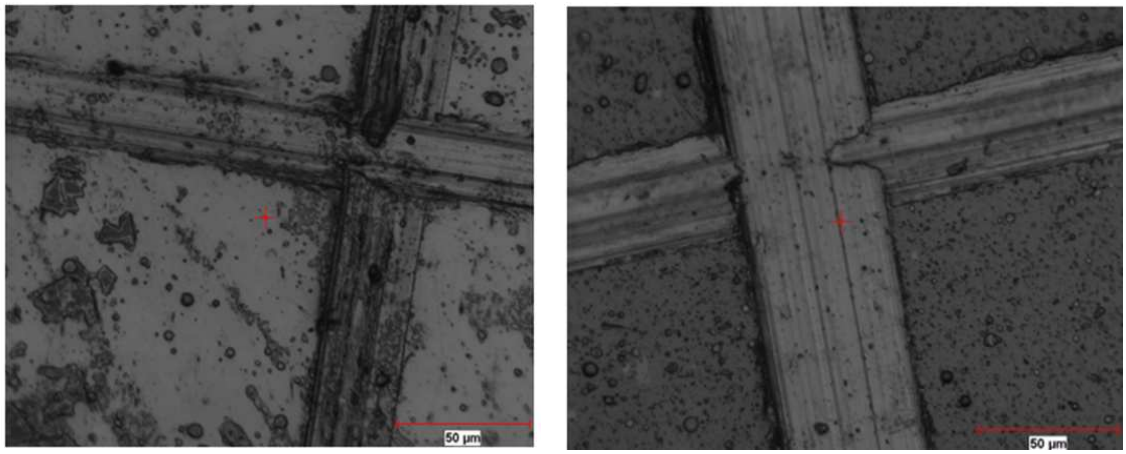

a) b)

Figure 3.31 Surface micrographs after adhesion test on Al_2O_3coated Ti6Al4V substrate at temperatures a) 300^0C and b) 450^0C

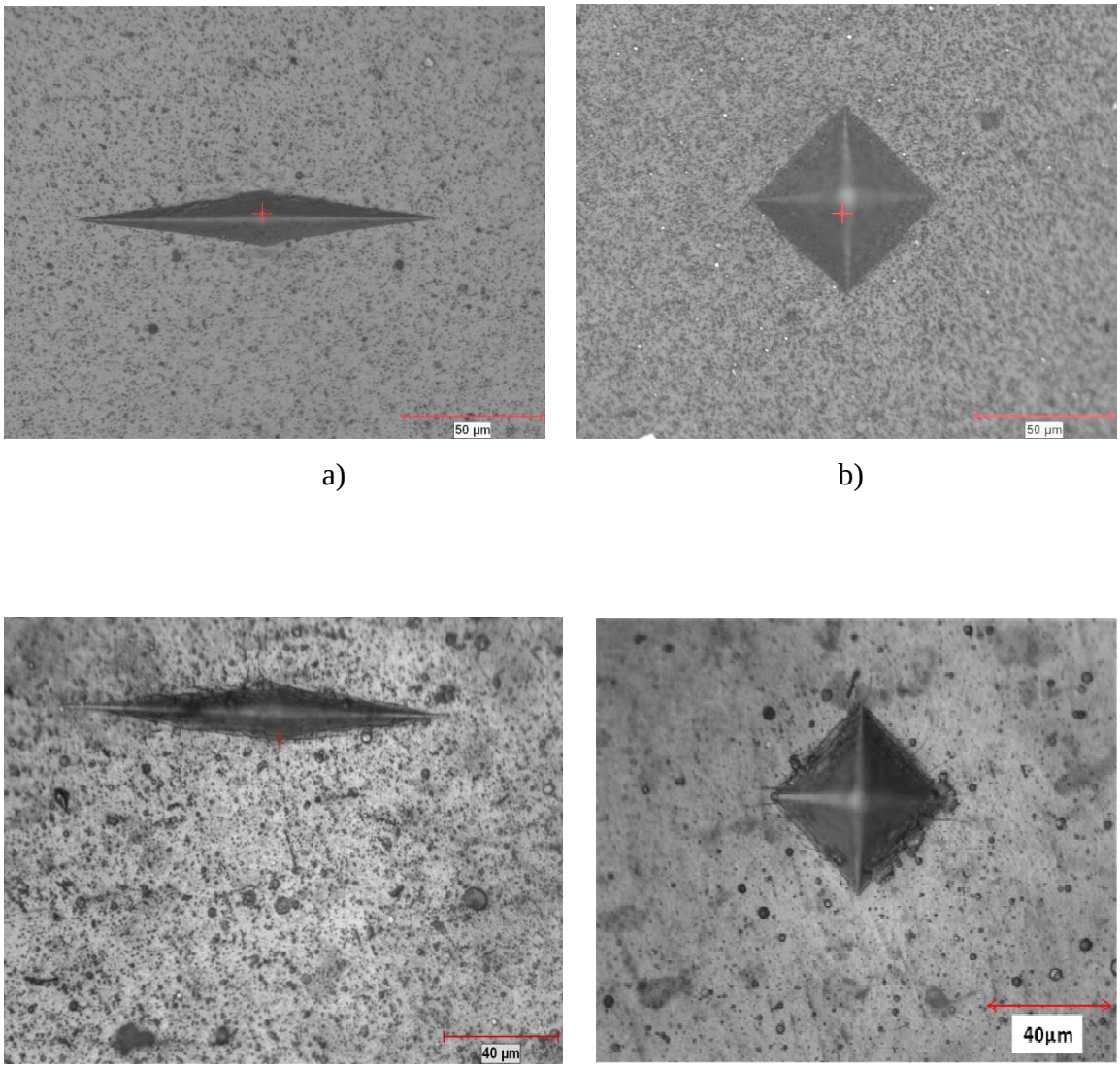

a) b)

d) d)

Figure 4.1 a) and b) Knoop and Vickers impression after indentation on SiC film c) and d) Knoop and Vickers impression after indentation on Al_2O_3 film.

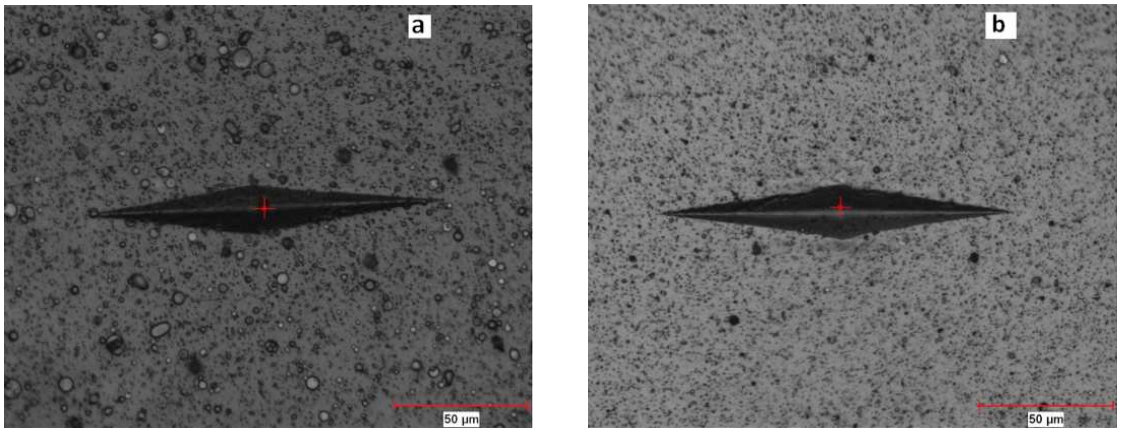

a) b)

Figure 4.2 Knoop indentation on a) Al_2O_3 b) SiC coated film on inconel substrate at 10N load.

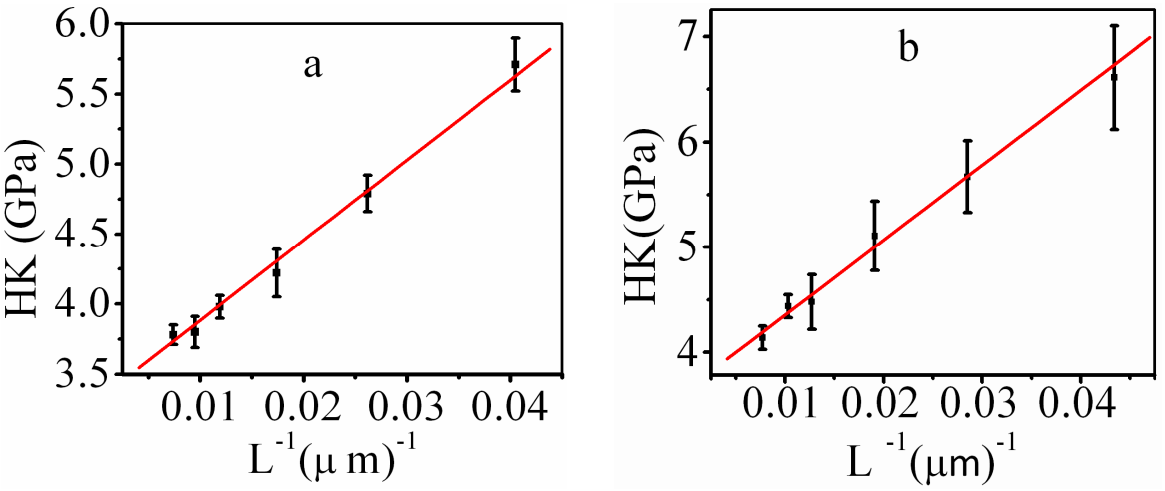

Figure 4.3. Knoop hardness variation with 1/L on a) Al_2O_3 and b) SiC coated film on inconel.

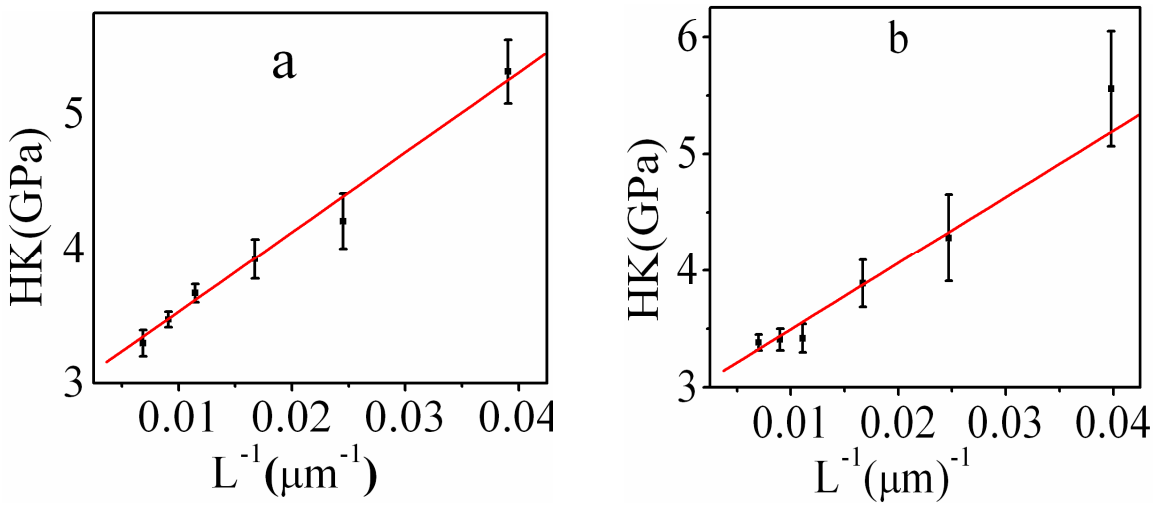

a) b)

Figure 4.4 Knoop hardness variations with 1/L on a) Al_2O_3 and b) SiC coated film on Ti6Al4V.

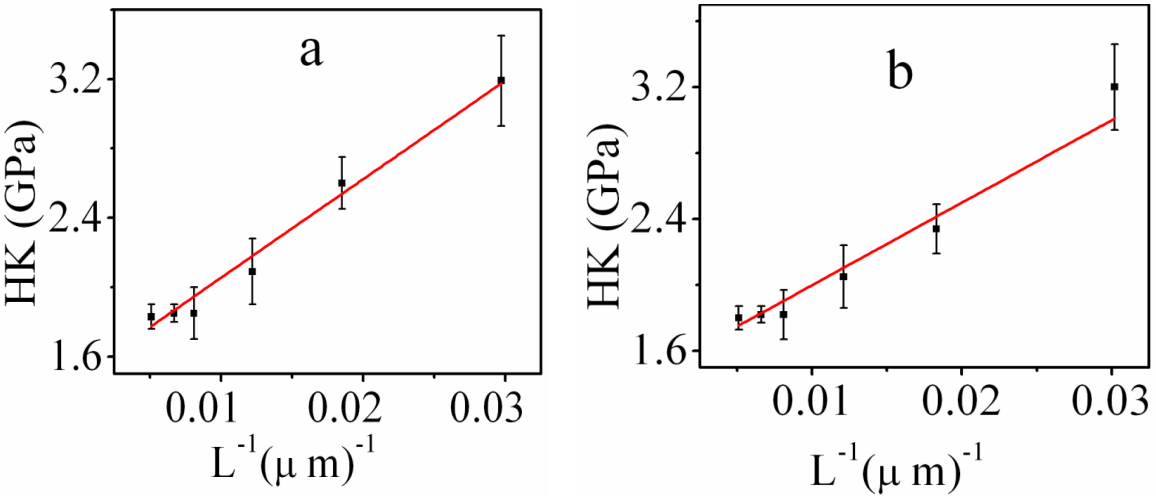

a) b)

Figure 4.5 a) Knoop hardness variations with 1/L on a) Al_2O_3 and b) SiC coated film on titanium.

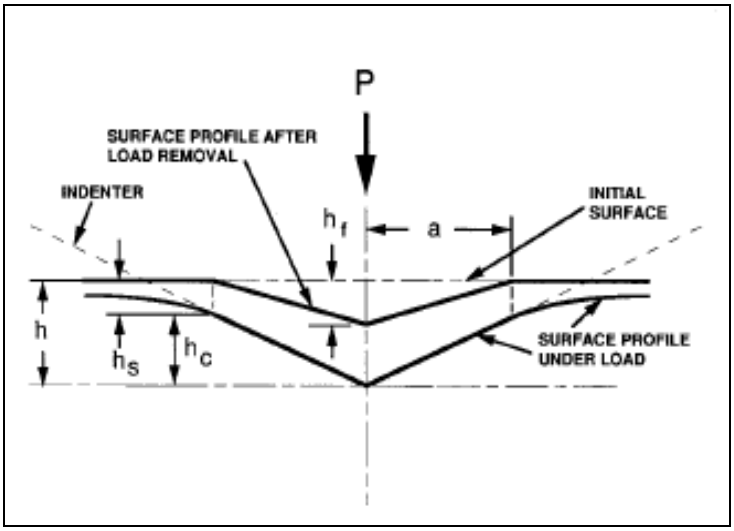

Figure 4.6 Schematic representation of a section through an indentation showing various quantities used in analysis.

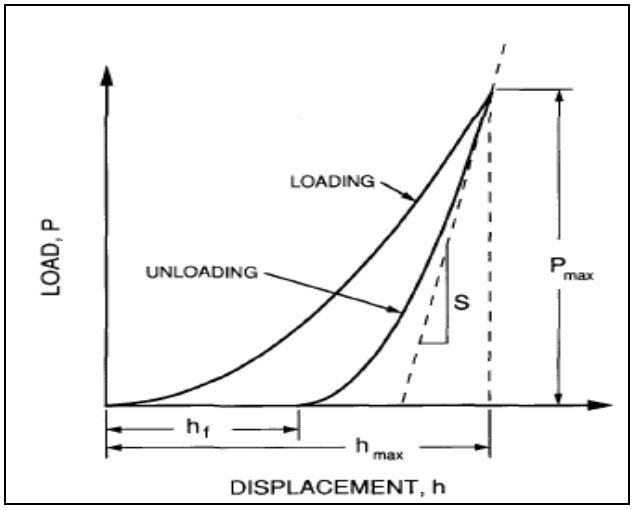

Figure 4.7 Schematic representation of indentation load (P) versus displacement (h) data obtained during one full cycle of loading and unloading.

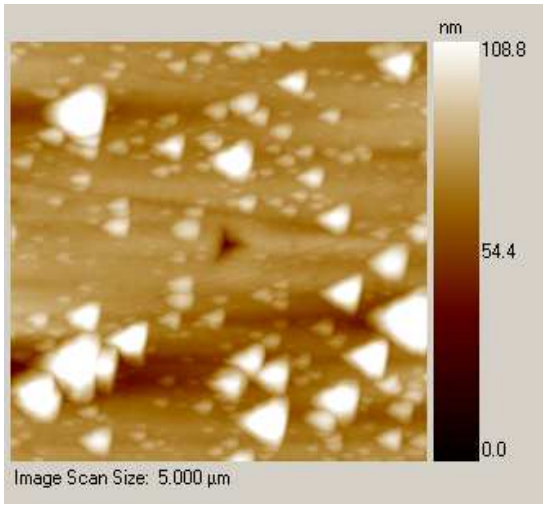

a) Al_2O_3 coating on inconel

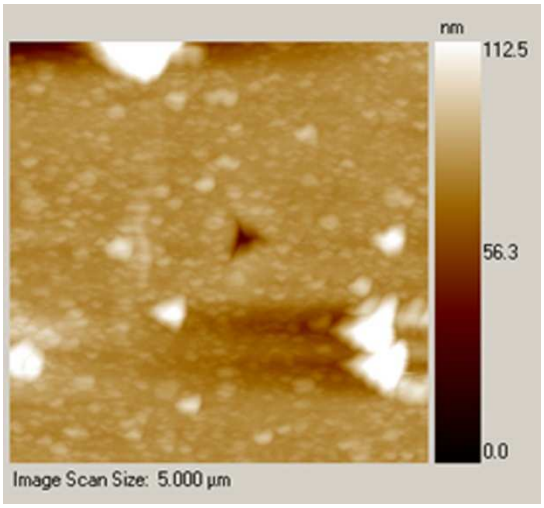

b) SiC coating on inconel

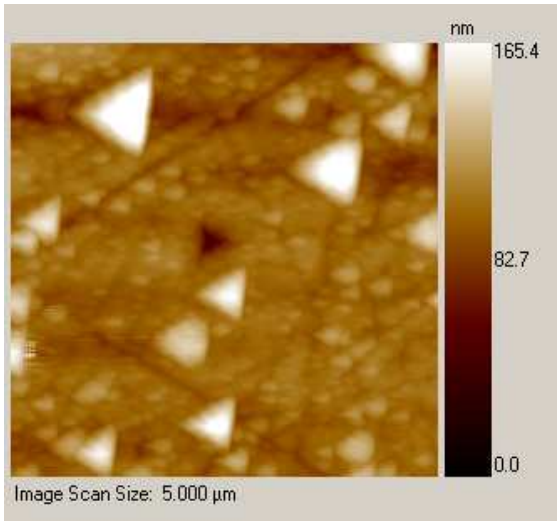

c) Al_2O_3 on Titanium substrate

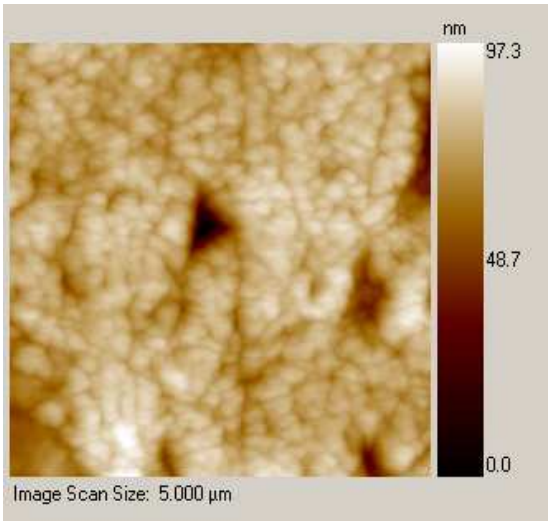

d) SiC on Titanium substrate

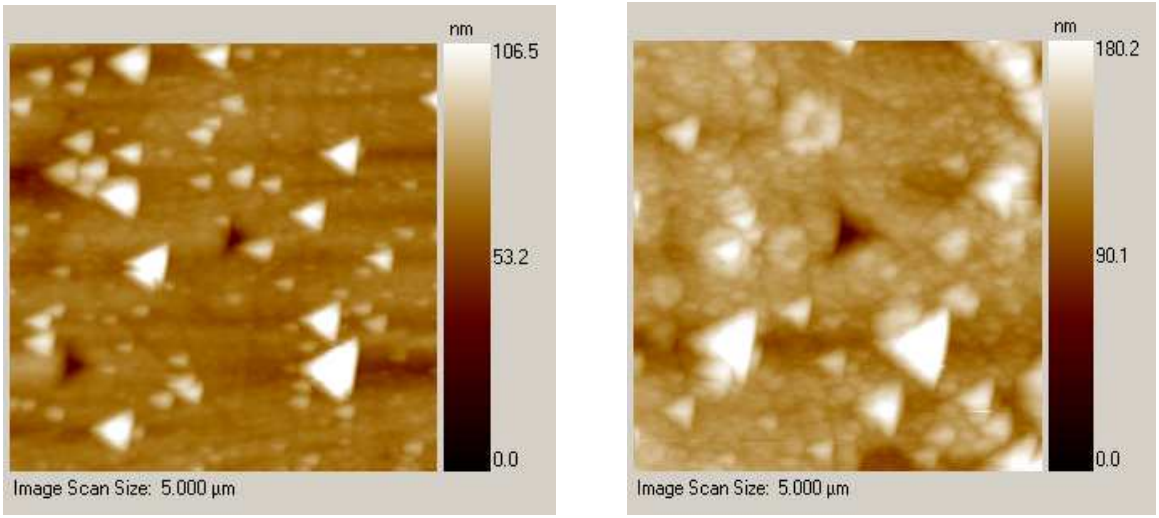

e) Al_2O_3 coating on Ti6Al4V f) SiC coating on Ti6Al4V

Figure 4.8 AFM images of the nanoindentation.

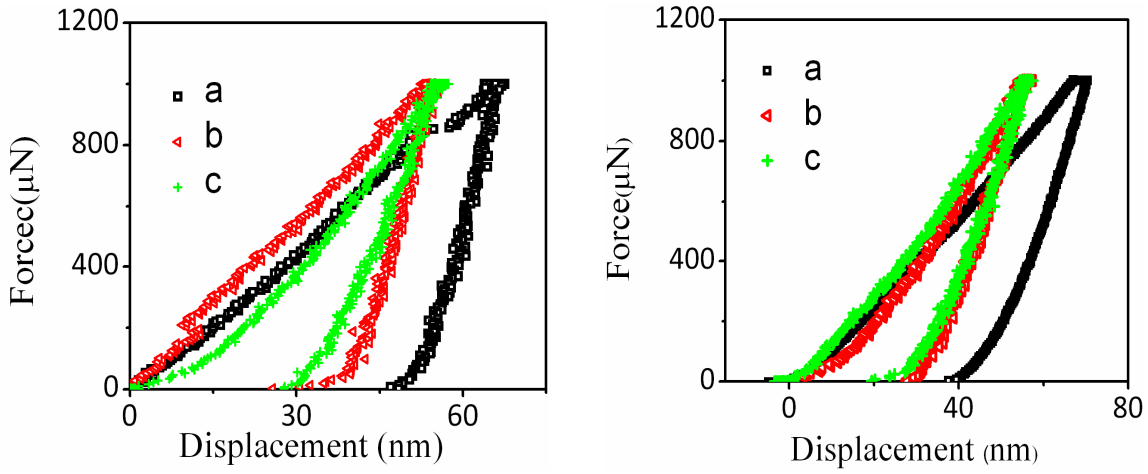

i) ii)

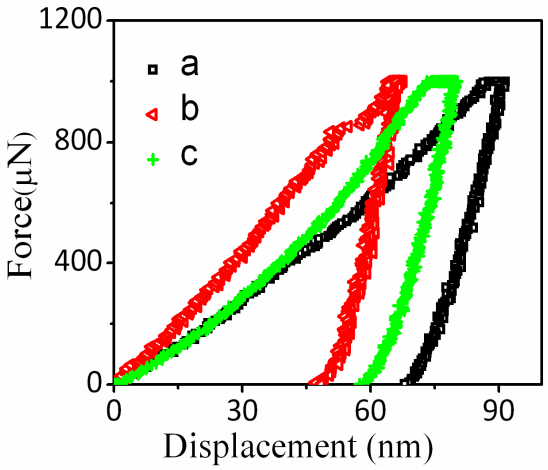

iii)

Figure 4.9 (i) Load variations with nanoindentation depth a) inconel substrate b) Al_2O_3 and c) SiC coating on inconel. ii) Load variations with nanoindentation depth a) Ti6Al4V substrate b) Al_2O_3 and c) SiC coating on Ti6Al4V. iii) Load variations with nanoindentation depth a) titanium substrate b) Al_2O_3 and c) SiC coating on titanium.

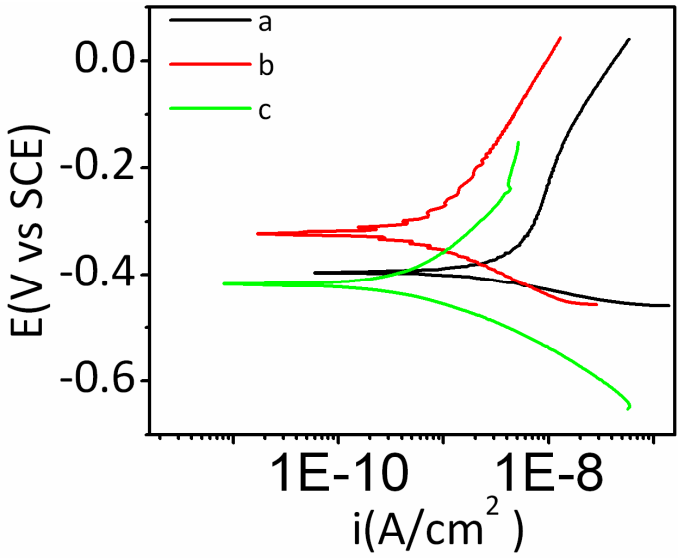

Figure 5.1 Potentiodynamic polarization curves of a) Ti6Al4V, b) Al_2O_3 coated Ti6Al4V and c) SiC coated Ti6Al4V.

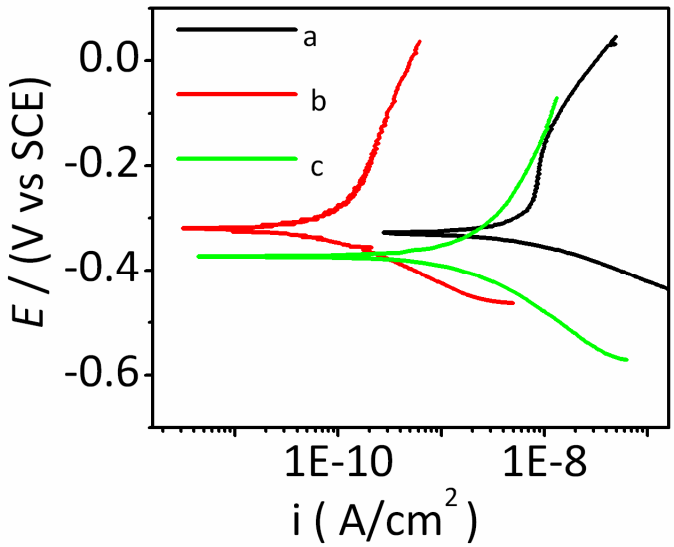

Figure 5.2 Potentiodynamic polarization curves of a) inconel, b) Al_2O_3 coated inconel and c) SiC coated inconel.

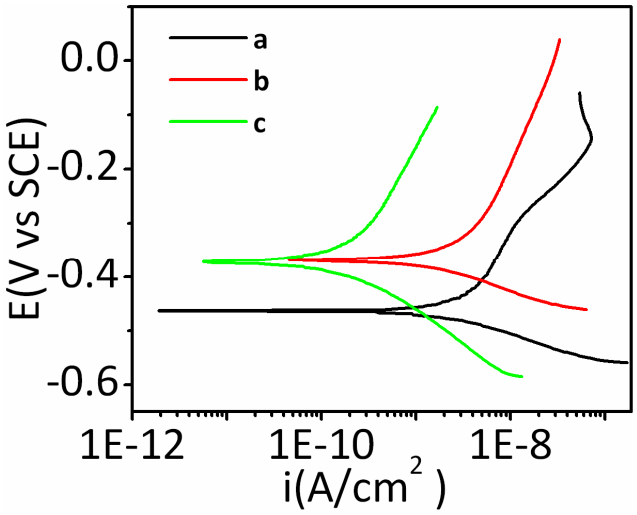

Figure 5.3 Potentiodynamic polarization curves of a) titanium, b) Al_2O_3 coated titanium and c) SiC coated titanium.

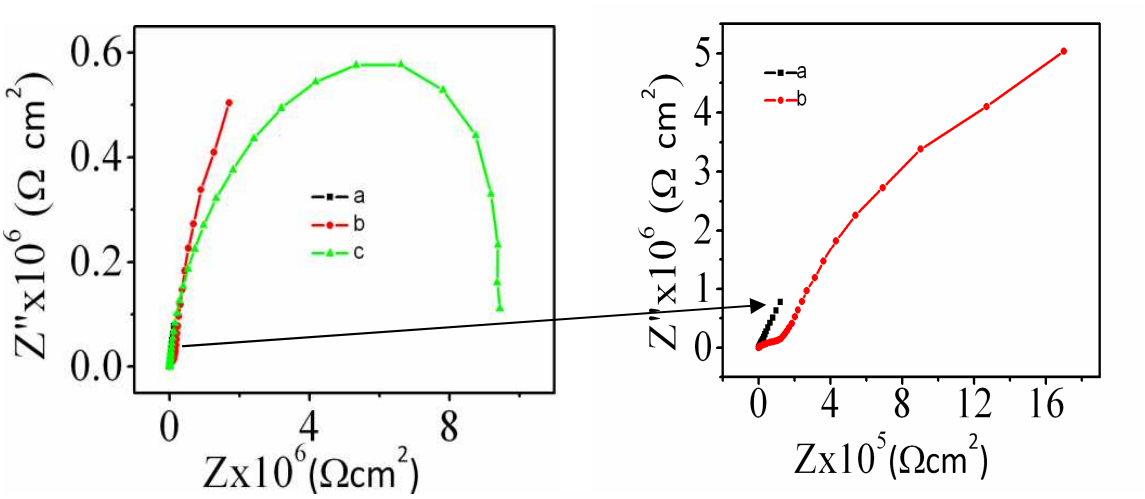

Figure 5.4 Nyquist plots of a) Ti6Al4V, b) SiC and c) Al_2O_3 coatings

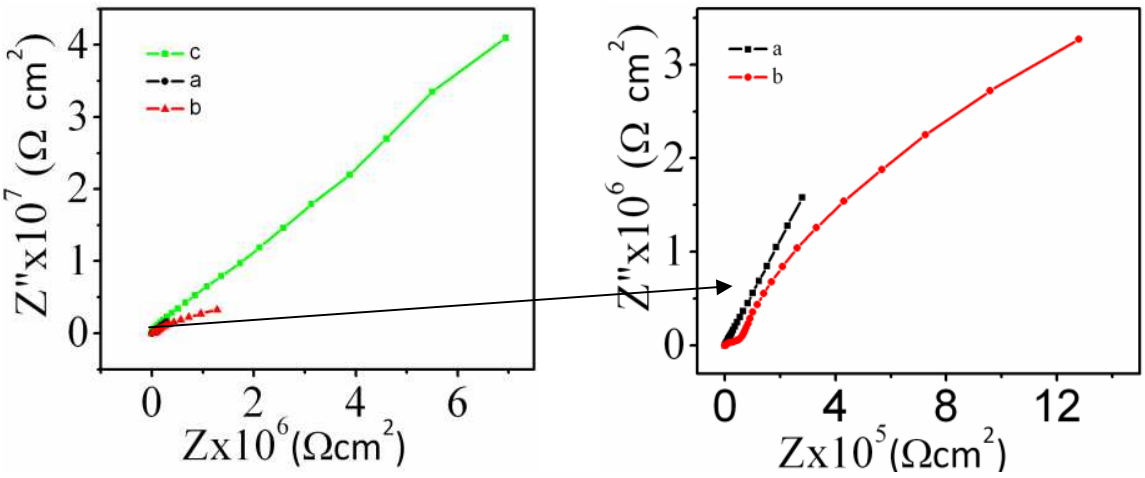

Figure 5.5 Nyquist plot of a) inconel, b) SiC and c) Al_2O_3 coatings

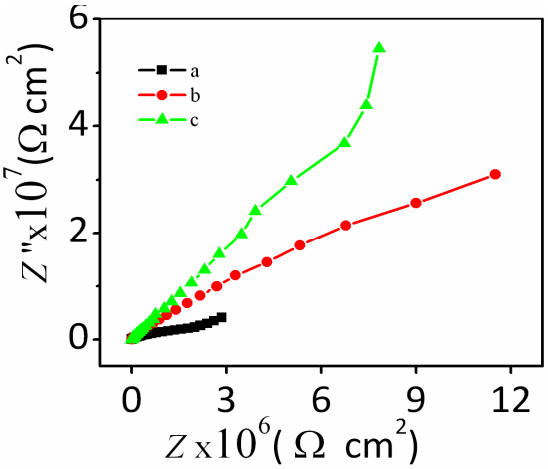

Figure 5.6 Nyquist plots of a) Titanium b) SiC and c) Al_2O_3 coatings

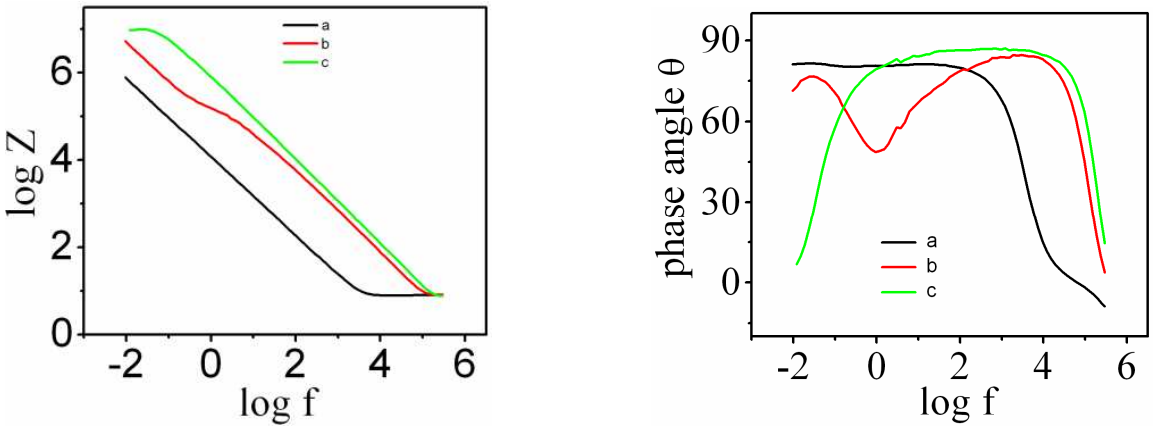

i) ii)

Figure 5.7 i). Bode plots of (log Z vs. log f) of a) Ti6Al4V b) SiC and c) Al_2O_3 coatings. ii). Bode plots of (phase angle Vs log f) of a) Ti6Al4V b) SiC and c) Al_2O_3 coatings.

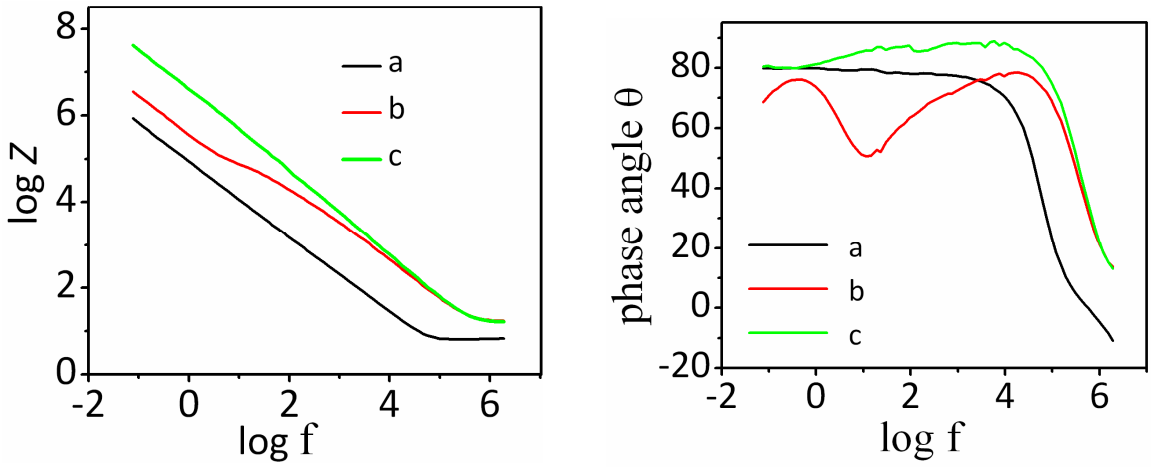

i) ii)

Figure 5.8.i) Bode plots (log |z| vs. log f) of a) inconel, b) SiC and c) Al_2O_3 coatings.

ii) Bode plots (phase angle vs. log f) of a) inconel, b) SiC and c) Al_2O_3 coatings.

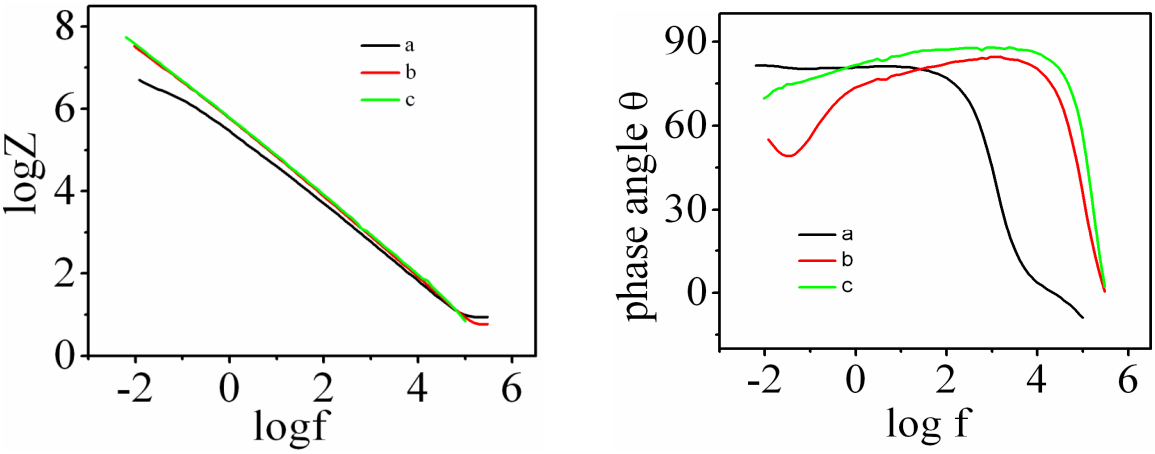

i) ii)

Figure 5.9. i) Bode plots (log |z| vs. log f) of a) titanium, b) SiC and c) Al_2O_3 coatings.

ii) Bode plots (phase angle vs. log f) of a) titanium, b) SiC and c) Al_2O_3 coatings.

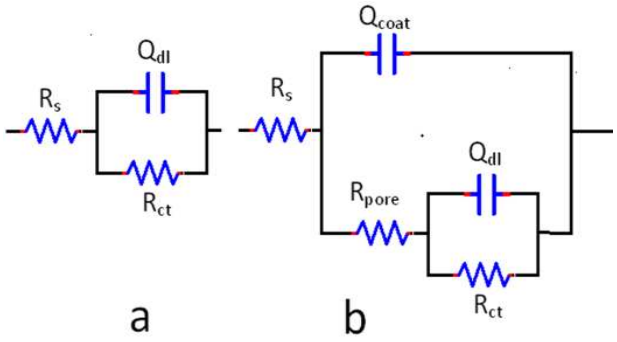

Figure 5.10 a) equivalent circuit to fit the electrochemical impedance data of the inconel substrate and b) equivalent circuit to fit the electrochemical impedance data of the coated substrate.

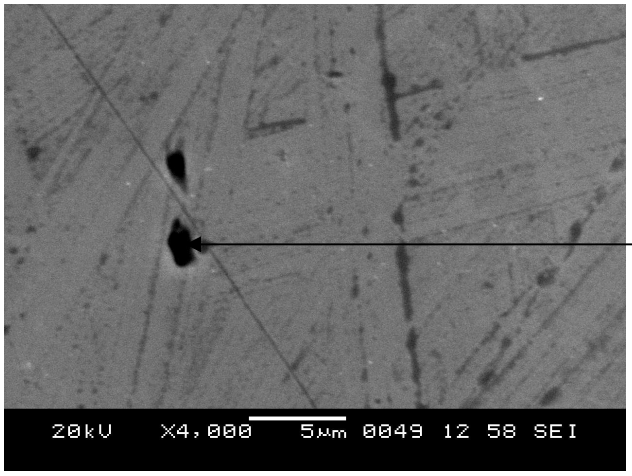

Ti6Al4V

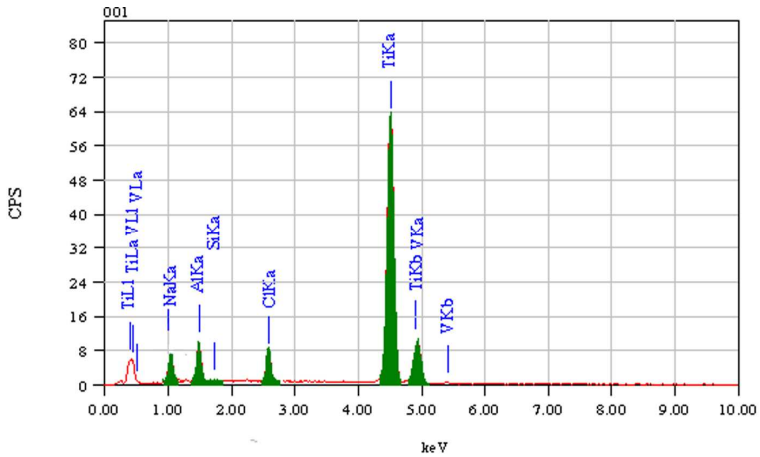

EDAX of Ti6Al4V

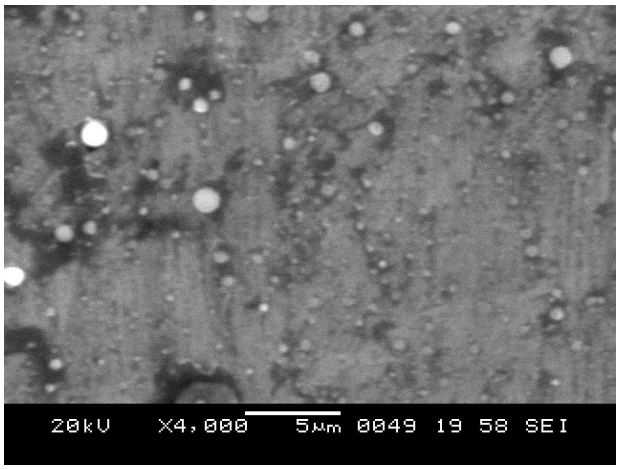

Al_2O_3 coating

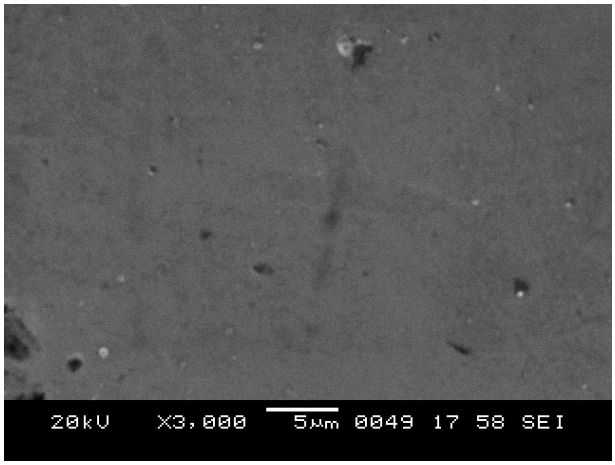

SiC coating

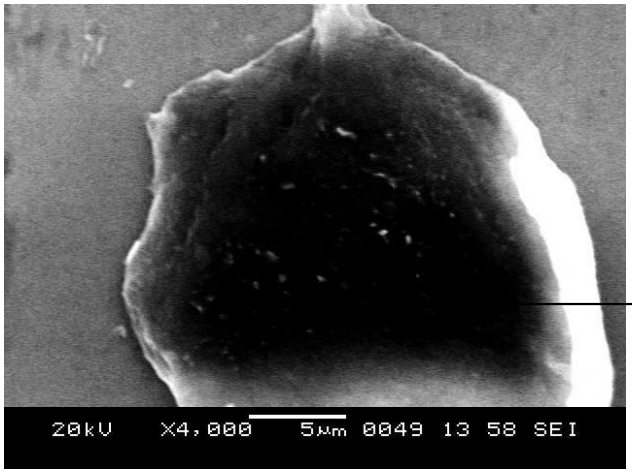

Titanium

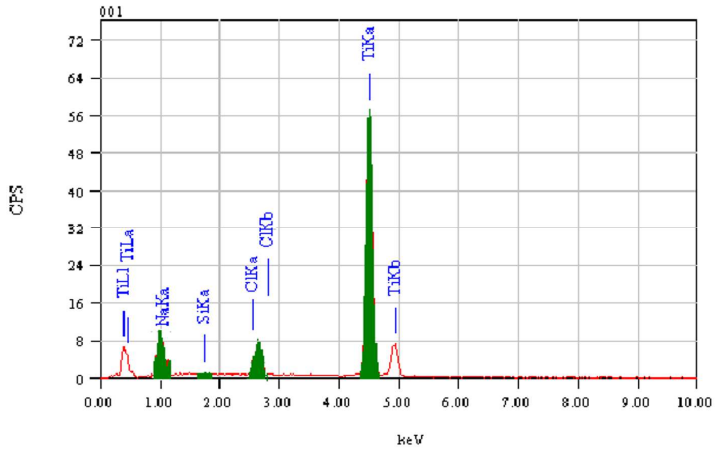

EDAX of Titanium

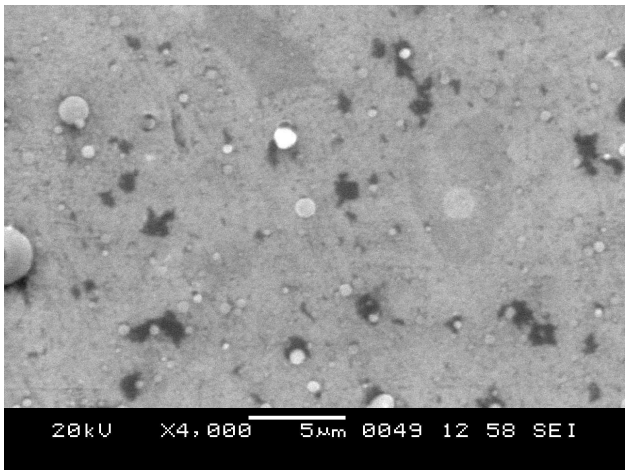

Al_2O_3 coating

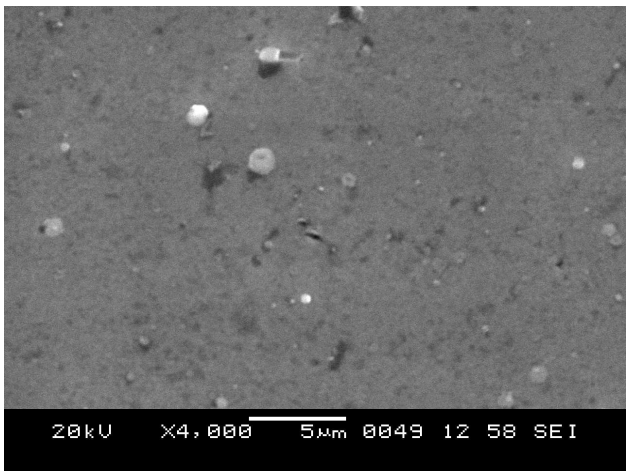

SiC coating

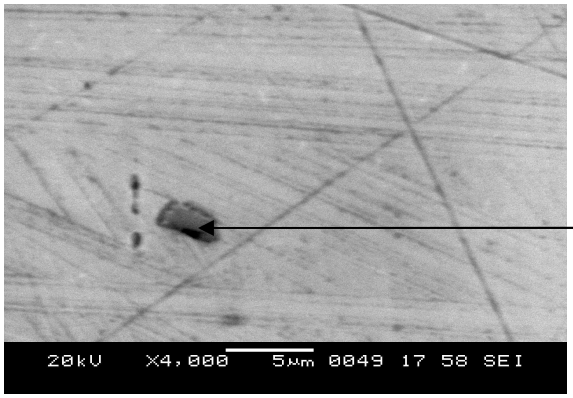

Inconel

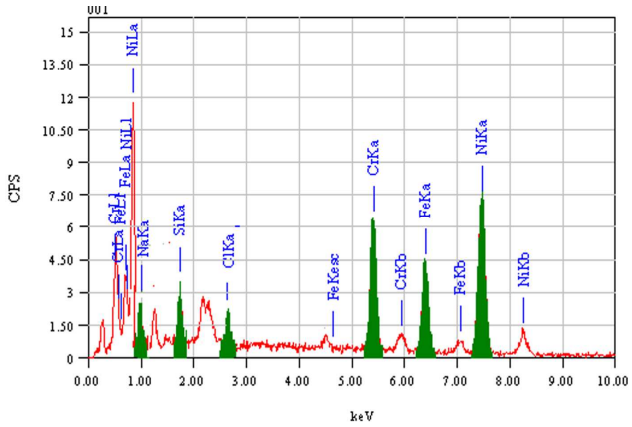

EDAX of Inconel

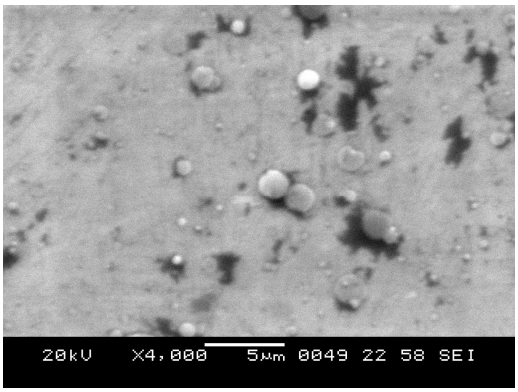

Al_2O_3 coating

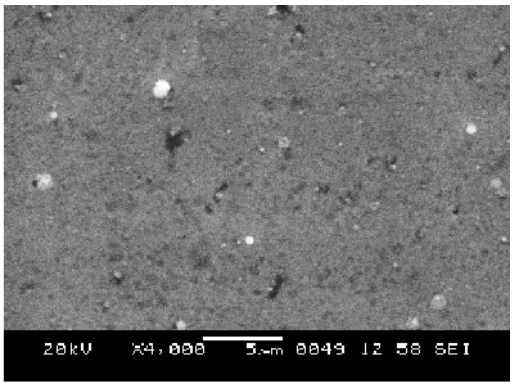

SiC coating

Figure 5.11 Surface morphology of the substrates with SiC and Al_2O_3 coating and EDAX of the substrates after corrosion test.

APPENDIX - II

Table 1.1

Physical properties of Silicon Carbide and Alumina

Item	Unit	Silicon Carbide	Alumina
True Density	Kg/m^3	3210	3980
Crystal system		Hexagonal	Hexagonal
Lattice constant	Å	a-3.0730 , c-15.11	a-4.7588; c-12.992
Knoop Hardness	GPa	25.51	19.6
Melting Point	K	2873	2,323
Specific Heat	KJ/Kg·K	0.63-1.26	0.92-1.26
Heat Conductivity at RT	W/mK	167.6	30.2
Index of refraction		2.55	1.77
Fracture toughness	MPa $m^{0.5}$	4.3	3.5
Coefficient of Thermal Expansion at RT	$\times 10^{-6}/K$	3.8	6.9

Table 3.1

Chemical composition of the titanium

	Titanium (at %)	Silicon (at %)	Iron (at %)
Chemical analysis	99.89	---	0.10
EDAX	99.77	0.23	---

Table 3.2

Chemical composition of the Ti6Al4V

	Titanium (at %)	Vanadium (at %)	Aluminium (at %)
Chemical analysis	92.72	3.91	3.22
EDAX	90.22	2.62	7.16

Table 3.3

Chemical composition of the inconel

	Nickel (at %)	Chromium (at %)	Iron (at %)	Silicon (at %)	Carbon (at %)
Chemical analysis	59.86	19.47	20.36	----	0.21
EDAX	55.88	20.36	19.87	3.89	---

Table.3.4

Comparison of microhardness and average roughness of films deposited at different distances.

Sample	Sample A (d=0.03m)			Sample B (d=0.05m)		Sample C (d=0.10m)
Region	I	II	III	II	III	III
Hardness GPa at 0.245N	10.50	8.58	7.09	8.94	6.91	7.22
Average surface roughness R_a in nm	309	107	87	105	84	79

Table 4.1

Hardness data of coating on Inconel using mathematical model

Coating material	t (μm)	B_s (GPa m^{-1})	B_c (GPa m^{-1})	c	H_{so} (GPa)	H_{fo} (GPa)
Al_2O_3	0.5	37.98	56.90	5.538	3.61	7.0
SiC	0.5	37.98	64.74	5.538	3.61	8.6

Table 4.2

Hardness data of coating on Ti6Al4V and Titanium using mathematical model

Substrates	Coating material	t (μm)	B_s (Gpa m^{-1})	B_c (Gpa m^{-1})	C	H_{so} (GPa)	H_{fo} (Gpa)
Ti6Al4V	Al_2O_3	0.5	23.78	59.27	5.538	2.8	9.2
	SiC	0.5	23.78	56.67	5.538	2.8	8.7
Titanium	Al_2O_3	0.5	37.37	0.012	5.538	1.69	4.0
	SiC	0.5	37.37	6.85	5.538	1.69	5.2

Table 4.3

Hardness and Young's modulus of the silicon carbide coating on different substrates by nanoindentation

Substrate	Hardness before coating (GPa)	Hardness after SiC coating (GPa)	Young's Modulus (GPa)
Inconel	5.64	8.65	197
Ti6Al4V	5.56	9.37	137
Titanium	3.62	5.69	123

Table 4.4

Hardness and Young's modulus of the alumina coating on different substrates by nanoindentation

Substrate	Hardness before coating (GPa)	Hardness after Al_2O_3 coating (GPa)	Young's Modulus (GPa)
Inconel	5.64	7.74	216
Ti6Al4V	5.56	8.7	147
Titanium	3.62	4.34	141

Table 4.5

Comparison of hardness values of SiC /Alumina coating on different substrates

Substrate	SiC coating		Al_2O_3 coating	
	Model	Nanoindentation	Model	Nanoindentation
Ti6Al4V	8.7	9.35	9.2	8.7
Inconel	8.6	8.65	7.0	7.74
Titanium	5.0	5.68	4.0	4.22

Table 5.1

Potentiodynamic polarization measurements.

	Ti6Al4V	SiC	Al_2O_3
b_a (V/decade)	613.6e-3	299.3e-3	164.2e-3
b_c (V/decade)	83.80e-3	112.2e-3	81.80e-3
I_{corr} ($\mu A/m^2$)	0.54	0.085	0.0457
E_{corr} (mV)	-395.0	-322.0	-419.0
Corrosion rate (μmpy)	47.55	23.76	12.78
Rp($M\Omega\ cm^2$)	5.93	41.7	51.9

Table 5.2

Potentiodynamic polarization measurements.

	Inconel	SiC	Al_2O_3
b_a (V/decade)	110.9 e-3	125.9e-3	62.59e-3
b_c (V/decade)	44.9e-3	78e-3	165.5e-3
I_{corr} ($\mu A/m^2$)	0.369	0.1007	0.0235
E_{corr} (mV)	-328.0	-372.0	-321.0
Corrosion Rate(μmpy)	44.00	29.95	12.78
Rp($M\Omega\ cm^2$)	3.76	19.6	83.9

Table 5.3

Potentiodynamic polarization measurements.

	Titanium	SiC	Al_2O_3
b_a (V/decade)	680 e-3	266e-3	363e-3
b_c (V/decade)	93 e-3	98e-3	136e-3
I_{corr} (nA/cm^2)	5.06	2.86	0.255
E_{corr} (mV)	-463.0	-369.0	-372.0
Corrosion Rate(µmpy)	43.68	37.96	7.139
Rp($M\Omega\ cm^2$)	7.02	10.9	168

Table 5.4

EIS data obtained by equivalent circuit simulation of SiC and Al_2O_3 coatings.

Sample	R_s (Ωcm^2)	$Q_{dl}-Y_0$ ($\mu F/cm^2$)	n_d	R_{ct} ($M\Omega cm^2$)	$Q_{coat}-Y_0$ ($\mu F/cm^2$)	n_c	R_{pore} ($M\Omega cm^2$)
Inconel	15.46	2.07	0.8	0.89			
Inconel/SiC	14.66	0.212	0.89	21.07	0.73	0.87	7.66
Inconel/Al_2O_3	15.82	0.16	0.99	108	0.085	0.74	18.6
Ti6Al4V	7.46	15	0.9	0.0324			
Ti6Al4V /SiC	7.37	0.411	0.94	14.3	1.9	0.86	11.7
Ti6Al4V / Al_2O_3	7.05	0.1305	1.0	50.9	0.0927	0.79	10.0
Titanium	5.4	0.3066	0.8	0.779			
Titanium / Al_2O_3	10	0.107	0.8	97.4	0.0605	0.76	12.2
Titanium / SiC	8.26	0.342	0.97	59	0.57	0.57	18.1

References

- Agostinelli, E., Kaciulis, S., Vittori-Antisari, M. (2000). “Great reduction of particulates in pulsed laser deposition of Ag–Co films by using a shaded off-axis geometry.” Appl. Surf. Sci. 156, 143.
- Askeland, D.R., (2007). “The Science and engineering of materials.” 2nd ed, page 443.
- Atul Khanna, Deepak, G.B, Adrian Harris, Ben, D.B. (2006). “Structure-property correlations in aluminum oxide thin films grown by reactive AC magnetron sputtering.” Surface and Coatings Technology, 20, 1109-1116.
- Audoly, B. (2000). “Mode-dependent toughness and the delamination of compressed thin films.” Journal of the Mechanics and Physics of Solids. 48, 2315–2332.
- ASM Metals Handbook (1990). Volume 2, 10th ed. Materials Park, Ohio, USA pp 586–591.
- Barry, C., Grant Norton, M. (2007). “Ceramic materials science and engineering.” Springer science, New Yark USA.
- Bauerle, D. (2000). “Laser processing and chemistry” 3rded, Spinger, Berlin, Heidelberg.
- Beegan D., Chowdhury S., Laugier M.T.(2008). “Modification of Composite Hardness Models to Incorporate Indentation Size Effects in thin Films.” Thin Solid Films. 516(2), 3813–3817.
- Boyd, W. (1996). “Thin Film Growth by Pulsed Laser Deposition.” Ceramics International 22, 429-434.
- Boyer, R. R. (1996). “An overview on the use of titanium in the aerospace industry.” Materials Science and Engineering A, 213, 103–114.
- Burnett, P.J., Rickerby, D.S. (1987). “The mechanical properties of wear-resistant coatings: I: Modelling of hardness behaviour.” Thin Solid Films, 148(1), 41-50.

- Cai, X., Bangert, H. (1995). “Hardness measurements of thin films-determining the critical ratio of depth to thickness using FEM.” Thin solid films 264(1), 59.
- Chicot, D. Lesage, J. (1995). “Absolute hardness of films and coatings.” Thin Solid Films, 254(2), 123-130.
- Chrisey, D. B. and Hubler, G. K. (1994). “Pulsed Laser Deposition of Thin Films.” John Wiley & Sons Inc., New York,
- Christoph, L. and Manfred, P. (2003). “Titanium and Titanium Alloys. Fundamentals and Applications.” WILEY-VCH Verlag GmbH & Co. KGaA, Weinheim, 1.3 – 9.
- Chopra, K. L., (1969). “Thin films phenomena.” McGraw- Hill book company, New York.
- Cibert, C., Hidalgo. H., Champeaux. C., Tristant, P., Tixier, C., Desmaison, J., Catherinot, A. (2008). “Properties of aluminium oxide thin films deposited by pulsed laser deposition and plasma enhanced chemical vapor deposition.” Thin solid films, 516(6), 1290- 1296.
- Colin, E.W., Julian, D.C.J. (2004). “Handbook of Laser technology and applications.” Taylor & Francis,Volume III, IOP publishing Ltd.
- Collings, E.W. (1984). “The Physical Metallurgy of Titanium Alloys, American Society for Metal.” Metals Park, Ohio.
- Dean, S. W. Houston, National Association of Corrosion Engineers, 1977, 52–60.
- Donachie, M. J. Jr., (2000). “Relationship among Structure, Processing and Properties, Titanium: A Technical Guide.” 2nd ed, American Society for Metals, Metals Park, Ohio.
- Esteve, J., Lousa, A., Martinez, E., Huck, H., Halac, E.B., Reinoso, M. (2001). “Amorphous Si_xC_{1-x} films: an example of materials presenting low indentation hardness and high wear resistance.” Diamond and related materials, 16(3), 1053-1057.

- Ferro, D. Barinov, S.M., Rau, J.V., Latini, A., Scandurra, R., Brunetti, B. (2006). "Vickers and Knoop hardness of electron beam deposited ZrC and HfC thin films on titanium." Surface Coatings and Technology, 200(16), 4701-4707.
- Galliano, F., Galvanetto, E., Mischler,S., Landolt, D. (2001). "Tribocorrosion behavior of plasma nitride Ti–6Al–4V alloy in neutral NaCl solution." Surface and Coatings Technology, 145 (3), 121-131.
- Garbacz, H., Widlickil, P. Wierzchoń, T., Kurzydłowski, G.H, Widlickil, P., Wierzchoń, T., Kurzydłowski, K. J. (2006). "Effect of the Al_2O_3+Ni–Al multilayer on the mechanical properties of Inconel 600 alloy." Surface & Coatings Technology, 200(22), 6206–6211.
- Geohegan, D.B., Puretzky, A.A., Rader, D.J. (1999). "Gas-phase nanoparticle formation and transport during pulsed laser deposition of $Y_1Ba_2Cu_3O_{7-d.}$" Appl. Phys. Lett., 74, 3788.
- Goodwin, T.J., Leppert, V.J., Risbud, S.H., Kennedy, I.M., Lee, H.W.H. (1997). "Synthesis of gallium nitride quantum dots through reactive laser ablation." Appl. Phys. Lett., 70, 3122.
- Gottmann. J., Husmann, A., Klotzbiicher, T., Kreutz, E.W. (1998). "Optical properties of alumina and zirconia thin films grown by pulsed laser deposition." Surface and Coatings Technology, 100, 415-419.
- Gottmann, J. Kreutz, E.W. (1999). "Pulsed laser deposition of alumina and zirconia thin films on polymers and glass as optical and protective coatings." Surface and Coatings Technology, 116, 1189-1194.
- Gruss, K. A. and Davis, R. F. (1999). "Adhesion measurement of zirconium nitride and amorphous silicon carbide coatings to nickel and titanium alloys." Surface and Coatings Technology, 114(3), 156-168.
- Guillemot, G., Iost, A., Chicot, D. (2010). "Comments on the paper "Modification of composite hardness models to incorporate indentation size effects in thin films", D. Beegan, S. Chowdhury and M.T. Laugier, Thin Solid Films 516 (2008), 3813–3817." Thin Solid Films, 518(8), 2097–2101.

- Haanappel, V.A.C., Van Corbach, H.D. Fransen, T. Gellings, P.J. (1995). "Properties of alumina films prepared by low-pressure metal-organic chemical vapour deposition." Surface coat. Tech, 72, 13.
- Harish,C., Barshilia, Yogesh, K., Rajam, K.S. (2006). "Deposition of TiAlN coatings using reactive bipolar-pulsed direct current unbalanced magnetron sputtering." Surface and Coatings Technology, 201(2), 329-337.
- Ho, S.K, Brechtel, F.J., Fowler, T.K. (1993). "A simple scaling approach to calculate activation radiological hazards in a silicon carbide first wall." Fusion Technology, 23, 321.
- Hirschauer, B. et al., (1997). "Highly oriented α-alumina films grown by pulsed laser deposition." Thin Solid Films, 305 243-247.
- Hirschauer, B., Soderholm, S., Paul, J., Flodstrom, A. S. (1996). "Large area synthesis of thin alumina films by laser ablation." Applied Surface Science, 99(4) 285-291
- Horwitz, J. S., Grabowski, K. S., Chrisey, D.B. and Leuchtner, R. E. (1991). "I*n situ* deposition of epitaxial $PbZr_xTi_{(1-x)}O_3$ thin films by pulsed laser deposition" Appl. Phys. Lett. 59, 1565.
- Horwitz J S, Grabowski K S, Chrisey D B and Leuchtner R E (1991). "*In situ* deposition of epitaxial $PbZr_xTi_{(1-x)}O_3$ thin films by pulsed laser deposition ." Appied. Physics. Letters. 59 1565
- http://www.tkk.fi/Units/AES/projects/prlaser/thesis/thesis.html 7.11.2005)
- http://www.schmitt-ind.com/support-technical-papers-scatter.shtml/ 10/12/2010.
- Iost, A. Bigot, R. (1996). "Hardness of coatings." Surface and Coatings Technology, 80(2), 117-120.
- Iost, A. (1998). "Knoop hardness of thin coatings." Scripta Materialia, 39: 231-238.
- Jamey, S. P, Matthew, E. R, Steven, M. D (2000), "Characterization of crystalline SiC films grown by pulsed laser deposition." Thin Solid Films, 371(2), 72-79.

- Jeong-Hoon Ahn, Dongil Kwon. (2000). “Micromechanical estimation of composite hardness using nanoindentation technique for thin-film coated system.” Materials Science and Engineering A, 285(2), 172–179.
- John, B.W. and Richard, A.H. (1993). “Ceramic films and coatings.” Noyes publications Park Ridge, New Jersey, U.S.A.
- Jonsson, B., Hogmark, S. (1984) “Hardness measurements of thin films.” Thin Solid Films, 114(3), 257.
- Jipo Huang, Lianwei Wang, Jun Wen, Yuxia Wang, Chenglu Lin, Mikael Ostling. (1999). “Effect of annealing on SiC thin films prepared by pulsed laser deposition.” Diamond and Related Materials, 8(12), 2099-2102.
- Katharria, Y.S., Sandeep Kumar, Choudhary, R.J., Ram Prakash, Singh, F., Lalla, N.P., Phase, D.M., Kanjilal, D. (2008). “Pulsed laser deposition of SiC thin films at medium substrate temperature.” Thin solid films,516(18),6083-6087)
- Kessler, O., Surm, H., Hoffmann, F., Mayr, P. (2002). “Enhancing surface hardness of titanium alloy Ti6Al4V by combined nitriding and CVD coating.” Surface Engineering, 18, 299-304.
- Kidoh, H., Morimoto, A., Shimizu, T. (1991). “Synthesis of ferromagnetic Bi-substituted yttrium iron garnet films by laser ablation.” Appl. Phys. Lett., 59, 237.
- Kingery, W.D. Bowen, H.K. and Uhlmann, D.R. (1976). “Introduction of ceramics.” 2nd ed., Weley: New York.
- Korsunsky, A.M., McGurk, M.R., Bull, S.J., Page, T.F. (1998) “On the hardness of coated systems” Surf. Coat. Technol., 99(2). 171-183.
- Kuzma, M., Bester, M., Pyziak, L., Stefaniuk, I., Virt, I. (2000). “Modeling of growth of thin solid films obtained by pulsed laser deposition.” Applied. Surface. Science 168, 132-135.
- Lowndes, D.H., Geohegan, D.B., Puretzky, A.A., Norton, D.P., Rouleau,C.M.,″ *(1996).* “Synthesis of Novel Thin-Film Materials by Pulsed Laser Deposition *Science.”* Science 273, 898-903.

- Lowndes, D.H., Miller, J.C., Haglund, R.F. (1998). “Experimental Methods in the Physical Sciences.” Vol. 30, Academic Press, New York, 475.
- Lidong, Z. and Erich, L. (2002). “Reactive plasma spraying of TiAl6V4 alloy.” Wear, 253(12), 1214-1218.
- Liu, C., Bi, Q., Leyland, A., Matthews, A. (2003), “An electrochemical impedance spectroscopy study of the corrosion behavior of PVD coated steels in 0.5 N NaCl aqueous solution: Part I. Establishment of equivalent circuits for EIS data modelling” Corrosion Science 45, 1243–1256.
- Liu, C., Bi, Q., Leyland, A., Matthews, A. (2003). “An electrochemical impedance spectroscopy study of the corrosion behavior of PVD coated steels in 0.5 N NaCl aqueous solution: Part I. Establishment of equivalent circuits for EIS data modelling.” Corrosion Science, 45(6), 1243-1256.
- Liu, C., Bi, Q., Leyland, A., Matthews, A. (2003) “An electrochemical impedance spectroscopy study of the corrosion behavior of PVD coated steels in 0.5 N NaCl aqueous solution: Part II. EIS interpretation of corrosion behavior.” Corrosion Science, 45(6), 1257-1273.
- Louis-Claude Dufour, Claude Monty, Georgette Petot-Ervas (1989). “Surfaces and Interfaces of Ceramic Materials.” Kluwer Academic, 779.
- Matthew, J. Donachie, Jr., “Relationship among Structure, Processing and Properties,” Titanium: A Technical Guide, 2nd, American Society for Metals, Metals Park, Ohio, 2000,.65-78.
- Mernagh, V.A., Kelly, T.C., Ahern, M., Kennedy, A.D., Adriaansen, A.P.M. and Ramaekers, P.P.J., McDonnell, L., Koekoek, R. (1991). “Adhesion improvements in silicon carbide deposited by plasma enhanced chemical vapour deposition.” Surface and Coatings Technology, 49(3), 462-467.
- Miller, J.C. and Haglund, R.F. (1998). “Laser Ablation and Desorption” Experimental Methods in the Physical Sciences Volume 30, Academic Press. New York.

- McKee, R. A., Walker, F. J. and Conner, J. R. (1991). “Molecular beam epitaxy growth of epitaxial barium silicide, barium oxide, and barium titanate on silicon.” Appl. Phys. Lett., 59, 782.
- Met, C., Vandenbulcke. L., Sainte Catherine M. C. (2003). “Friction and wear characteristics of various prosthetic materials sliding against smooth diamond-coated titanium alloy.” Wear, 255 (12), 1022-1029.
- Metev, S. and Meteva, K. (1989). “Nucleation and growth of laser-plasma deposited thin films.” Applied Surface Science, 43(4), 402.
- Mischler, S. Debaud, S. Landolt, D. (1998) “Wear accelerated corrosion of passive metals in tribocorrosion systems.” J. Electrochem. Soc 145(3) pp 750-758.
- Morkoç, H. Strite, S. Gao, G.B. Lin, M.E. Sverdlov, B. and Burns, M. (1994). “Large -band -gap SiC, III-V nitride, and II-VI ZnSe-based semiconductor device technologies ” J applied Phy 76, 1363.
- Muraleedharan, T.M. and Meletis, E.I. (1992). “Surface modification of pure titanium and Ti6A14V by intensified plasma ion nitriding.” Thin Solid Films, 221(2), 102-104.
- Myer Kutz. (2002). “Handbook of Materials Selection.” John Wiley & Sons, Inc., New York.
- Nestor, P.(2004), *Electrochemistry and Corrosion-Science*, Kluwer Academic Publishers New York, Boston, Dordrecht, London, Moscow.
- Otsubo.S, Maeda, T., Minamikawa, T., Yonezawa, Y., Morimoto, A., Shimizu, T. (1990). “Preparation of $Pb(Zn_{0.52}Ti_{0.48})O_3$ Films by Laser Ablation.” Jpn. J Appl. Phys. 29, L133.
- Park, J., Rouleau, C.M. and Lowndes, D. H. (1998). “Study of Substrate Diffusion in Epitaxial n-Type CdSe Films Grown on GaAs (001) by Pulsed-Laser Ablation.” MRS Symp. Proc. 526, 27.

- Park, Y. J., Park, Y. W., Chun, J. S., (1998). “The bond structures and properties of chemically vapour deposited amorphous SiC.” Thin Solid Films, 166(2), 367-374.
- Pieraggi, B. (1987) “Effect of creep or low cycle fatigue on the oxidation or hot corrosion behavior of nickel-base superalloys.” Materials Science and Engineering, 88, 199-204.
- Pillonnet, A., Garapon, C., Champeaux, C., Bovier, C., Jaffrezic, H., Mugnier, J. (2000). “Optical, structural and fluorescence properties of nanocrystalline cubic or monoclinic Eu:Lu_2O_3 films prepared by pulsed laser deposition.” Journal of Luminescence, 108, 787-789.
- Prusseit, S. Corsépius, M. Zwerger, P. Berberich, H. Kinder, O. Eibl, Jaekel, C. Breuer, U. and Kurz, H. (1992). “Epitaxial $YBa_2Cu_3O_{7-\delta}$ films on silicon using combined YSZ/Y_2O_3 buffer layers A comprehensive study” Physica C: Superconductivity 201(4) 249.
- Puchi-Cabrera, E.S. (2002). “A new model for the computation of the composite hardness of coated systems.” Surf. Coat. Technol., 160(2), 177.-186.
- Qiu, X, Conrad, J.R, Dodd, R., Worzala, F.J. (1990). “Plasma source nitrogen ion implantation of Ti6Al4V.” Metallurgical and Materials Transactions A, 21, 1663 -1667.
- Rose, V., Podgursky, V., Costina, I., Franchy, R.(2003). “Growth of ultra-thin amorphous Al_2O_3 films on CoAl (1 0 0).” Surface Science 541(3), 128–136.
- Schutz, R.W. and Thomas, D.E. “Corrosion of Titanium and Titanium Alloys.” Corrosion, Vol. 13, ASM Handbook, ASM International, 1987, pp. 669-706.
- Singer, F. and Singer, S.S., (1963). Industrial Ceramics, Chapman Hall Ltd, London.
- Smith, H. M., Turner, A. F. (1965). “Vacuum Deposited Thin Films Using a Ruby Laser.” Appl Opt., 4(1), 147.

- Sridharan, M., Sillassen, M., Bottiger, J., Chevallier, J., Birkedal, H., (2007). "Pulsed DC magnetron sputtered Al_2O_3 films and their hardness." Surface & Coatings Technology 202, 920–924.
- Tang, Y.H., Sham, T.K., Yang, D. Xue**,** L. (2006). "Preparation and characterization of pulsed laser deposition (PLD) SiC films." Applied Surface Science, 252(10), 3386-3389.
- Tauc J, (1972). "Optical properties of solids." F.Abels Edition, North-Holland, Amsterdam, p 277.
- Tian, Y.S, Chen, C.Z, Li S, Huo, Q.H, (2005). "Research progress on laser surface modification of titanium alloys." Appl. Surf. Sci., 242, (2), 177-184.
- Torregrosa, F., Barrallier, L., Roux, L., (1995). "Phase analysis, microhardness and tribological behaviour of Ti-6Al-4V after ion implantation of nitrogen in connection with its application for hip-joint prosthesis." Thin Solid Films, 266(2), 245-253.
- Tsuboi, Y., Goto, M., Itaya, A. (1999). "Thin films formation of poly (N-vinylcarbazole) by laser ablation deposition." J. Appl. Phys. 85, 4189.
- Tsuboi, Y., Itaya, A. (1998). "Thin Film Formation of a Protein by Laser Ablation Deposition Technique." Chem. Lett. 27, 521.
- Valentin, N. and Moiseyev. (2006). "Titanium alloys Russian aircraft and aerospace applications." Taylor & Francis Group 6000, Broken Sound Parkway N W, Suite 30.
- Urbach, F. (1953). "The Long-Wavelength Edge of Photographic Sensitivity and of the Electronic Absorption of Solids**.**" Physics Review, 92, 1324.
- Wang, L.D., Kwok, H.S. (2000). "Pulsed laser deposition of organic thin films." Thin Solid Films, 363, 58.
- Wang, J., Yu, Y.H., Lee, S.C., Chung, Y.M. (2001). "Tribological and optical properties of crystalline and amorphous alumina thin films grown by low-temperature reactive magnetron sputter-deposition." Surface and Coatings Technology, 189, 146-147.

- William, G.V.K., Ezhil, S.V., Harish, C.B., Rajam, K.S. (2006). “Effect of electroless nickel interlayer on the electrochemical behavior of single layer CrN, TiN, TiAlN coatings and nanolayered TiAlN/CrN multilayer coatings prepared by reactive dc magnetron sputtering.” Electrochimica Acta, 51, 3461–3468.
- Yi-Shung, C., Nripen, R. (1990). “Reactions at the aluminum oxide-ferrite interface.” Thin Solid Films, 193-194, Part 2, 959-964.
- Zaytouni, M. and Riviere, J.P. (1996). “Wear reduction of TiAl6V produced by SiC coatings deposited by dynamic ion mixing.” Wear, 197, 56-62.
- Zhang, Y., Gu. H., Iijima, S. (1998). “Single-wall carbon nanotubes synthesized by laser ablation in a nitrogen atmosphere.” Appl. Phys. Lett., 73, 3827.
- Zhu, X.M., Lei M.K. (2005). “Surface engineering of biomedical metallic materials by plasma-based low-energy ion implantation.” Curr. Appl. Phys., 5(5), 522-525.
- Zopal, J.C., Tellent, M., Skowronski, M. (2005). “Advances in Silicon Carbide Electronics.” Materials Research Society Bull., 30, 273.

BRIEF BIO-DATA

Contact address

Sujaya C ,
Mathakripa, Kodange House
Koliyoor Post
Manjeshwara, Kasaragod, 671323
Email. sujayachendel@gmail.com
Mobile +919449615068

Qualification: Bachelor of Science (Physics, Electronics, Mathematics),
Master of Science (Materials Science)

Academic achievements:

- 1st Rank holder in M Sc (Materials Science), Winner of Gold Medal for the year 2000-2001.
- First prize in poster presentation in International Conference on "Metals and Alloys: Past, Present and Future 'METALLO'" 07-10 Dec. 2007, IIT Kanpur.

Research experience:

- Project Assistant, Dept of Mechanical Engineering, IISc Bangalore - 560 017, India.
- Project fellow ISRO RESPOND project entitled "Laser processing of ceramic coatings onAl,Ti and other aerospace alloys"

Teaching experience:

Worked as an assistant lecturer in the Department of Physics, NITK Surathkal, for two years.

List of publications

International Journals

1. Hardness and electrochemical behavior of ceramic coatings on inconel, C. Sujaya, H.D.Shashikala, G. Umesh , A. C. Hegde, J. Electrochem. Sci. Eng. **2(1)** (2012) 19-31; doi: **10.5599/jese.2011.0007**
2. Hardness and electrochemical behavior of ceramic coatings on CP Titanium by Pulsed laser deposition, C. Sujaya, H. D. Shashikala, Surface Engineering and Applied Electrochemistry, 2012, Vol. 48, No. 2, pp. 133–140.
3. Microhardness of laser ablated alumina coatings on Ti-6Al-4V, Sujaya C., H.D.Shashikala, G. Umesh, K. Narayana Prabhu, Satyapal Hegde, Trans.Indian Inst.Met, volume 61, No 2, April 2008.

International conferences

1. Microhardness of laser ablated alumina coatings on Ti-6Al-4V, C. Sujaya, H. D. Shashikala, G. Umesh, K. Narayana Prabhu, Satyapal Hegde. International Conference on "Metals and Alloys: Past, Present and Future 'METALLO' " 07-10, Dec. 2007, IIT Kanpur.
2. Microhardness and Corrosion Behaviour of Pulsed Laser Deposited Al_2O_3 Coatings on Ti-6Al-4V, Titanium and Inconel, Sujaya C, H.D.Shashikala, Shelar Vikas M, G. Umesh, Yogesha .S, A. C. Hedge, International Conference on Recent Trends in Materials Charecterization , RETMAC 2010 , 14^{th} – 15^{th} Feb 2010., NITK Surathkal.

National conferences

1. Laser processing of Al_2O_3 coatings on Ti-6Al-4V, C. Sujaya, H.D.Shashikala, G.Umesh, National Symposium for Materials Research Scholars MR-08, 17-18 May, 2008, IITB Bombay.
2. Microhardness and Corrosion Behaviour of Pulsed Laser Deposited Al_2O_3 and SiC Coatings on Ti-6Al-4V, C. Sujaya, H.D.Shashikala, G. Umesh, DAE-BRNS 5^{th} national symposium on Pulsed laser deposition of thin films and nano structured materials, PLD 2009, Dec 2-4, IIT Madras.